DISSERTATION

# QUANTIFICATION OF HYDRAULIC EFFECTS FROM TRANSVERSE INSTREAM STRUCTURES IN CHANNEL BENDS

Submitted by

Stephen Michael Scurlock

Department of Civil and Environmental Engineering

In partial fulfillment of the requirements

For the Degree of Doctor of Philosophy

Colorado State University

Fort Collins, Colorado

Spring 2014

Doctoral Committee:

Advisor: Christopher I. Thornton

Steven R. Abt
Subhas K. Venayagamoorthy
Ellen E. Wohl

ABSTRACT

QUANTIFICATION OF HYDRAULIC EFFECTS FROM TRANSVERSE INSTREAM STRUCTURES IN CHANNEL BENDS

Meandering river channels possess hydraulic and geomorphic characteristics that occasionally place anthropogenic interests at risk. Loss of valuable land holdings and infrastructure due to outer-bank channel encroachment from erosion processes and complications for channel-bend navigation have prompted development of techniques for reconfiguration of instream hydraulics. Transverse instream structures are one type of technique and have been implemented in channel bends to reduce outer-bank erosivity and improve navigability. Instream structures use less material and have ecological and habitat benefits over traditional revetment type bank protection. Structures are typically constructed in series, extend from the outer-bank into the channel center, and are designed with various crest heights and slopes. Current design recommendations for the structures in natural channels provide generalized ranges of geometric parameters only; no specific information pertaining to hydraulic reconfiguration is provided. Understanding specific hydraulic response to alteration of geometric structure parameters is requisite for educated structure design.

Focusing on two types of transverse instream structures, the spur-dike and vane, a mathematical design tool was developed for the quantification and prediction of induced hydraulic response. A series of dimensionless groupings were formulated using parameters obtainable from field data of natural channels and grouped using dimensional analysis. Each

dimensionless grouping had an identifiable hydraulic influence on induced hydraulics. A conglomerate mathematical expression was established as the framework for induced instream structure quantification.

The mathematical model was tailored to produce twenty-four hydraulic relationships through regression analysis utilizing a robust physical model dataset collected within rigid-bed, trapezoidal channel bends. Average and maximum velocity and boundary shear-stress data were segmented into outer-bank, centerline, and inner-bank regions and then normalized by bend-averaged baseline conditions. Velocity equations were developed for an all-structure dataset, a spur-dike dataset, and a vane dataset. Boundary shear-stress equations were developed for spur-dike structures only. Regression equations quantified laboratory hydraulics to a high level of accuracy. Equation response to independent parameter alteration coincided with continuity principles and physical hydraulic expectations. Methods performed well in application to extraneous natural channel data from the literature.

Developed methodologies from this research presented a fundamental addition to the current design procedures for the installation of structures in migrating channel bends. Quantification of the reduction of outer-bank erosive potential and increase at the shifted conveyance zone within natural channels was made possible using readily measured field data and the proposed methodology. Equations allow for previously unattainable investigation of configuration geometry combinations to meet installation objectives using simple mathematical formulas. Configuration geometry optimization to meet hydraulic design criteria using the proposed methods may hold substantial economic benefit over traditional design protocols.

# ACKNOWLEDGEMENTS

Completion of this research would not have been possible without significant support from those I have been fortunate enough to be surrounded by. Dr. Christopher Thornton provided an incredible opportunity to be involved with the hydraulics laboratory and has devoted his time and resources to fund the duration of my graduate school. He and Dr. Steven Abt have provided welcomed inspiration, guidance, and encouragement throughout this project and throughout my graduate school journey. My committee members, Dr. Karan Venayagamoorthy and Dr. Ellen Wohl, helped steer my graduate course work and gave instrumental commentary to the benefit of the final research. Dr. Drew Baird and Dr. Amanda Cox significantly contributed in the development of the research concepts and fundamental research objectives presented within this dissertation.

My family has given unwavering support during this endeavor and their love and pride was felt throughout the duration of this research. My best friend and beautiful wife, Whitney, deserves special mention for her patience and understanding during the completion of this project.

TABLE OF CONTENTS

1. Introduction ..... 1
1.1. Transverse instream structures ..... 4
1.2. Objectives ..... 5
1.3. Methodology ..... 6
2. Literature review ..... 8
2.1. Channel-bend hydraulics ..... 8
2.2. Instream structure design ..... 12
2.3. Instream structure hydraulics ..... 17
2.3.1. Single configuration and structure hydraulics ..... 18
2.3.2. Hydraulic prediction models ..... 36
2.4. Literature review summary ..... 42
3. Physical modeling and analysis database ..... 44
3.1. Physical model description ..... 44
3.2. Instrumentation ..... 46
3.2.1. Volumetric flow rate ..... 47
3.2.2. Water-surface elevation ..... 47
3.2.3. Flow depth ..... 47
3.2.4. Velocity ..... 48
3.2.5. Boundary shear stress ..... 48
3.3. Instream-structure configurations ..... 49
3.4. Data-collection locations ..... 51
3.5. Compiled research dataset ..... 53

3.6. Physical modeling summary ..... 54
4. Predictive model development ..... 55
4.1. Parameter normalization ..... 55
4.2. Velocity distributions ..... 60
4.3. Boundary shear-stress distributions ..... 65
4.4. Quantification of induced structure hydraulics ..... 68
4.5. Predictive model development ..... 75
4.5.1. Channel curvature ratio ..... 78
4.5.2. Spacing ratio ..... 79
4.5.3. Lateral contraction ratio ..... 80
4.5.4. Submergence ratio ..... 81
4.5.5. Planimetric angle ratio ..... 82
4.5.6. Area contraction ratio ..... 83
4.5.7. Predictive mathematical model ..... 84
4.6. Model optimization ..... 85
4.7. Predictive mathematical models ..... 89
4.7.1. Velocity relationships ..... 90
4.7.2. Boundary shear-stress relationships ..... 96
4.8. Parameter response and sensitivity ..... 98
4.8.1. Laboratory data ranges ..... 98
4.8.2. Summarized parameter response ..... 100
4.9. Model development summary ..... 104
5. Developed methodology analyses and design application ..... 106
5.1. Equation application to natural-channel topography ..... 106

5.2. Application of methodology for field design ..... 114
5.3. Methodology analysis summary ..... 117
6. Conclusions and recommendations ..... 118
6.1. Research summary and discussion ..... 118
6.2. Conclusions ..... 123
6.3. Recommendations for further research ..... 124
7. References ..... 127
Appendix ..... 137
A1. Data used for analysis ..... 137
A2. Normalized hydraulic ratios ..... 141
A3. Parameter response and sensitivity ..... 146
A.3.1 Velocity ratios ..... 146
A.3.2. Boundary shear-stress ratios ..... 153
A4. Literature comparison ..... 155
List of Abbreviations ..... 157

LIST OF FIGURES

Figure 1. Middle Rio Grande River prototype area (Google, 2012).....3

Figure 2. Installed instream structures (Rhoads, 2003).....3

Figure 3. Channel-bend flow from Sellin et al. (2003).....9

Figure 4. Channel bend hydraulic schematic, from Ottevanger et al. (2011).....10

Figure 5. Boundary shear-stress distribution within trapezoidal bend, from Ippen and Drinker (1960).....11

Figure 6. Boundary shear-stress distribution from field site, from Dietrich et al. (1979).....11

Figure 7. Instream structure geometric parameter definitions.....14

Figure 8. Simulated boundary shear-velocity distributions (left) and streamlines (right) around bendway-weir configurations of Abad et al. (2008).....20

Figure 9. Results from Jia et al. (2011). Vertical section velocity vectors (top left), bed velocity vectors (top right), water-surface velocity vectors (bottom left), and physical model confetti lines (bottom right).....22

Figure 10. Normal secondary current rotation (top) and bendway-weir rotation (bottom) as reported from Jia et al. (2011).....22

Figure 11. Perspective and planimetric views of velocity streamlines around first encountered structure as reported by McCoy et al. (2007).....23

Figure 12. Planimetric view of streamlines around structures from McCoy et al. (2007).....23

Figure 13. Spur-dike velocity cross-sectional contours and recirculation zones (Duan, 2009).....24

Figure 14. Streamwise velocity contours before and after vane installation (Jamieson et al., 2013).....25

Figure 15. Cross-sectional velocity magnitudes and circulation moving past a vane structure; flow encounters vane at arrow moving downwards in cross-section (Bhuiyan et al., 2010).....26

Figure 16. Planimetric velocities within bendway-weir field from Lyn and Cunningham (2010)28

Figure 17. Bernalillo bendway-weir installation site; before and after, Google (2007).....29

Figure 18. Bernalillo bendway-weir installation schematic (BIO-WEST, 2006) .....29

Figure 19. Bendway-weir configurations from Scurlock et al. (2013a).....31

Figure 20. Normalized bendway-weir velocity plots from Scurlock et al. (2013a) .....32

Figure 21. Instream structure schematics from Scurlock et al. (2013b) .....34

Figure 22. Normalized instream structure velocities from Scurlock et al. (2013b).....35

Figure 23. Trapezoidal model plan view.....36

Figure 24. Constructed trapezoidal channel model.....37

Figure 25. Profile view schematic of evaluated structures in trapezoidal model .....38

Figure 26. Planimetric geometries of channel bends from the Middle Rio Grande study reach (Heintz, 2002).....45

Figure 27. Constructed instream structure in trapezoidal physical model .....51

Figure 28. Structure data points from Heintz (2002).....52

Figure 29. Full data-collection point distribution for structure field in upstream bend.....53

Figure 30. Calculation of bend-averaged friction slope for 8 cfs .....58

Figure 31. Calculation of bend-averaged friction slope for 12 cfs .....59

Figure 32. Calculation of bend-averaged friction slope for 16 cfs .....60

Figure 33. Normalized velocity for configuration W01; flow direction down-page.....62

Figure 34. Normalized velocity for configuration W04.....63

Figure 35. Normalized velocity for configuration W13.....64

Figure 36. Normalized boundary shear stress for configuration W01 .....66

Figure 37. Normalized boundary shear stress for configuration W04 .....67

Figure 38. Normalized boundary shear stress for configuration W10 .....68

Figure 39. Regional analysis for upstream W04, 12 $ft^3/s$.....72

Figure 40. Regional and point-based analysis data distribution .....74

Figure 41. Migration rate as a function of $R_C/T_W$ from Nanson and Hickin (1986).....79

Figure 42. Parameter estimation error propagation in power-type prediction equations.....89
Figure 43. Velocity ratios for all-structure dataset .....92
Figure 44. Velocity ratios for spur-dike dataset .....94
Figure 45. Velocity ratios for vane dataset.....95
Figure 46. Spur-dike ratios for spur-dike dataset .....97
Figure 47. Evaluation of developed methodologies with literature data .....111
Figure 48. Ranges of laboratory data compared to design recommendations.....140
Figure 49. All-structure velocity equation parameter response.....148
Figure 50. Spur-dike velocity equation parameter response .....150
Figure 51. Vane velocity equation parameter response .....152
Figure 52. Spur-dike boundary shear-stress equation parameter response .....154

LIST OF TABLES

Table 1. Design guidelines for bendway-weirs from literature (variables defined in Figure 7) ..15

Table 2. Design guidelines for spur-dikes from literature (variables defined in Figure 7).....16

Table 3. Design guidelines for vanes from literature (variables defined in Figure 7) .....17

Table 4. Type-I and Type-III trapezoidal model bend characteristics .....45

Table 5. Calculated normalization parameters for 8 cfs.....57

Table 6. Calculated normalization parameters for 12 cfs.....58

Table 7. Calculated normalization parameters for 16 cfs.....59

Table 8. Normalization conditions for velocity and shear stress.....60

Table 9. $R^2$ and regression coefficients for Equation 11; all-structure velocity ratios.....91

Table 10. $R^2$ and regression coefficients for Equation 11; spur-dike velocity ratios.....93

Table 11. $R^2$ and regression coefficients for Equation 11; vane velocity ratios.....93

Table 12. $R^2$ and regression coefficients for Equation 11; spur-dike boundary shear-stress ratios .....96

Table 13. Static median values and ranges of laboratory data .....99

Table 14. Parameters determined for method evaluation from the literature.....108

Table 15. Computed velocity ratios for comparison.....109

Table 16. Methodology optimization results.....116

Table 17. Instream structure tests and associated geometric parameters.....137

Table 18. Configuration maximum and average velocity ratios, regional analysis.....141

Table 19. Configuration maximum and average boundary shear-stress ratios, point-based analysis .....143

Table 20. Velocities from literature with normalization conditions .....155

Table 21. Predicted velocity ratios using Equation 11 and literature data .....155

Table 22. Absolute error between observed and predicted values, literature studies to Equation 11.....156

# LIST OF VARIABLES

| | |
|---|---|
| $\gamma$ | specific gravity of water [F/L³] |
| $\theta$ | planimetric angle of structure crest with bankline tangent |
| $\phi$ | crest slope angle measured down from horizontal |
| $\tau_0$ | normalization boundary shear stress [M/L²] |
| $\tau_{AVG}$ | array average of shear-stress measurements at location *i* [F/L²] |
| $\Delta z$ | difference between structure crest elevation and water-surface elevation [L] |
| $A$ | cross sectional flow area [$L^2$] |
| $Avg$ | average value |
| $AVR_i$ | normalized average velocity at location i |
| $A_W$ | projected weir area blocking the flow [$L^2$] |
| $A\tau R_i$ | normalized boundary shear stress at location *i* |
| $b$ | bottom width of channel [L]; |
| $C$ | location index for centerline |
| $D_B$ | baseline flow depth [L] |
| $D_R$ | submergence ratio |
| $H$ | horizontal |
| $h_W$ | height of structure above bed datum measured at the end of the crest [L] |
| $h_{W,TOE}$ | height of structure above bed datum measured at the channel toe [L] |
| $i$ | location index |
| $I$ | location index for inner-bank |

| | |
|---|---|
| $k$ | number of cross sections |
| $L$ | structure length [L] |
| $L_{ARC}$ | arc length between weirs along design waterline [L] |
| $L_{CW\text{-}PROJ}$ | projected length of weir crest measured from the baseline water surface along the horizontal plane to a cross section perpendicular to the flow [L] |
| $L_{W\text{-}PROJ}$ | projected length of weir measured from the baseline water surface along the horizontal plane to a cross section perpendicular to the flow [L] |
| $m$ | cross-sectional index |
| $M$ | maximum value |
| $MVR_i$ | normalized maximum velocity at location $i$ |
| $n$ | Manning roughness value |
| $O$ | location index for outer-bank |
| $Q$ | volumetric flow rate [$L^3$] |
| $R$ | hydraulic radius [L] |
| $R^2$ | coefficient of determination |
| $R_C$ | Radius of curvature for channel bend [L] |
| $S$ | structure spacing [L] |
| $s$ | structure-type index |
| $S_F$ | slope of total mechanical energy head in flow direction |
| $T_W$ | channel top width [L] |
| $u_0$ | bend-averaged normalization velocity [L/T] |
| $u_{AVG\text{-}i}$ | array average of mean-flow resultant velocity at location $i$ [L/T] |

| | |
|---|---|
| $V$ | vertical |
| $W$ | structure width [L] |
| $y$ | flow depth [L] |
| $Z$ | ratio of horizontal to vertical distance at outer-bank slope |
| $Z_W$ | ratio of horizontal to vertical distance on projected weir crest tip tie-in |

# 1. Introduction

River environments are complex and dynamic systems wherein localized and regional geologic, geographic, ecologic, meteoric, and anthropogenic influences dictate the characteristics of flow path and behavior. River systems under relatively constant stimulus variables, i.e. annual hydrograph and sediment load, commonly exhibit quasi-equilibrium states with recurring and predictable responses in planimetric and profile form. Such equilibrium states have been categorized under braided or meandering geomorphic regimes, both of which have numerous sub-categorizations (Leopold and Wolman, 1957). Braiding channels are typically regulated within a straight and defined flow path while meandering channel boundaries change over time within the confines of the river corridor. Significant alteration of the quantity or duration of flow, or of the qualities of the watershed, may result in a breach of a geomorphic threshold separating one regime from another and cause substantial effects to riparian areas.

A shift from braiding to meandering regimes increases planimetric flow path variability as noted by Cencetti et al. (2004), Surian and Rinaldi (2003), and Crosato (2008). Valuable land holdings which were once removed from the flow path, and infrastructure designed for the braiding conditions, may be placed in jeopardy as the emerging, migrating channel path encroaches upon them. Infrastructure designed without acknowledging channel-bend hydraulics, or unrealistic expectations of a meandering river system, may also produce undesired encroachment from natural migration within an equilibrium meander belt. Navigation requirements may dictate a meandering channel to become static for ease and reliability of passage. Regardless of the origin of the encroachment or intention for the river, measures for the protection of resources from migrating channel banks have been implemented extensively.

Scientists and engineers have developed a variety of methodologies to combat erosive forces associated with channel-bend hydraulics.

Examples of installation of mitigation measures to combat undesired bank erosion associated with meandering rivers and stabilize banks are numerous. In 1975, the Cochiti Dam was installed in a braiding geomorphic regime of the Middle Rio Grande River upstream of Albuquerque, New Mexico. The installation of the Cochiti Dam effectively disrupted sediment supply to the downstream reach of the channel, resulting in a geomorphic shift from a braiding to slightly meandering geomorphic regime (Richard and Julien, 2003). Previous channelization work conducted on the river, and a minimal berth for lateral mobility, placed infrastructure and valuable land holdings at risk. In response, the Albuquerque Area Office of the United States Bureau of Reclamation (Reclamation) identified a variety of transverse instream structures as potential mitigation measures of undesired channel migration within the targeted reach of the Middle Rio Grande River depicted in Figure 1 (Heintz, 2002).

Control of undesired river migration through transverse instream structures has also been implemented in Illinois. Rivers in the region are subject to watershed perturbations, have become channelized, and exhibit problematic migration characteristics (Rhoads, 2003). Figure 2 depicts an example of transverse instream structures installed in a channel bend in Illinois from Rhoads (2003).

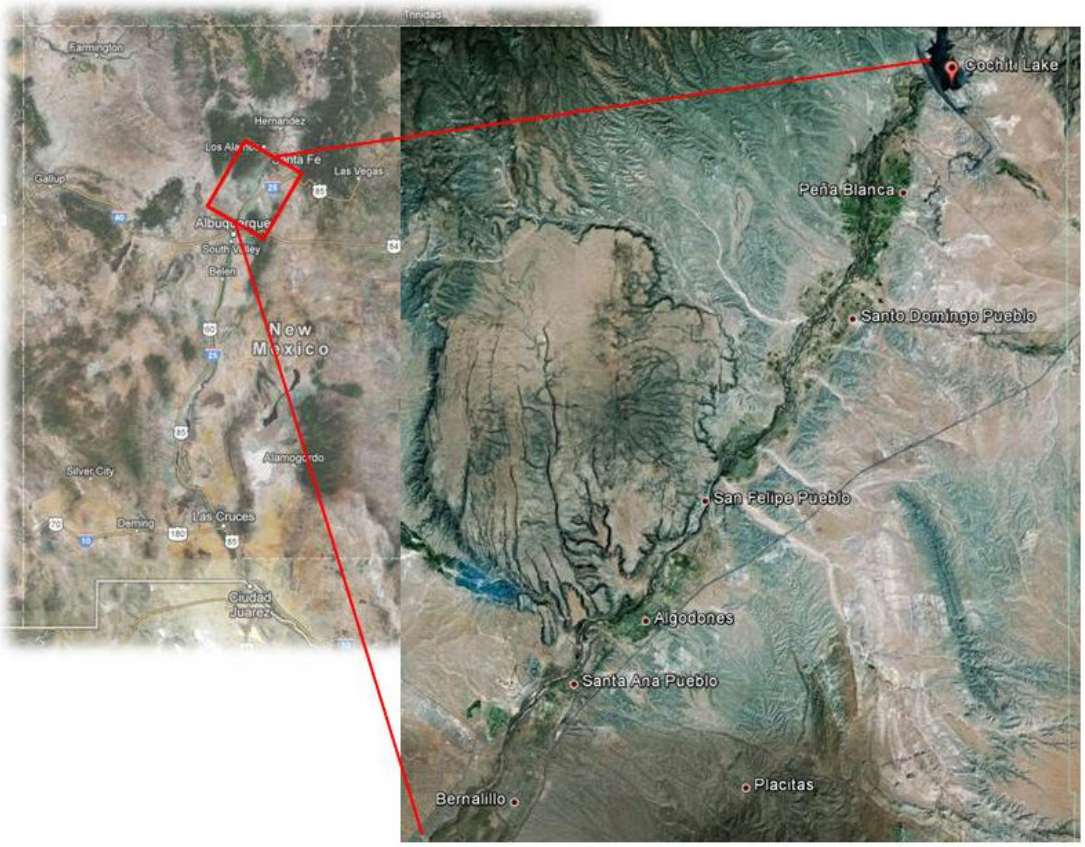


**Figure 1.** Middle Rio Grande River prototype area (Google, 2012)

**Figure 2.** Installed instream structures (Rhoads, 2003)

Instream structures possess benevolent environmental characteristics over traditional bank revetment methods and typically require less construction material for installation as noted by Shields et al. (1998) and Piper et al. (2001). Implemented structures redirect bulk conveyance to the channel center and away from the outer-bank in an effort to minimize erosive forces. A variety of structure types exist and are classified by intended hydraulics and geometric design.

## 1.1. Transverse instream structures

Instream structure nomenclature is dependent upon the design elevation of the structure crest relative to the design flow depth, structure plan angle, structure profile angle, and intended objective for installation. Spur-dikes, vanes, bendway weirs, Iowa vanes, jetties, hardpoints, retards, groynes, and guide-banks are examples of structures designed to train channel-bend flows to a desired pathway (Federal Highway Administration, 2009). Redirection structures are installed in the channel center and run parallel to the desired flow path. Iowa vanes and guide-banks are classified as redirection structures and are typically implemented for navigation purposes, yet have also been installed for morphological reasons (Fitzpatrick et al., 2013). Transverse instream structures extend from the outer-bank into the main channel, divert conveyance to the channel center, and create relatively stagnant or recirculating flow zones in the leeward zone of the structure. Spur-dikes, vanes, and bendway weirs are classified as transverse structures and have been recently scrutinized for their effectiveness for bank erosion and migration control.

Current design criteria for transverse instream structures are rudimentary and anecdotal, typically providing generalized ranges for structure geometry parameters, spacing, and orientation. Designers have limited information pertaining to specific structure configurations

and geometries for reduction of outer-bank erosive forces and increase of hydraulic forces at the channel center and inner-bank which occur as a result of installation. State parameters of interest for transverse instream structure design are the velocity magnitude and boundary shear stress at the outer-bank, channel center, and inner-bank. Formulation of design guidelines for the prediction of hydraulic response from transverse instream structure installation in channel bends is addressed in this study.

## 1.2. Objectives

Objectives for the current investigation are as follows:

1) Identify the geometric parameters of transverse instream structures, and hydraulic parameters of the channel and flow, which are influential on velocity and boundary shear-stress effects;
2) Organize the parameters into dimensionless groupings which have physically identifiable meaning and hypothesized effects on state parameters;
3) Quantify maximum and average velocity and boundary shear-stress for various instream structure types at different channel-bend locations from a physical model dataset;
4) Perform regression analyses to determine statistical significance and develop mathematical models for the prediction of the maximum velocity, average velocity, maximum shear stress, and average shear stress relative to baseline conditions for different structure types;
5) Apply developed models to field, numerical, and physical model data from the literature; and
6) Provide a comprehensive summary of results with application of methods to field installation, recommendations, and limitations.

Completion of the six objectives for this research will significantly improve and expand the current knowledge regarding transverse instream hydraulics and provide an important design tool for engineers and field practitioners.

## 1.3. Methodology

Completion of the objectives was performed systematically. A comprehensive literature review of the current guidelines for the design of transverse instream structures was performed and scrutinized. Studies detailing the hydraulic response of the structures are investigated. Documented flow hydraulics from the literature are attributed to geometric design variables when applicable to ascertain response mechanisms. Pertinent geometric parameters of the structures, the channel bend, and the conveyed flow are compiled for the development of original predictive model development. Parameters governing the hydraulics of transverse instream structures were selected based upon physical expectations gained from the literature review and are grouped into ratios using dimensional analysis. Dimensionless groupings were organized into a mathematical model able to be tailored through regression procedures for the prediction of the velocity and boundary shear-stress distributions at a variety of channel locations.

Data were obtained from a prismatic physical model constructed and evaluated at Colorado State University (CSU) and maximum and average velocity and boundary shear-stress values were determined at three channel regions. Values were normalized by bend-averaged velocity and shear-stress conditions, respectively. Using the developed mathematical model, regression analyses were performed to determine statistically significant predictive relationships for the maximum and average normalized velocities and boundary shear stresses at the outer-bank, channel center, and inner-bank for two different structure types evaluated in the physical

model. Regression procedures were conducted to ensure minimization of error in parameter prediction, correct mathematical variable response with physical expectations of parameter changes, and applicability to non-prismatic, natural channels.

Predictive relationships were compared to data collected from physical models of natural river topographies, numerical models, and field studies. Comparative analysis between results of the prismatic regression relationships and natural channel results was performed, offsets are applied to the equations, and limitations of the developed methodologies are presented. Applications of the equations for design purposes, limitations of the dataset and mathematical model, recommendations to expand the current research for more robust application to field design, and conclusions from the research are provided.

# 2. Literature review

Transverse instream structures are installed in channel-bends to address problematic, yet recurring and predictable, trends in hydraulic behavior. This section details the nature of such problematic channel-bend hydraulic behavior, structural characteristics of instream structures, intended goals of the structures, and hydraulic findings from laboratory, numerical, and field studies. Channel-bend hydraulics without structures are detailed, including cross-sectional and planimetric descriptions of velocity and boundary shear-stress patterns and distributions. Transverse instream structure design protocols are examined and summarized, specifically for spur-dike, vane, and bendway-weirs. Investigations into induced hydraulics from the structures yield pertinent information to structure geometric parameter influence and key findings are documented. State of the knowledge prediction methodologies are investigated and applied to datasets from the literature.

## 2.1. Channel-bend hydraulics

Meandering river geomorphic regimes are characterized by a sinuous flow path, migrating laterally and longitudinally within the confines of a meander belt or river corridor. Channel-bend hydraulics are three-dimensional, turbulent, and complex, and have been the focus of extensive empirical and theoretical study. A balance of form and function, induced hydraulics and topographic patterns from channel-bends have found to be characteristic and recurring throughout observed laboratory and real-world meandering systems. Channel-bend hydraulics may be generally described by differences in velocity and boundary shear-stress distributions from the case of one-dimensional, straight channel flow.

Flow entering a channel bend is redirected and affected by the centrifugal force of a curved bank-line and thalweg. Figure 3 illustrates a schematic of helical flow development

through a meandering stream from Sellin et al. (1993). Figure 4 provides a perspective view of the flow path and details the super-elevation of the water surface and outer-bank conveyance shift from Ottevanger et al. (2011). Water-surface super-elevation that occurs on the outer-bank of the channel bend generates a pressure gradient that drives a secondary current of transverse and vertical flow. Secondary circulation results in both increased erosivity, as noted by Bathurst et al. (1979), and complicates nautical navigation as detailed by Scott et al. (2001). Blanckaert and Graf (2001) noted the presence of a secondary rotation current formed at the far outer-bank in channel-bend flows and hypothesized that the cell served to protect the outermost-bank and adjacent bottom from erosive forces.

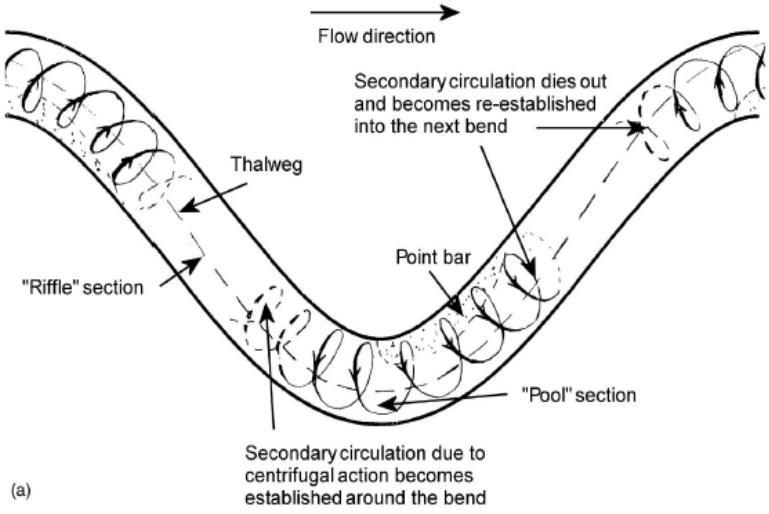


**Figure 3.** Channel-bend flow from Sellin et al. (2003)

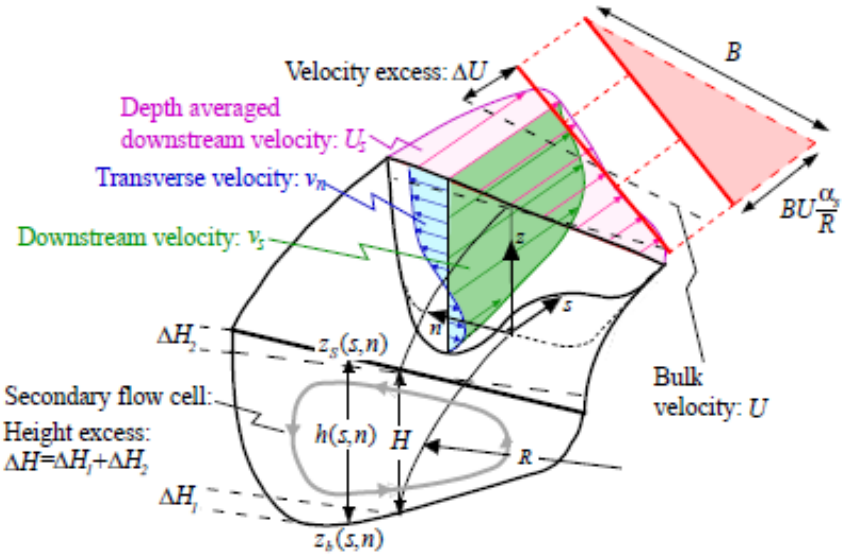


**Figure 4.** Channel bend hydraulic schematic, from Ottevanger et al. (2011)

Conveyance increase to the outer-bank of a channel bend is accompanied by boundary shear-stress increase along the outer-bank. Boundary shear-stress distributions in channel bends of varying shape and curvature have been examined extensively. Figure 5 depicts a boundary shear-stress distribution in a prismatic, trapezoidal laboratory model from Ippen and Drinker (1960). Figure 6 shows a distribution observed within a natural stream meander from Dietrich et al. (1979). An area of high shear stress is commonly noted at the inner-bank near the bend entrance, and at the outer-bank near the bend exit. Increased boundary shear stress coupled with the helicoidal flow within channel bends results in a tendency for river meanders to migrate, eroding and encroaching on land at the outer-bank and depositing and retreating at the inner-bank. As noted by Blanckaert and Graf (2001), and reinforced by experimental studies of Fitzpatrick et al. (2013), and Rhoads (2003), the highest erosive potential is centered at the channel toe. Channel toe erosion routinely serves as the precursor for bank failures as noted by Thorne (1978).

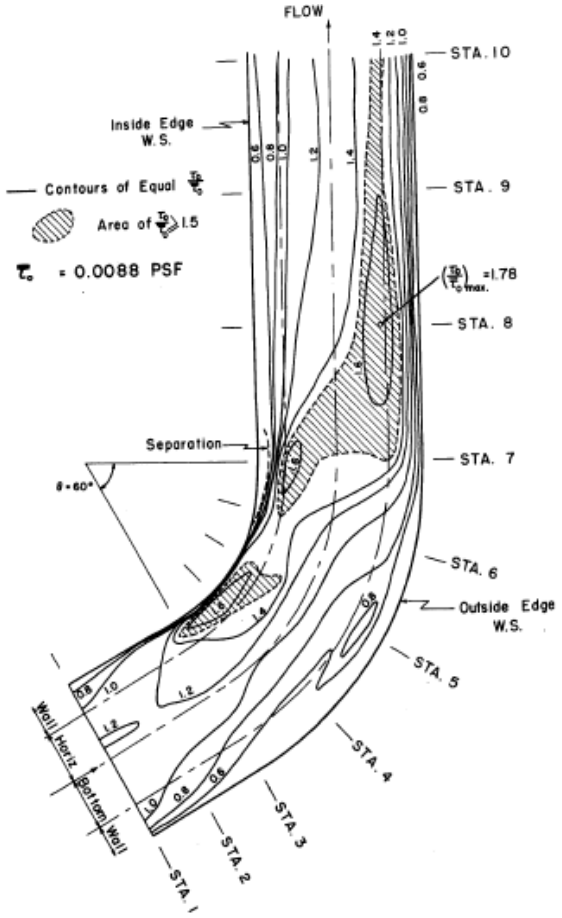


**Figure 5.** Boundary shear-stress distribution within trapezoidal bend, from Ippen and Drinker (1960)

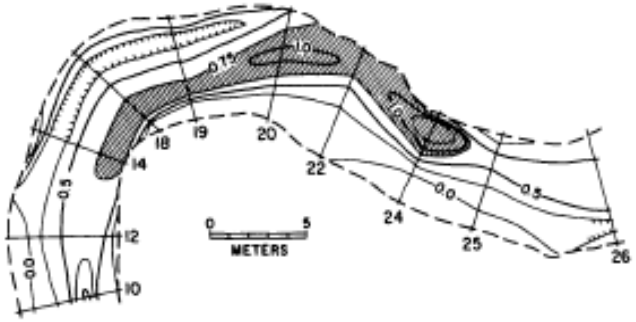


**Figure 6.** Boundary shear-stress distribution from field site, from Dietrich et al. (1979)

Channel-bend hydraulics and meander belts are a naturally occurring phenomenon that may exist in a dynamic equilibrium without disrupting anthropogenic requirements from the surrounding landscape. However, meandering channels are associated with alluvial river corridors containing fertile agricultural valleys, are aesthetically appealing, and are typically

located in desirable living environments. Meandering river corridors are linked by these factors with a propensity for development and human inhabitance. Occasionally, localized bank erosion within the river corridor is determined as hazardous to valuable infrastructure, buildings, or landholdings. Recent stream transitions exacerbate deleterious erosional effects, such as a meandering geomorphic regime transition from a historically straight or braided channel (Schumm and Brackenridge, 1987), or when significant channelization or alteration to the bathymetry has occurred in proximal reaches of the river (Crosato, 2008). Mitigation measures against undesired channel migration have recently emphasized the employment of transverse instream structures.

Transverse instream structures for bank erosion mitigation have gained in popularity due to potential reduction in material cost over bank revetment, habitat enhancement (Shields et al., 2000), and promotion of natural stream aesthetic (Rosgen, 2006). Transverse instream structures are typically installed in series along the outside of the channel bend and are designed to deflect outer-bank channel bend conveyance to the channel-center, increase flow resistance near the base of the outer-bank, and inhibit helical motion and redistribution of momentum near the outer-bank (Derrick, 1997). As summarized by Radspinner et al. (2010) and Baird et al. (2014), spur-dikes, vanes, and bendway-weirs are classes of transverse instream structures with specific geometric design and hydraulic characteristics.

## 2.2. Instream structure design

Bendway-weir, spur-dikes, and vanes are types of instream structures, planimetrically identical, yet different in their cross-sectional geometries and intended hydraulic effects. Planimetric and cross-section schematics of the three identified instream structures are provided in Figure 7 which expounds differences between structure classifications in the cross-sectional

view. In a general hydraulic sense, bendway-weirs redirect conveyance perpendicularly and over the top of the structure crests, spur-dikes shift flows around the structure tip, and vanes combine both crest overtopping and shifted flow to redirect conveyance to the channel center. A field installation of an instream structure configuration was provided in Figure 2. Physical and numerical research has been undertaken to describe hydraulic trends associated with the various instream structure types. Typical geometric parameters of interest for instream-structure design are the structure width, *W*, length, *L*, spacing, *S*, elevation difference between the water-surface elevation and structure crest elevation, $\Delta z$, and planform angle, $\theta$. Codified guidelines for the construction and installation of instream structures in channel bends as functions of the geometric parameters exist in an anecdotal and non-specific pertaining to induced hydraulic effects. This section details the current state of knowledge of design criteria and hydraulic characteristics of bendway weirs, spur-dikes, and vanes.

Bendway-weirs were initially developed by the U.S. Army Core of Engineers to increase channel width and improve navigation in bends of the Mississippi River (Derrick et al. 1994). Structures are typically placed in series along the outside of a channel bend, are angled upstream, and have a submerged crest elevation at design flow. Flows encountering the crest are redirected over and perpendicular to the structure axis to the channel center. Three primary sources for documentation and interpretation of bendway-weir design and construction guidance were identified as McCullah and Gray (2005), Lagasse et al. (2009), and Julien and Duncan (2003). Recommendations summarized from the literature are detailed in Table 1. Currently, design guidelines for bendway-weir configurations are anecdotal, and have largely been developed on the basis of expert judgment (Rhoads, 2003).

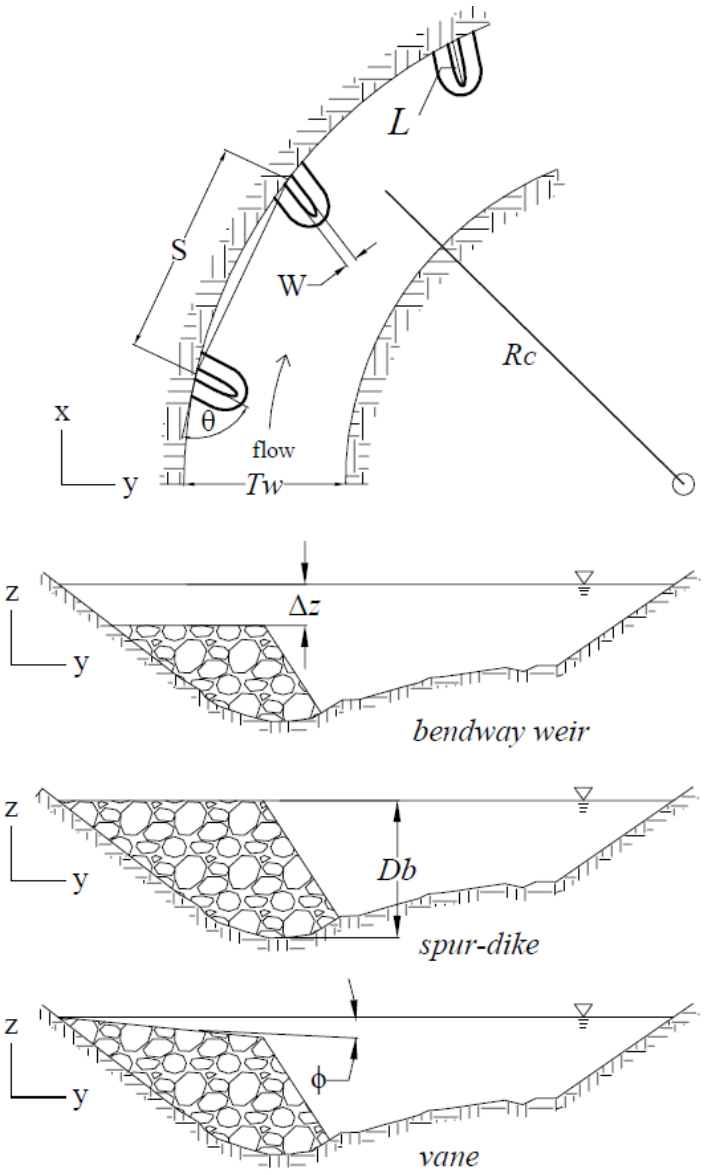


**Figure 7.** Instream structure geometric parameter definitions

**Table 1.** Design guidelines for bendway-weirs from literature (variables defined in Figure 7)

| | Length | | Height | | Top width | | Spacing | | θ | | Transverse slope | |
|---|---|---|---|---|---|---|---|---|---|---|---|---|
| Source | min | max | min | max | min | max | min | max | min | max | crest slope | key |
| McCullah and Gray (2005) | $T_W/3$ | $T_W/2$ | $W/2$ | $W$ | $2d_{100}$ | $3d_{100}$ | $1.5L$ | $1.5L$ | 80º | 70º | flat | flat |
| Lagasse et al. (2009)* | $T_W/10$* | $T_W/3$* | 0.3 $D_B$ | 0.5 $D_B$ | $2d_{100}$ | $3d_{100}$ | $4L$ | $5L$ | 60º | 85º | flat | 1$V$:5$H$ |
| Julien and Duncan (2003) | longer is better | | max permitting navigation | | none | none | $2L$ | $3L$ | 60º | 60º | none | none |

* Lagasse et al. (2009) also recommends structure length to fall between annual mean flow and annual low flow water surface elevations

Spur-dikes, also referred to as groynes or jetties, extend into the flow from the outer-bank, are placed in series throughout a channel bend, and are set perpendicular or angled upstream or downstream to the stream flow direction. In contrast to bendway weirs, spur-dike crest elevations are constructed at the design water-surface elevation such that no flows are intended to be conveyed over the structure crest. Crest elevation design encourages sedimentation within the structure field and outer-bank erosion protection (Radspinner et al., 2010). Design guidelines for spur-dikes are summarized by the Federal Highway Admninistration publications of Brown (1985) and Lagasse et al. (2009) as detailed in Table 2.

**Table 2.** Design guidelines for spur-dikes from literature (variables defined in Figure 7)

| | Length | | Top width | | Spacing | | θ | |
|---|---|---|---|---|---|---|---|---|
| Source | min | max | min | max | min | max | min | max |
| Brown (1985) | For impermeable spurs, less than $T_W/6$ at bankfull stage, and less than $T_W/4$ otherwise | | n/a | n/a | Line from DS structure tip, parallel to bank tangent at tie-in, to intersection of US bank | | 90° | 150° |
| Lagasse et al. (2009) | n/a | $T_W/5$ for impermeable | 3 ft | n/a | $3.27L$* | | 90° | 90° |

* Lagasse et al. (2009) reports spacing to be $S = L\cot\theta$, where θ = expansion angle = 17° constant for impermeable spurs

Vanes, synonymous with barbs, represent a hybrid between the bendway weir and spur-dike structures. They are constructed with a crest elevation at the design discharge water-surface elevation at the outer-bank and extend into the channel at a downward angle to allow increasingly more flow to overtop the structure crest moving away from the outer-bank key-in. Similar to the other transverse instream structure types, vanes are typically constructed in series and set perpendicular or angled upstream to the flow direction. Unique publications of geometric design criteria, including summarizations from Rosgen (2001), McCullah and Gray (2005), and others are reported by the United States Department of Agriculture (USDA) (2005), Johnson et al. (2001), and Maryland (2000), which are summarized in Table 3.

**Table 3.** Design guidelines for vanes from literature (variables defined in Figure 7)

| | Length | | Top width | | Spacing | | θ | | Transverse slope | |
|---|---|---|---|---|---|---|---|---|---|---|
| Source | min | max | min | max | min | max | min | max | min | max |
| USDA (2005) | Must cross thalweg, dependent upon horizontal angle, not to exceed $T_W/3$ | | $d_{100}$ | $3d_{100}$ | Line from DS structure tip, parallel to bank tangent at tie-in, to intersection of US bank | | 20° | 30° | 5% | 8% |
| Johnson et al. (2001) | $T_W/4$ | $T_W/3$ | Constructed from large boulders | | n/a | n/a | 20° | 30° | n/a | n/a |
| Maryland (2000) | n/a | $T_W/3$ | n/a | n/a | $5T_W$ | $7T_W$ | 20° | 30° | 3% | 7% |

Bendway-weirs, spur-dikes, and vanes generally redirect flow away from the outer-bank and have been validated in natural channels. Field data from studies such as Scott et al. (2001), Rhoads (2003), Smith and Wittler (1998), and Wardman and Papanicolaou (2006) for bendway weirs, and Dahle (2009) for vanes, have confirmed that transverse instream structure configurations are typically effective at the redirection of bulk channel conveyance to the central channel. Investigations into specific flow patterns associated with single structures and configuration fields have been conducted utilizing physical and numerical modeling. Hydraulics associated with transverse instream structures have been reported as three-dimensional and complex, yet the literature reports specific and recurring trends of flow behavior across independent sources.

## 2.3. Instream structure hydraulics

Instream structures have been the focus of analytical, numerical, and physical investigation. Studies found within the literature largely focus upon specific hydraulic trends

associated with single instream structures or isolated configurations. Investigations of how the flow is redirected by the structure, generated turbulence, scour effects, and numerical modeling efficacy have been the primary research goals. Physical hydraulic modeling was performed by Heintz (2002), Darrow (2004), and Schmidt (2005) at CSU on instream structures to quantify the effects of influential geometric parameters on channel-bend flow. The first section of the investigation into transverse instream structure hydraulics centers on specific hydraulic trends found from the literature. The second section focuses on the methodologies for induced hydraulic prediction, primarily on testing and results found from CSU. The third section details the application of the most recent prediction methods to available datasets from the literature and identifies methodology shortcomings to function as a design tool.

### 2.3.1. Single configuration and structure hydraulics

Investigations of single transverse instream structure configuration installations, and the incited flow fields and hydraulic responses, are the most prevalent within the literature. Studies typically focus upon velocity streamlines, areas of scour and deposition, and evaluating numerical modeling schemes with physically collected data. While most studies generally note a lack of design guidelines available for geometric parameter determination as the impetus for research, few address the effects of the variation of such design parameters on resulting hydraulics. Pertinent studies and findings relating to transverse instream structures are detailed.

Abad et al. (2008) coupled surveyed field data with a three-dimensional numerical model to emulate flow characteristics at various flow depths around a bendway-weir configuration installed in an Illinois meander bend. Key insights from the study included areas of convective acceleration and high boundary shear-stress at the tips of the structures, increased velocity and shear-stress over the crest of the structure at the bankline, and locally increased bed shear

downstream of the crest due to plunging flows. Flow was observed to be conveyed to the channel center and away from the outer-bank of the channel. Figure 8 details numerical results from Abad et al. (2008) of boundary shear-velocity and streamlines within the bendway-weir field at various flow stages. At the lowest flow illustrated, the modeled bendway-weirs did not experience overtopping flows, therefore behaving as spur-dikes. Acceleration and increased boundary shear stress at the structure tips, over the structure crest at the bankline, and at the overtopping jet and bed interface were noted in the graphical output. Analyzing select cross-sections within the numerical model, Abad et al. (2008) reported that secondary circulation patterns were not altered significantly from the helicoidal fluid motion in channel bends without instream structures as depicted in Figure 3. However, validation for the numerical model was only collected for non-submerged crest conditions.

Jia et al. (2002), Jia et al. (2005), and Jia et al. (2011) investigated the efficacy of bendway-weirs to disrupt helical secondary currents in channel bends and documented flow patterns using numerical and physical modeling on a single structure angled 70º upstream of the bankline tangent. Acceleration of the flow velocity over the weir crest and around the structure tip, and a vertical recirculation zone directly behind the structure were reported. Figure 9 depicts results from Jia et al. (2011) illustrating the flow vectors around the evaluated bendway-weir. Contradictory to Abad et al. (2008), Jia et al. (2011) reported substantial deviation from an unaffected secondary current cell in the vicinity of bendway-weirs. A counter-rotating current, opposite that of the expected helical motion of the channel bend, was observed to form from interaction with the structure and flow. Figure 10 illustrates results of secondary currents observed by Jia et al. (2011) with and without the presence of a bendway-weir structure. It is

noted that the zone of counterrotation was reported to diminish in strength moving downstream from the structure crest to an eventual return to typical channel-bend rotation.

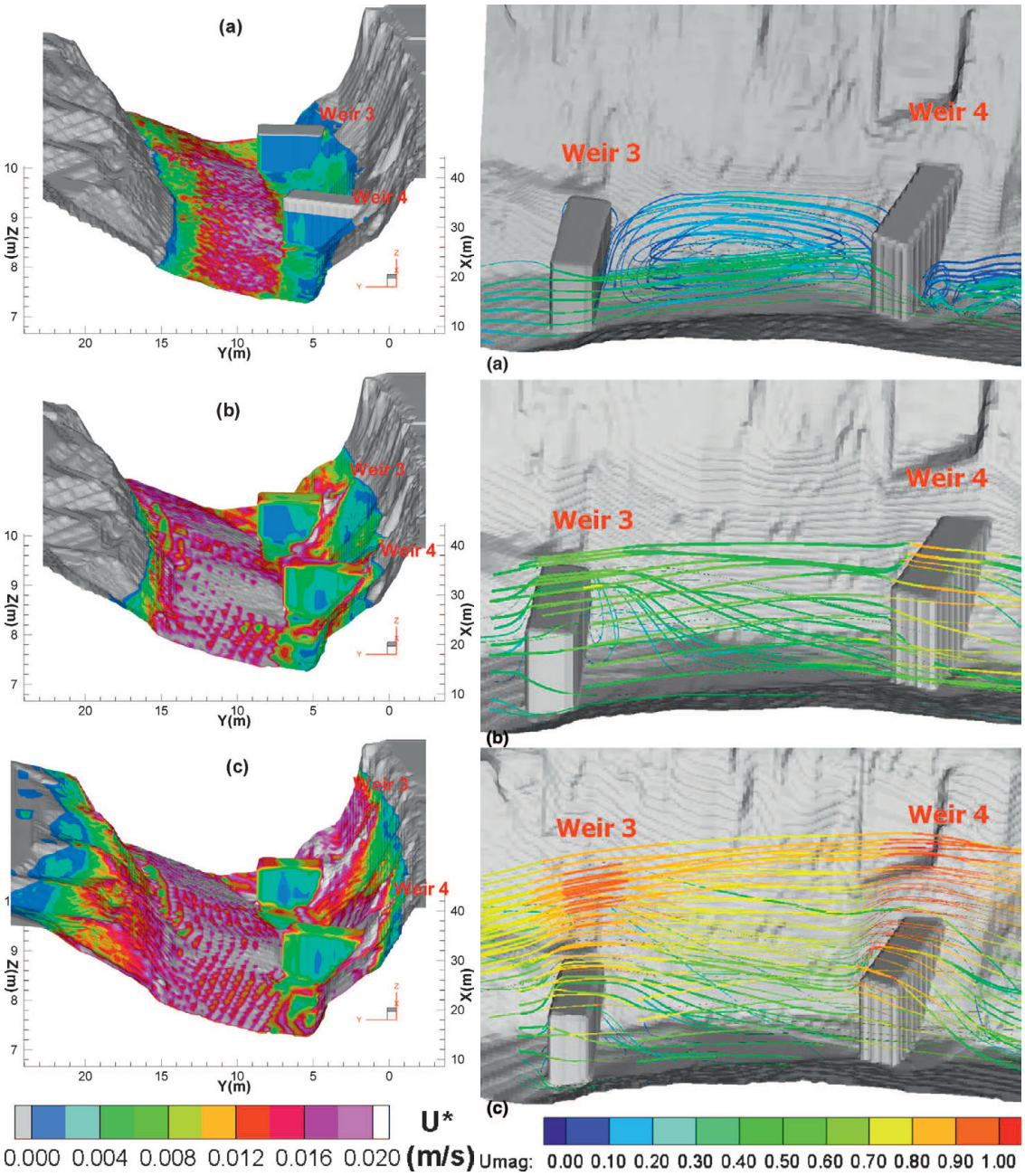


**Figure 8.** Simulated boundary shear-velocity distributions (left) and streamlines (right) around bendway-weir configurations of Abad et al. (2008)

McCoy et al. (2007) detailed numerical modeling results of flow encountering submerged, bendway-weir like structures angled perpendicular to the approach flow. Evaluated

structures had abrupt, blunt noses instead of gradually angled into the channel-center. Authors noted significant convective acceleration over the structure crest and around the blunt structure tip as illustrated in Figure 11. Flow encountering the first structure in the configuration series separates at a stagnation velocity zone at the structure face, and was redirected over and around the obstruction. Recirculation zones were observed to form behind the structures and between adjacent structures as depicted in Figure 12. Streamlines were not shown to exhibit substantial planimetric circulation in the upper water column and the effects of the structure field diminished within two structure lengths of the downstream crest. Conveyance was observed to shift to the inner channel, away from the increased roughness of the modeled structure series.

Duan (2009) performed physical modeling on a spur-dike installed in a straight laboratory channel with a mobile bed under clear-water conditions. Results of the study included documentation of flow separation downstream of the structure, strong planimetric recirculation in the upper water-column which decayed moving deeper into the flow, induced cross-sectional rotation, and high tip velocities. Figure 13 illustrates the velocity contours and recirculation zones associated with the induced spur-dike hydraulics. Reynolds stresses were noted to be altered due to the flow interaction with the spur-dike with positive values corresponding to sweep and ejection flows and negative values corresponding to recirculation and deposition areas. Values of mean and turbulent kinetic energy were reported with a balance between the two parameters. Flow interaction with the spur-dike shifted the conveyance and bulk mean kinetic energy to the outside of the tip of the structure and incited circulation and increased turbulent kinetic energy downstream and behind the structure crest.

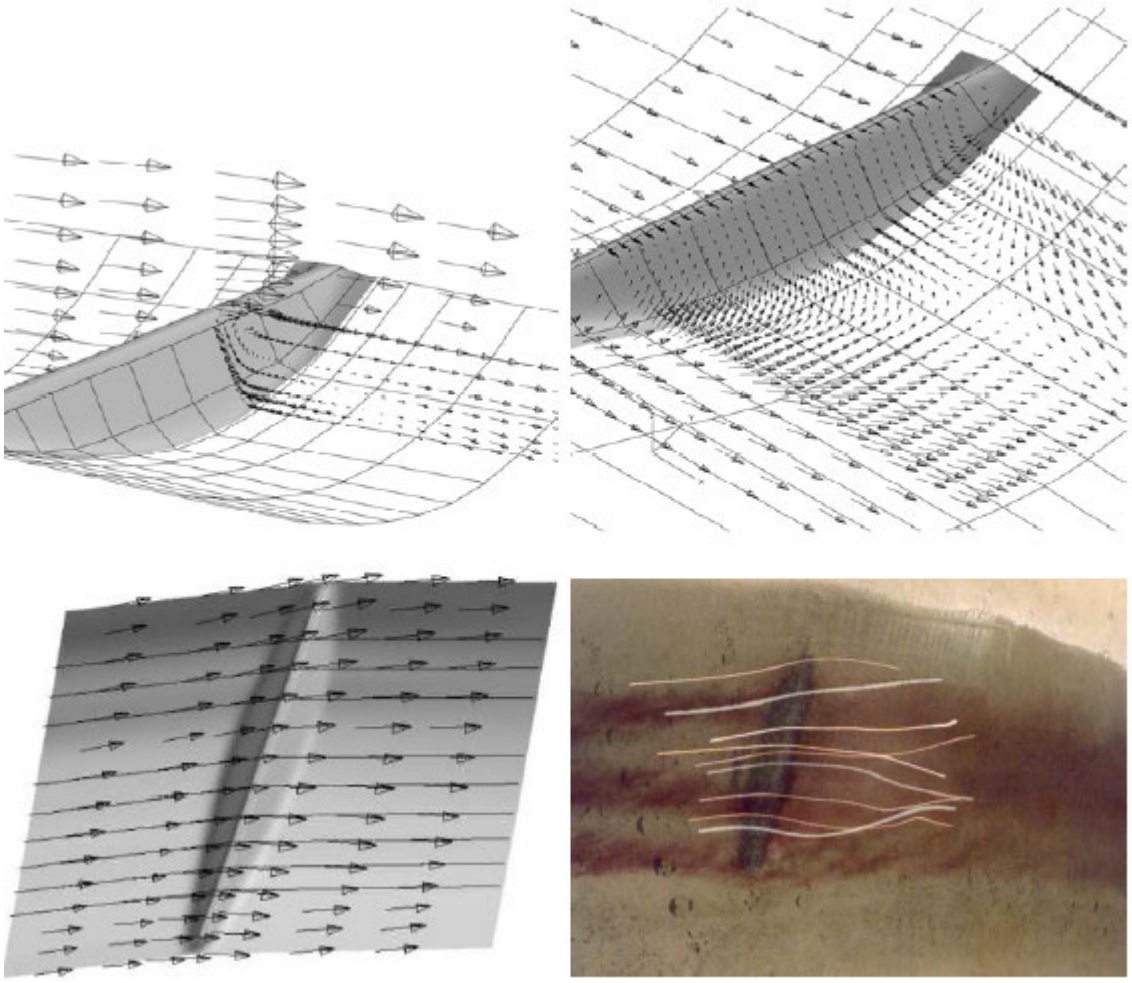

**Figure 9.** Results from Jia et al. (2011). Vertical section velocity vectors (top left), bed velocity vectors (top right), water-surface velocity vectors (bottom left), and physical model confetti lines (bottom right).

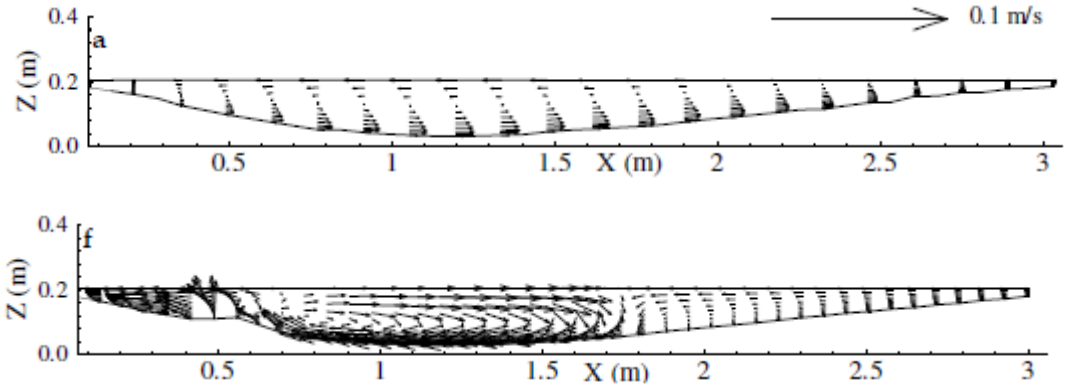


**Figure 10.** Normal secondary current rotation (top) and bendway-weir rotation (bottom) as reported from Jia et al. (2011)

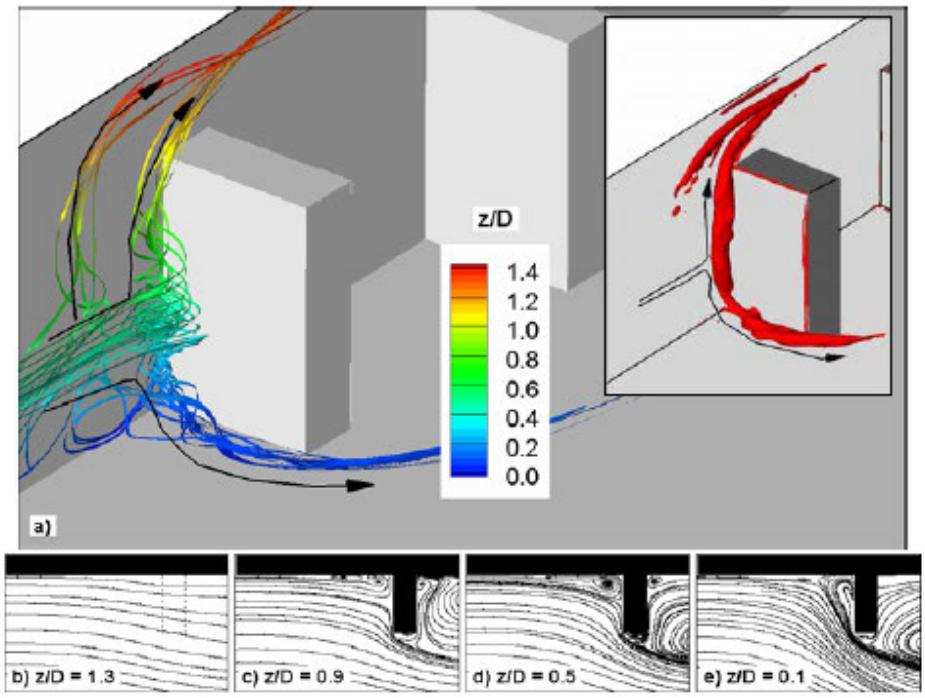


**Figure 11.** Perspective and planimetric views of velocity streamlines around first encountered structure as reported by McCoy et al. (2007)

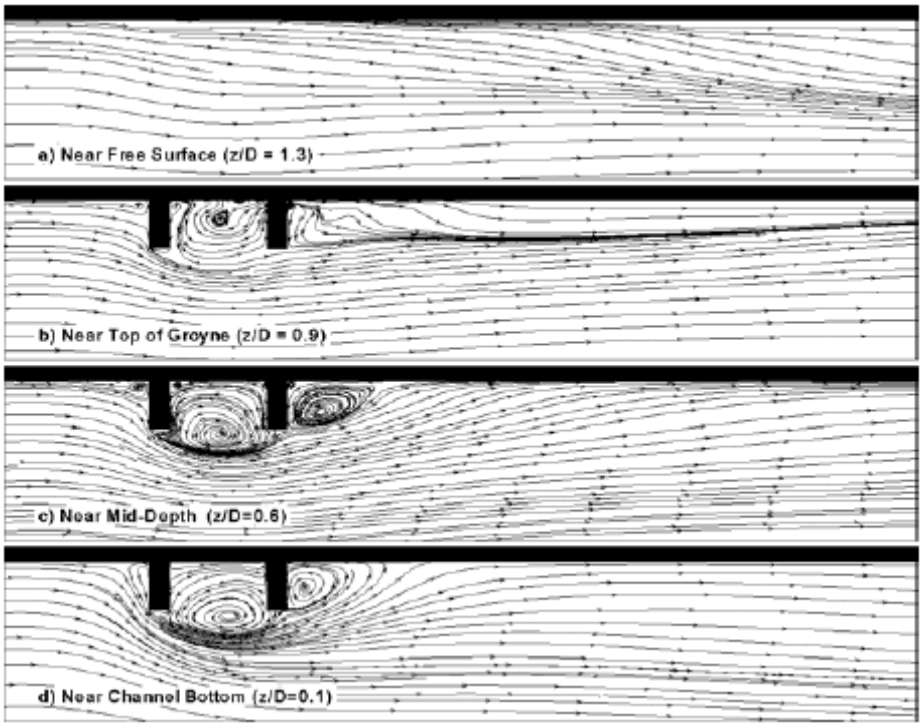


**Figure 12.** Planimetric view of streamlines around structures from McCoy et al. (2007)

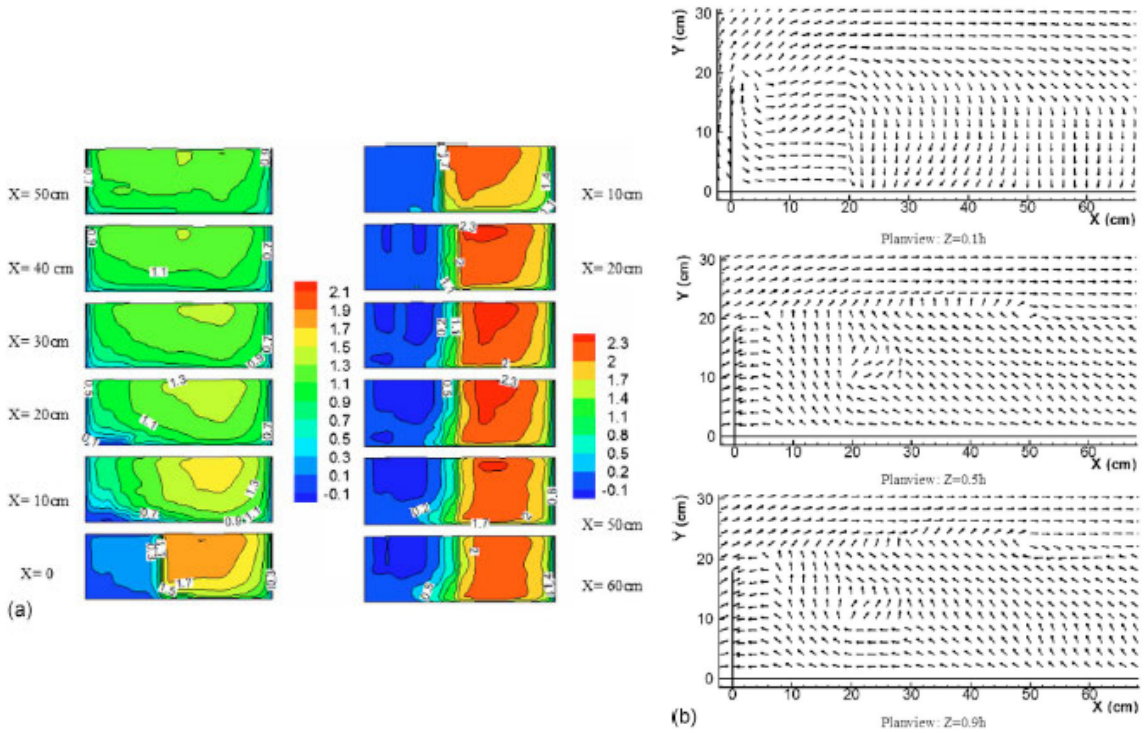


**Figure 13.** Spur-dike velocity cross-sectional contours and recirculation zones (Duan, 2009)

Jamieson et al. (2013) installed vanes constructed from scaled rip-rap in a mobile-bed, trapezoidal laboratory channel bend and collected bathymetry and velocity data. Vanes were imbricated in series and constructed according to USDA (2005) guidelines. Planimetric interpolations of velocity measurements are depicted in Figure 14 which illustrate an effective conveyance shift from the outer-bank at baseline conditions (TR1, TR3) to the channel center with the installed structure configurations (TR5, TR10). Authors noted scour formation downstream of the vane crests which was attributed to the combination of plunging crest flow and local acceleration around the vane tip. When vanes were constructed with the bank key-in point below the water-surface elevation, increased outer-bank erosion was noted, similar to bank key-in flow acceleration noted for bendway weirs (McCoy et al. 2007, Abad et al., 2008).

Disruption of the secondary current was noted to various degrees for the installed vane configurations and was attributed to the strength of plunging flow over the vane crest.

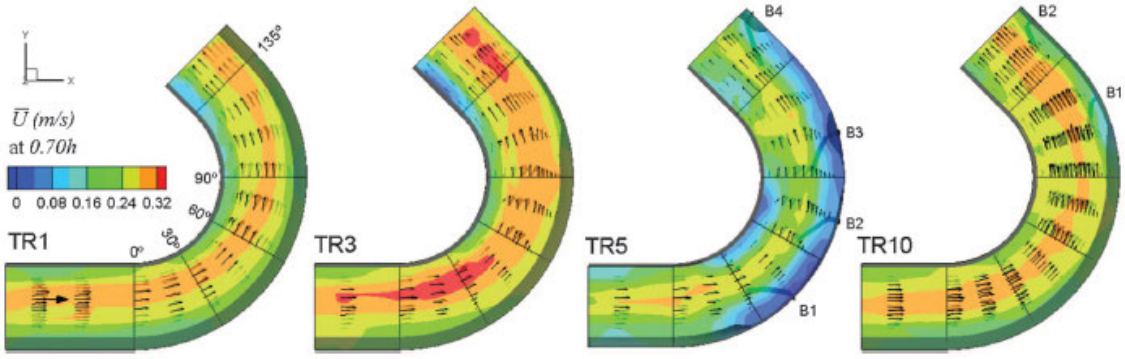


**Figure 14.** Streamwise velocity contours before and after vane installation (Jamieson et al., 2013)

Bhuiyan et al. (2010) investigated structures resembling vanes installed in a mobile-bed, rectangular laboratory flume. Structures were thin, triangular shaped plywood templates attached at the bank and extended downwards to the channel bed at crest angles much greater than maximum crest slopes recommended in design guidelines of Table 3. Flow velocity, bathymetry, and topographic scour data were collected and displayed. Reported hydraulic effects of vanes included a reduction of velocity at the bend apex of 60% compared to baseline condition and a general conveyance shift from the outer-bank to channel center due to structure installation. Velocity data coupled with observed scour patterns around the structures indicated zones of high velocity and boundary shear stress at the structure tip and crest end. Figure 15 depicts cross-sectional velocity magnitude contours and velocity vectors associated with flow passing one laboratory vane. Secondary currents were reported to be shifted towards the inner bank and counter-rotating cells were observed due to plunging flow over the vane crest. Counter-rotating cells were determined to be in roughly the same location as those observed in baseline channel-bend flows by Blanckaert and Graf (2001), and the authors indicate the rotating cell may be strengthened by the vanes.

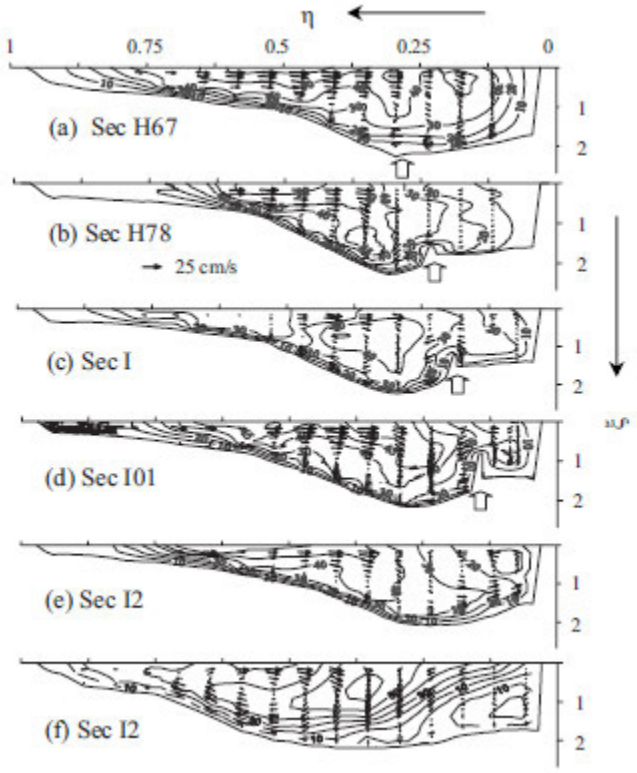


**Figure 15.** Cross-sectional velocity magnitudes and circulation moving past a vane structure; flow encounters vane at arrow moving downwards in cross-section (Bhuiyan et al., 2010)

Matsuura and Townsend (2004) performed a laboratory study on vanes and documented sedimentation effects due to configuration installations. They concluded that the structures effectively shifted the thalweg, and main conveyance, away from the outer-bank. Thalweg scour depth was found to increase for structures with planimetric angles that were larger and blocked more of the outer-bank conveyance. Vane crest height was found to be directly related to thalweg relocation away from the outer-bank.

Laboratory experiments were performed on a single vane and a two-vane configuration in a straight, rectangular mobile-bed flume by Fox et al. (2005). Vanes were scaled from field data in the Pacific Northwest region of the United States, had a projected length of approximately 1/3 of the channel top-width, and were angled at 50° upstream to the bankline tangent. Results of the testing and analyses indicated velocity increases in the main channel of 1.2 times the mean

channel baseline velocity, and decreases at the outer-bank to 0.24 of the baseline velocity. A zone of high Reynolds stress was noted at the area above the structure nose that was five times greater than the bed shear stress.

Lyn and Cunningham (2010) evaluated three physically modeled bendway-weir configurations in a mobile bed channel bend at variable boundary conditions. Three baseline conditions were determined from equilibrium bend scour formed in an initially trapezoidal channel bend. Structures were placed at 75° angled upstream, were set with full structure length of one-quarter initial top width, and with three crest heights. A total of six independent combinations of flow depth, discharge, and structure crest height were tested. One bendway-weir configuration was designed with the crest height set at approach flow depth, such that the structures behaved like spur-dikes. Design specifications were concordant with recommendations from HEC-23 (Lagasse et al., 2009) and were placed at a ratio of 3.7 weir lengths. Velocity and bathymetric data were collected throughout the structure configurations at sufficient resolution to interpolate planimetric trends throughout the full flow area. A planimetric view of interpolated velocity data collected within the bendway-weir field with crest heights at 50% approach flow depth is presented in Figure 16. Conveyance was noted to be shifted to the channel center and typically reduced within the structure field apart from a large velocity zone near the bend apex. Authors noted significant display errors as a result of interpolation from planimetrically sparse cross-sectional data to the extents of the waterline. Substantial erosion was observed at the outer-bank key-in above the bendway-weir crest, and it was determined that the current HEC-23 guidelines are not fully appropriate for bendway-weir structure design since such erosion is not addressed.

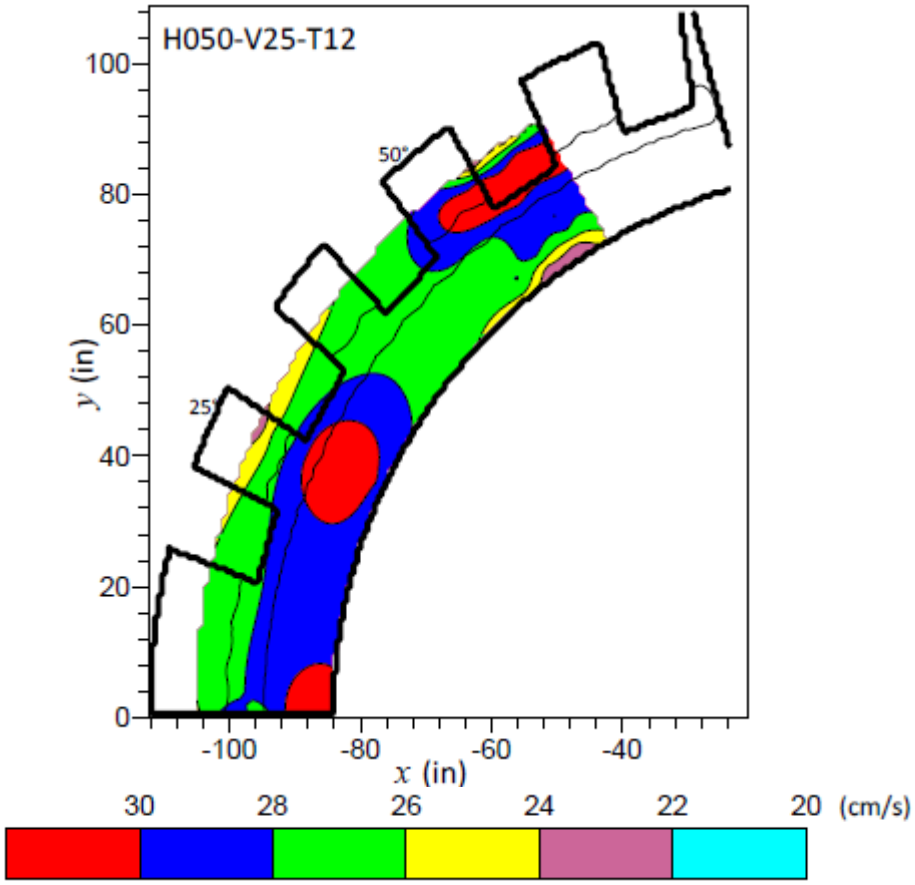


**Figure 16.** Planimetric velocities within bendway-weir field from Lyn and Cunningham (2010)

Bui (2011) investigated a field installation of bendway weirs near Bernalillo, NM on the Middle Rio Grande River. Figure 17 presents the site before and after bendway-weir installation and Figure 18 is a structure schematic of the field installation. The geometry of the weirs and the channel properties were determined. Weir crests extended 25 ft into the channel angled 70° upstream to the flow direction. Structures were spaced at 75 ft intervals measured between the centerline of each weir and had cross-sectional areas of 87.5 ft². Velocity data analyzed were collected at three different discharges at different dates within the structure field and the channel. General observed hydraulic trends indicated velocities within the structure field were reduced and the bulk conveyance was shifted into the center of the channel.


**Figure 17.** Bernalillo bendway-weir installation site; before and after, Google (2007)

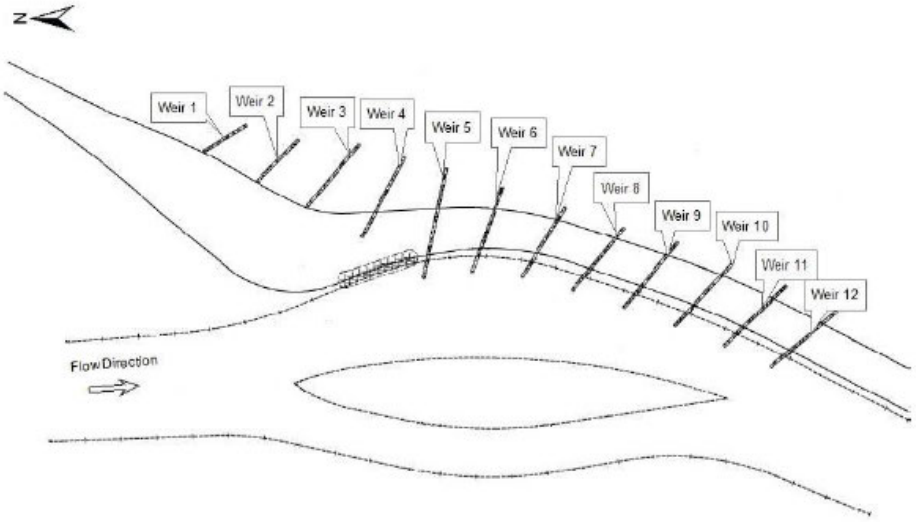


**Figure 18.** Bernalillo bendway-weir installation schematic (BIO-WEST, 2006)

Thornton et al. (2011) evaluated four spur-dike configurations in a physical model emulating the natural pool-riffle and planimetric characteristics of two channel bends in the Middle Rio Grande River. Structures were designed according to specified area ratios and met design requirements as specified in Table 2 with the exception of the planimetric angle. Spur-dikes evaluated were either installed perpendicularly to the bankline tangent or angled upstream, as opposed to the recommended downstream angle orientation. Two geometric structure

configurations were evaluated in two channel bends. The first configuration was set perpendicularly to the bankline tangent, was designed at 10.75% flow blockage at baseline conditions, and had a spacing of 5.9 times the crest length. The second configuration was set at 60° angled upstream to the flow direction, was designed at 19.4% flow blockage at baseline conditions, and had a spacing of 3.4 crest lengths. Velocity, shear stress, and water-surface elevation data were collected throughout the flow field. The first configuration was found to not reduce velocity at the outer-bank compared to baseline conditions, yet the second configuration did exhibit reduced erosive potential. Results indicated that decreased structure spacing and increased flow area blockage are directly related to outer-bank erosive force reduction.

Scurlock et al. (2013a) investigated four bendway-weir configurations installed in the physical model constructed by Thornton et al. (2011). Velocity, shear stress, and water-surface elevation data were collected and interpolated in cross-section and planimetric views. Impermeable structures were designed according to the current design specifications as detailed in Table 1 and illustrated in Figure 19. Crest elevation was set at one-third of the baseline, bend-averaged hydraulic depth. Secondary current effects due to bendway-weir installation were noted to be significant, with commonly reversed flow circulation in the vicinity of the structures. These results coincide with those found from Jia et al. (2011). Conveyance was effectively shifted to the channel center, a region of high velocity was noted at the bankline key-in similarly to Lyn and Cunningham (2010), and localized acceleration was noted at the structure tip and over the crest. Hydraulics were noted to return to approximately normal channel-bend conditions at three to six times the projected weir length distance downstream of the configuration. Figure 20 illustrates normalized velocity magnitudes at 60% flow depth from the water-surface from Scurlock et al. (2013a).

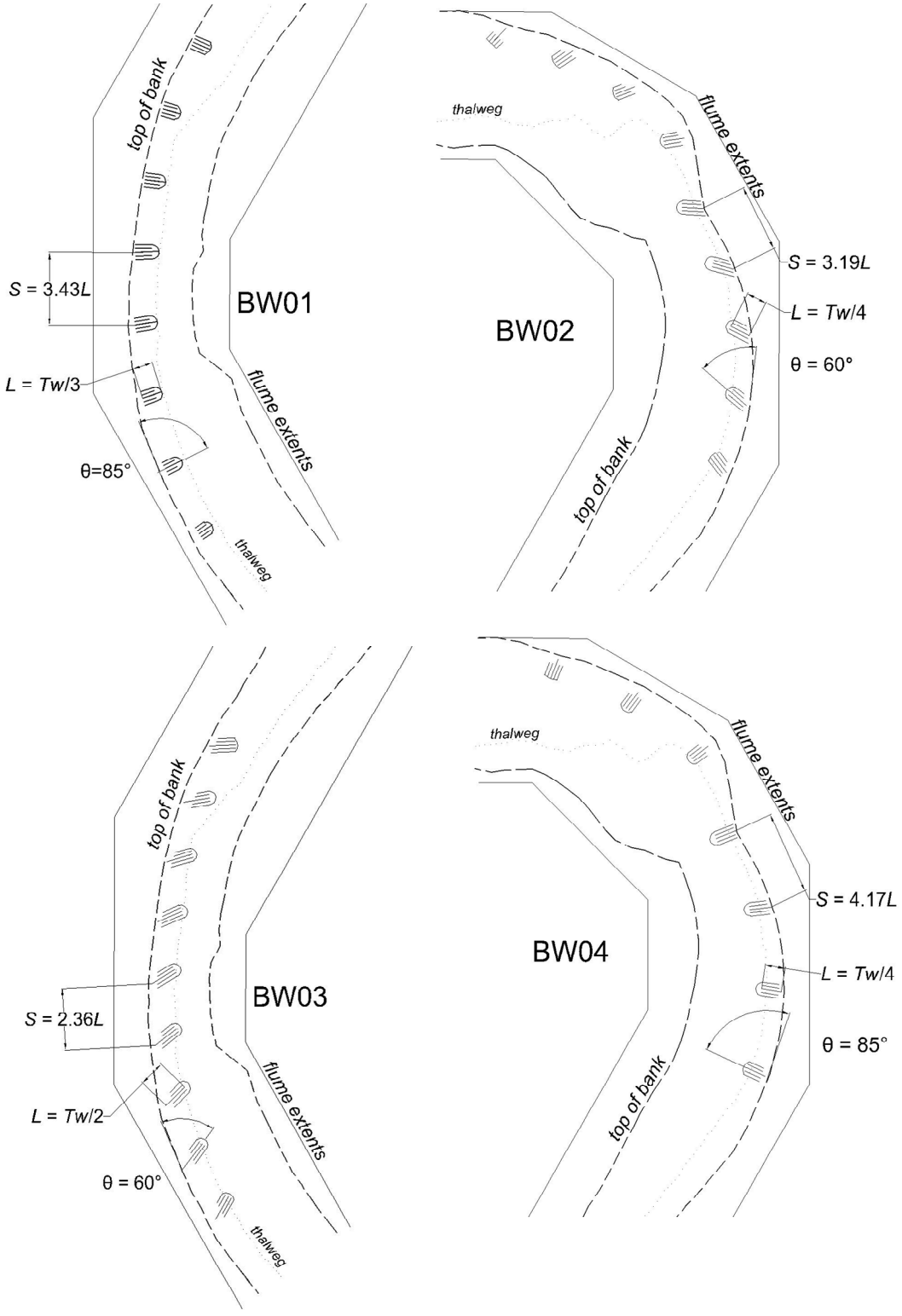


**Figure 19.** Bendway-weir configurations from Scurlock et al. (2013a)

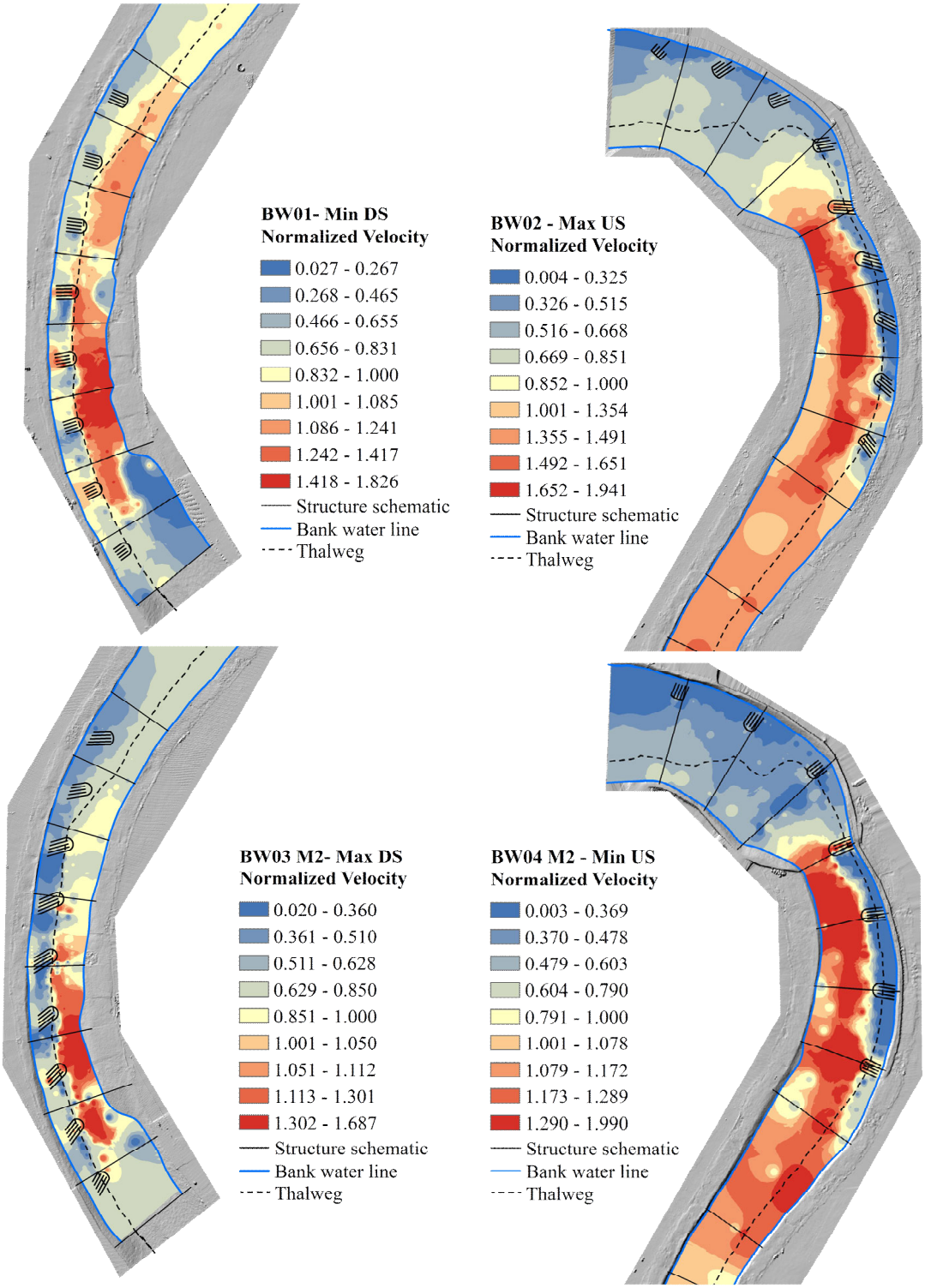


**Figure 20.** Normalized bendway-weir velocity plots from Scurlock et al. (2013a)

Scurlock et al. (2013b) investigated two bendway-weir configurations, one spur-dike, and one vane configuration in the same natural channel physical model as Thornton et al. (2011). Structures were designed and constructed according to the current recommended specifications from the literature and were impermeable. Spur-dike configurations were angled upstream, which is in contradiction to recommended design protocol. Vanes were angled upstream at a more moderate angle than recommended from the literature at 60°. Deviations from the recommendations of the design methods were performed for structure comparisons within the current research and to other studies. Figure 21 details a planimetric schematic of the structures installed. Comprehensive velocity, shear stress, and water-surface elevation data were collected and hydraulic distributions were analyzed. Figure 22 illustrates interpolated normalized velocity magnitude fields collected for the configurations. Consistent with other results from the literature, conveyance was noted to shift to the channel center off of the tips of the instream structure fields and was reduced in the outer-bank zone. Bendway-weirs exhibited an outer-bank zone of higher conveyance over the crest at the bankline key-in. Secondary currents were notably affected, Reynolds stress distributions were concentrated at the structure tips, and a balance between turbulent kinetic and mean kinetic energy was found throughout the flow field.

Results from the literature indicate a recurring set of hydraulic trends for instream structures which are pervasive throughout field, physical, and numerical studies. The primary focus of the structures, outer-bank erosion protection through conveyance diversion, was achieved in almost all instances. Secondary current effects, shear-stress distributions, erosion and sedimentation patterns, and localized velocity effects were documented for specific structures and individual configurations. Of the reported studies, minimal specific information

regarding expected state parameter effects due to structure geometry variability were developed or presented.

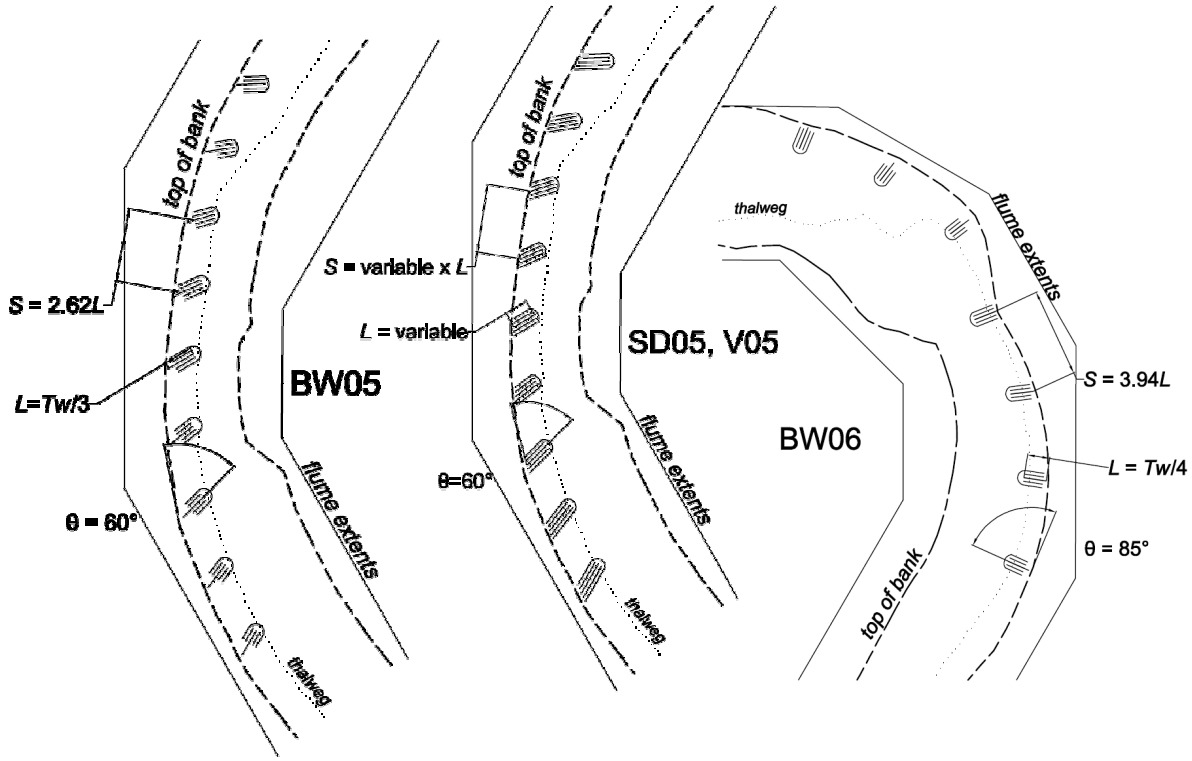


**Figure 21.** Instream structure schematics from Scurlock et al. (2013b)

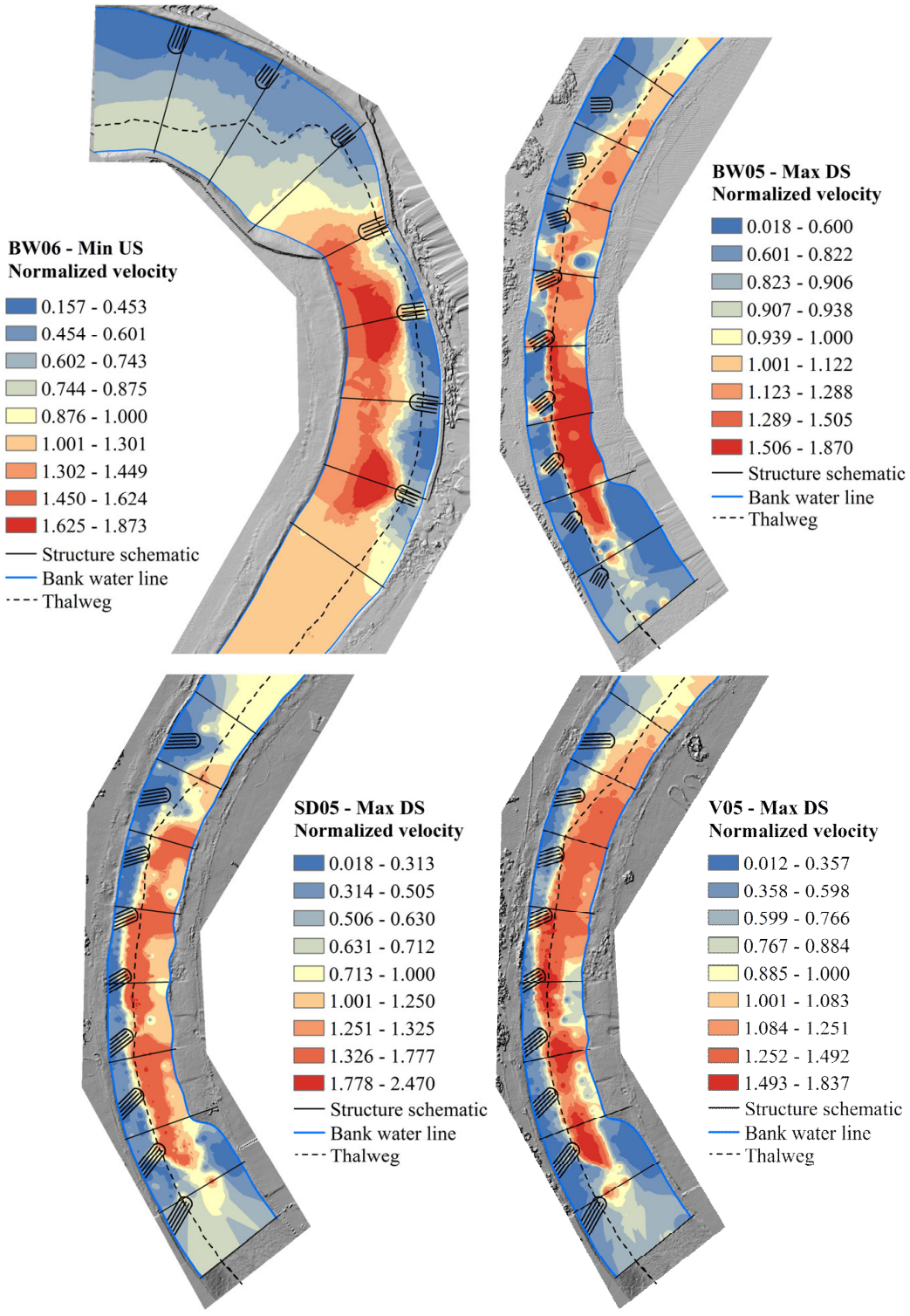


**Figure 22.** Normalized instream structure velocities from Scurlock et al. (2013b)

### 2.3.2. Hydraulic prediction models

The number of studies addressing hydraulic effects from parameter variability for instream structure design purposes is small considering the quantity of research found from the literature. A series of studies detailing design methodologies were conducted at CSU under contract from Reclamation. Heintz (2002), Darrow (2004), and Schimdt (2005) report physical modeling and data analyses of a variety of transverse instream structure configurations installed in a two-bend, trapezoidal flume.

Focusing upon implementing transverse instream structure to meet the objectives of the Middle Rio Grande maintenance project, Reclamation contracted CSU to conduct a physical model to investigate structure-induced hydraulic conditions and to develop design criteria. A concrete, trapezoidal, 1:12 Froude-scaled physical model was constructed in 2001 at CSU consisting of two representative channel bends of the Middle Rio Grande placed in series and connected with a transition zone. Figure 23 presents a schematic of the planform geometry, and Figure 24 portrays a picture of the constructed prismatic model. Heintz (2002) details the rationale behind the selection of bend geometries and construction methods which are elaborated upon in the physical modeling section of this report.

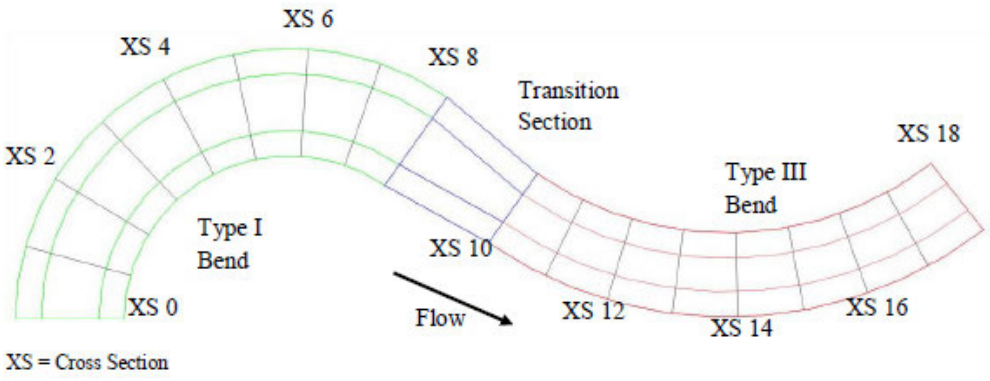


**Figure 23.** Trapezoidal model plan view

**Figure 24.** Constructed trapezoidal channel model

Heintz (2002) installed and collected data on spur-dikes with various geometric configurations. Certain flow rates tested for the constructed spur-dikes reported by Heintz (2002) overtopped the designed crest elevation, producing hydraulic conditions resembling bendway weirs. Spur-dikes with overtopping flow evaluated by Heintz (2002) were set with crest elevations not contained within recommended bendway-weir design guidelines. The combination of overtopping flow hydraulics with crest elevations exceeding design guidelines led to the designation of such structures as submerged spur-dikes. Assuming that the structures were designed as bendway-weirs for the submerging flows tested, submerged structures were set approximately 40% higher than the limiting bendway-weir design criteria of one-half bankfull hydraulic flow depth (Lagasse et al., 2009). Flow depth, velocity, and boundary shear-stress data were collected throughout the physical model.

Darrow (2004) expanded the work conducted by Heintz to investigate effects of spacing ratios between the structures. Schmidt (2005) reconfigured the spur-dikes and submerged spur-dikes established by Heintz (2002) to include sloping structure crests. Structures evaluated by Schmidt (2005) did not follow typical design protocol for vanes; the tie-in elevation was constructed above any water-surface elevation evaluated. Traditional vanes, with crests that intersect the bank at the design water-surface elevation, remain classified as vanes when the flow elevation drops below the design flow elevation. While not tied into the bank at the design discharge, constructed lab structures by Schmidt (2005) function as vanes at flow elevations lower than those associated with the design discharge. Figure 25 shows a cross-section schematic of the spur-dike, submerged spur-dike, and vane structures evaluated in the CSU trapezoidal model.

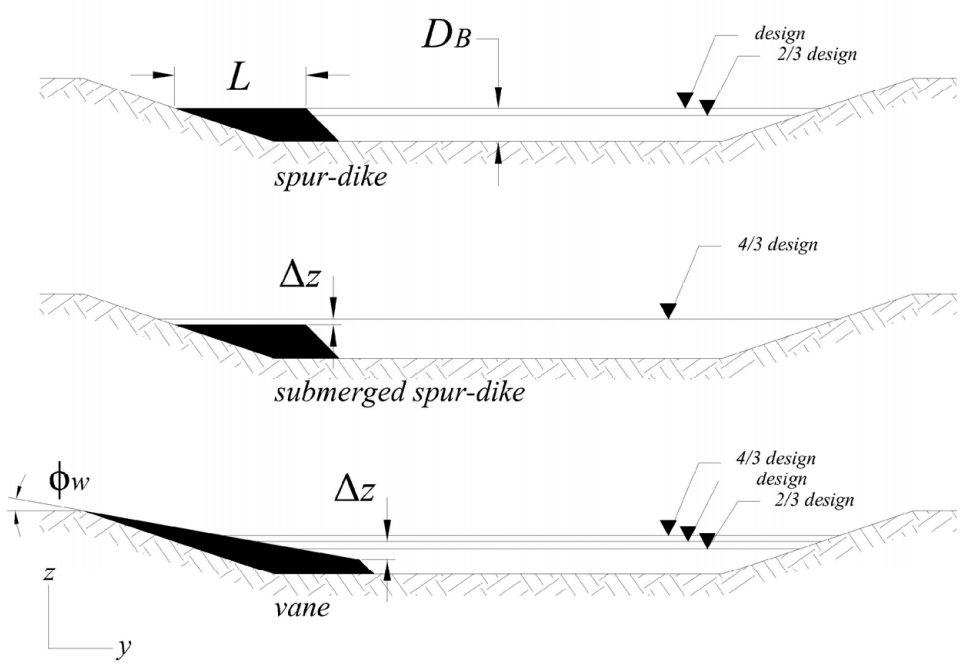


**Figure 25.** Profile view schematic of evaluated structures in trapezoidal model

In addition to an expansive database for instream structure examination, researchers at CSU contributed the sets of hydraulic quantification models representing the first step in relating structure geometry to induced hydraulic fields. Originally defined by Heintz (2002), and then utilized by Darrow (2004) and Schmidt (2005), the concept of the maximum velocity ratio, *MVR*, observed within a structure field as compared to baseline conditions was quantified and predictive methodologies were developed in each study. The concept of *MVR* as utilized by Heintz (2002), Darrow (2004), and Schmidt (2005) is expressed as Equation 1.

$$MVR = \frac{MV_j}{MV_{c-base}} \tag{1}$$

where:

$MV_j$ = maximum velocity measured at channel location $j$, $j$ = (outer-bank, centerline, and inner-bank) [L]; and

$MV_{c\text{-}base}$ = maximum velocity measured at the channel centerline at baseline condition [L].

Each of these three studies implementing *MVR* developed unique predictive methodologies. Heintz (2002) developed offsets for *MVR* based on 95% confidence intervals of the data distributions. Darrow (2004) and Schmidt (2005) identified influential parameters on *MVR*, formed dimensionless groupings from those variables, and performed statistical sensitivity analysis to extract insignificant parameters from the final equation format. Prediction models were formed from significant parameters using regression analyses to determine weighting coefficients. The prediction model of Darrow (2004) described laboratory data with coefficient of determination ($R^2$) values of 0.577, 0.591, and 0.540 for the outer-bank velocity ratio ($MVR_O$), the centerline velocity ratio ($MVR_C$), and the inner-bank velocity ratio ($MVR_I$), respectively.

Schmidt (2005) described laboratory data with coefficients of determination of 0.640, 0.658, and 0.711 for $MVR_O$, $MVR_C$, and $MVR_I$, respectively.

Examination of the most current prediction methods developed by Schmidt (2005) reveals problematic areas in the theory used for development and potential applicability for design. Relationships for the evaluation of *MVR* at the outer-bank, centerline, and inner-bank are presented in Equation 2, Equation 3, and Equation 4, respectively.

$$MVR_O = e^{-2.981} \frac{\left(L_{ARC}\right)^{0.632}\left(L_{CW-PROJ}\right)^{2.768}}{\left(L_{W-PROJj}\right)^{3.40}\left(\sin\phi+1\right)^{1.961}}\left(\frac{y}{h_{W,TOE}}\right)^{0.246}\left(\frac{A}{A_W}\right)^{0.891} \quad (2)$$

$$MVR_C = e^{-1.10} \frac{\left(T_W\right)^{0.895}\left(h_{W,TOE}\right)^{0.037}}{\left(L_{cw,proj}\right)^{0.526}\left(y\right)^{0.406}}\left(\frac{L_{W-PROJj}}{b}\right)^{0.855} \quad (3)$$

$$MVR_I = e^{-2.34} \frac{\left(T_W\right)^{2.194}\left(L_{CW-PROJ}\right)^{0.887}\left(h_w\right)^{0.0345}\left(\sin\theta\right)^{0.127}}{\left(y\right)^{0.8335}\left(b\right)^{1.423}\left(L_{W-PROJj}\right)^{0.859}\left(\sin\phi+1\right)^{0.958}} \quad (4)$$

where:

$L_{ARC}$ = arc length between weirs along design waterline [L];

$L_{CW\text{-}PROJ}$ = projected length of weir crest measured from the baseline water surface along the horizontal plane to a cross section perpendicular to the flow [L];

$L_{W\text{-}PROJ}$ = projected length of weir measured from the baseline water surface along the horizontal plane to a cross section perpendicular to the flow [L];

$h_W$ = height of structure above bed datum measured at the end of the crest [L];

$h_{W,TOE}$ = height of structure above bed datum measured at the channel toe [L];

$A$ = cross sectional flow area [$L^2$];

$A_W$ = projected weir area blocking the flow [$L^2$];

$y$ = flow depth at baseline [L];

$b$ = bottom width of channel [L];

$T_W$ = channel top width [L];

$\phi$ = crest slope angle measured down from horizontal; and

$\theta$ = planform angle of structure crest.

Equation 2, Equation 3, and Equation 4 describe hydraulics within the physical model well, with adjusted $R^2$ values exceeding 0.64. However, application of the models to natural channel topography as a field design tool requires significant assumptions.

Data used to develop the regression expressions were obtained from a prismatic channel, and certain terms included by Schmidt (2005) do not transfer well to situations of natural channel design. The height of the weir at the toe of the channel and the channel bottom width are parameters included in the predictive equations which are challenging for a designer to determine without subjectivity. The methodologies further implement two weir length parameters which counteract each other in the equations, yet are fundamentally related. Increased structure crest length generally increases the length of overall structure. Necessary assumptions for the terms in the absence of direct measurements may cause improper variable response.

Quantitative hydraulic models were developed to describe hydraulics in a physical model at CSU. The current predictive methodologies from Schmidt (2005) were tailored specifically to the prismatic channel dataset and were not created specifically for application in field design in natural channels. Parameters were incorporated which are specific to the examined physical model only; estimation in a natural bathymetry would be challenging and subjective. The

current quantification methodologies are appropriate for describing observed hydraulics within the physical model dataset, but a need for design tools for field applications is still needed.

## 2.4. Literature review summary

A review of the literature to date indicated that designers are implementing transverse instream structures in river restoration projects with growing frequency, yet with inadequate design guidelines. Current guidelines are largely anecdotal and focus on geometric parameter ranges for specific structure types. Information regarding specific hydraulic effects of parameter variation within the ranges is sparse. The majority of research to date performed on transverse structures focused on local hydraulics around a single structure, the velocity field for a single configuration, or the application of numerical models to emulate flow fields.

Data collection and flow analyses of transverse instream structures from the literature illuminated a recurring set of flow characteristics. The bulk flow conveyance is shifted towards the channel-center, acceleration occurs around the structure tip, and for submerged crests acceleration is observed along the outer-bank at the bank key-in and at the structure tip. Recirculation zones occur behind each structure and eddies may establish between the structures. The secondary current is affected by the structure presence to varying intensity, with the rotational direction potentially reversed, and has been linked to the degree of crest overtopping. While valuable for full realization of the flow fields and hydraulic effects associated with transverse instream structures, this information does not provide comprehensive design guidance for outer-bank erosion control or conveyance increase. Effects on the hydraulics due to variability in geometric design parameters were identified throughout the literature as important for structure design; however, limited studies were conducted which focused specifically on structure geometry optimization for desired hydraulics. Three studies were found which provide

a substantial transverse instream structure dataset and a series of methods for prediction of the maximum velocities within the channel as functions of configuration geometry.

Design methods developed by Heintz (2002), Darrow (2004), and Schmidt (2005) represent a significant step for efficient and effective installation of instream structure configurations in the field. Quantification models developed from the research related observed velocity trends to geometric parameters of the structure configurations. The current iteration of design guidelines focused on maximum velocity design conditions and incorporated independent parameters which are complicated to evaluate in a natural channel. As such, there is a need for redevelopment of the quantification models to describe induced instream structure hydraulics with formulas that may be readily calculated using natural channel field data.

# 3. Physical modeling and analysis database

Development, accuracy, and applicability of numerical prediction methodologies is dependent upon the size and quality of the available database. Physical modeling research conducted by Heintz (2002), Darrow (2004), and Schmidt (2005) varied transverse instream structure geometries across a wide array of values and was selected to serve as the conglomerate database for methodology development. Other studies from the literature were found not to provide the quantity of information required to derive statistically significant methodologies; however, reported data substantiate validation of developed models. Physical model facilities, instrumentation, data collection, and reported data from the studies conducted by Heintz (2002), Darrow (2004), and Schmidt (2005) are detailed. A consolidated summary for the full testing program in the trapezoidal physical model is provided. Individual study reports contain further information about the physical modeling process conducted under each investigator.

## 3.1. Physical model description

A large physical model was constructed in the Hydromachinery Laboratory at the Engineering Research Center, Colorado State University. Model design was conducted to fulfill objectives of Reclamation to research hydraulic trend quantification and design procedure development for transverse instream structure installations in the Middle Rio Grande River. Measures were taken to ensure that the physical model was the most effective representation of the problematic reaches of the Middle Rio Grande while conforming to flume and facility limitations. Two prismatic, trapezoidal bends were constructed with a transition section in between. Model surfaces was capped with concrete to form a rigid surface. Figure 23 presented a schematic of the flume and Figure 24 presented a picture of the completed model.

The two modeled channel bends were chosen as representations of the full set of channels within the focus reach of the Middle Rio Grande. Channel bend $R_C/T_W$ was quantified through analysis of aerial photography and demarcations between different classifications of the ratio were made. Figure 26 illustrates $R_C$ plotted against $T_W$ and three zones of channel classification identified. In order to span the full range of the surveyed channel bends, a Type I channel curve with a small radius of curvature to top-width ratio and a Type III channel with a larger ratio were selected. Table 4 details the planimetric geometry parameters chosen for the model bends.

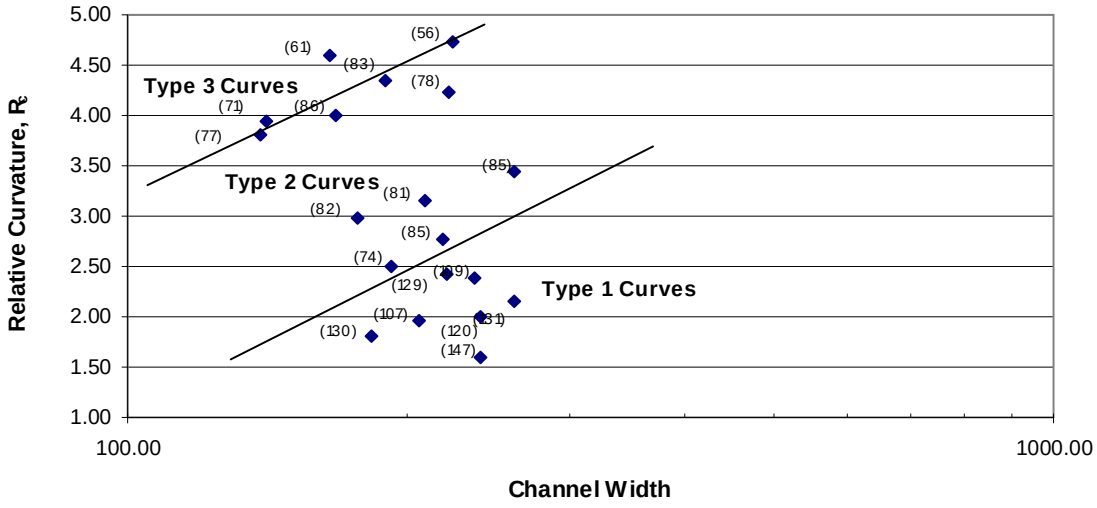


**Figure 26.** Planimetric geometries of channel bends from the Middle Rio Grande study reach (Heintz, 2002)

**Table 4.** Type-I and Type-III trapezoidal model bend characteristics

| Type | Top Width | Radius of Curvature | Bend Angle | Relative Curvature | Channel Length |
|---|---|---|---|---|---|
| | ft (m) | ft (m) | (degrees) | $R_C/T_W$ | ft (m) |
| I | 19.2 (5.9) | 38.75 (11.81) | 125 | 2.02 | 84.5 (25.8) |
| III | 15 (4.6) | 65.83 (20.06) | 73 | 4.39 | 83.5 (25.5) |

Prototype geometries were scaled according to undistorted 1:12 Froude similarity. Modeled bends were constructed at a side slope at one-vertical (V) to three horizontal (H) units and were set with a constant bed gradient of 0.000863 V:H. The Type I channel bend was

constructed in the upstream model section and the Type III channel bend was constructed in the downstream section. The transition between the structures occurred at a 10:1 contraction ratio, connecting the 19.2 ft upstream width and the 15 ft downstream width over a 42 ft straight section. The model was constructed from cross-sectional plywood templates with steel flashing at the gradient breaks in topography and filled with sand material. A brushed concrete surface was placed between the plywood templates. Prototype roughness characteristics were determined to have a Manning *n* value of 0.027. Roughness was scaled and the concrete material installed on the model bed surface had an appropriate *n* of 0.018.

Three discharges were evaluated within the model for the transverse instream structures which corresponded to one-third increments of the bankfull, design discharge. Design, prototype discharge was determined at 6,000 $ft^3/s$, which scaled to 12 $ft^3/s$ within the model. Other evaluated model discharges were two-third design at 8 $ft^3/s$ and at three-half design at 16 $ft^3/s$. Flows were delivered from the model sump to the headbox in a recirculating system. Tailwater conditions were established at normal depth conditions for all flow rates within the model. Once a flow condition had been established, collection of data throughout the model ensued. Specific instrumentation was used to establish flow rate, water-surface elevation, flow depth, velocity, and boundary shear stress.

## 3.2. Instrumentation

The key parameters for measurement within the model were the bed topography, volumetric flow rate, water-surface elevation, flow depth, mean-flow velocity fields, and boundary shear-stress distributions. High-quality, precise instrumentation was employed to collect the required data to achieve project goals and objectives.

### 3.2.1. Volumetric flow rate

Flow delivered from the sump to the headbox was measured through connecting 12-inch diameter pipes using two George Fischer SIGNET 2250 Insertion Magmeters®. The precision of each instrument was ±2% of the measured flow rate. Control of flow was maintained in each line by a butterfly valve mounted on a sump bypass line, and an additional downstream butterfly valve to create pump back-pressure. An alternate 12-inch line was used for non-recirculating flows which were monitored by a Brooks Mag 7000 flow meter which was precise to ±0.5%. Flow rates were monitored with Newport Infinity® digital readout boxes and cumulative observed flow in the model was maintained to within ±1% of the desired testing condition. Heintz (2002) and Schmidt (2005) utilized recirculating flows during experiments while Darrow (2004) used non-recirculating flow.

### 3.2.2. Water-surface elevation

Water-surface elevation within the model was controlled with the use of downstream stop-logs which were staggered vertically to allow through-flow and lessen stagnant velocity effects. For any structure configuration or for baseline conditions, a combination of discharge and stop-log configuration would result in a unique water-surface elevation profile in the model. The water-surface elevation for each discharge, tailwater, and structure configuration was measured with a point gage of ±0.001 ft precision.

### 3.2.3. Flow depth

A data-collection cart was installed on rails on top of the flume walls, and spanned the width of the physical model. The cart was capable of travelling along the thalweg axis and

allowed for transverse and vertical positioning of instrumentation. Local flow-depth readings at each data-collection location were ascertained with the use of a point gage of ±0.001 ft precision as the difference between the measured water-surface elevation and bed surface.

### 3.2.4. Velocity

Velocity data were collected at 60% flow depth measured from the water-surface elevation as an approximation of the depth-average velocity profile. Mean-flow and turbulent velocity characteristics were obtained using an acoustic Doppler velocimeters (ADV). A SonTek® ADV of ±1% measured accuracy was utilized (SonTek, 1999). ADV data collection has been used extensively in laboratory and field applications, and further details may be found in Voulgaris and Trowbridge (1998), Wahl (2000), McLelland and Nicholas (2000), and Strom and Papanicolau (2007). ADV instruments operate at a high frequency ($\geq$ 25 Hz) and allow for the determination of mean and fluctuating velocity components over the course of a sampled time period. A minimum of 1500 velocity data were obtained at each data-collection location. Data were processed using WinADV as detailed by Wahl (2000), and data used for instream-structure analyses typically had percentage-good scores greater than 70%, correlation values greater than 70, and signal-to-noise values greater than 15.

### 3.2.5. Boundary shear stress

Boundary shear stress was quantified through differential pressure measurements collected with a modified Pitot-static tube known as a Preston tube, details of which are described by Head and Rechenberg (1962). The installed Preston tube was configured to average differential pressure over a one-minute duration using a Rosemount 3051 Pressure Transmitter of ±0.04% measured accuracy. Calibration of the Preston-tube pressure differential

to calculated one-dimensional boundary shear stress over native-topography bed material was conducted by Heintz (2002), and the relationship of Equation 5 was generated for shear-stress estimation for the trapezoidal model roughness.

$$\tau_b = 1.739 dP \tag{5}$$

where:

$\tau_b$ = boundary shear stress [lb/ft$^2$]; and

$dP$ = differential pressure [inches].

## 3.3. Instream-structure configurations

The three studies conducted in the trapezoidal model evaluated different instream structure configurations which may be described as spur-dikes, submerged spur-dikes, and vanes, as presented in Figure 25. The initial study of Heintz (2002) varied structure spacing throughout the bends, keeping the structure width, height, angle, and length constant. Darrow (2004) expanded the dataset to include variable length, angle, and additional spacing. Schmidt (2005) investigated different planimetric angles than Darrow (2004) and included structures with crest slopes of 10 degrees. Cumulatively, a total of 130 individual tests on 22 structure configurations were performed. Appendix A1 details the instream structure tests and associated geometric parameters for the different studies.

Constructed configurations spanned the ranges of design recommendations for spur-dikes and vanes, provided by Table 2 and Table 3, respectively, with some exceptions. Figure 48 in

Appendix A1 illustrates the ranges of spacing, length, and planimetric angle tested in the laboratory compared to design recommendations. Spur-dikes were angled upstream to the flow direction at 60º to 90º in the physical model as opposed to the recommended downstream angles of 90º to 150º from Table 2. Length and spacing generally encompassed and exceeded design recommendations. Vane angles did not coincide with design guidelines, with evaluated values of 60º to 90º instead of the 20º to 30º recommendations from Table 3. Spacing was also outside of the design recommendations; however, structure length encompassed and exceeded values from Table 3.

For all experiments, structures were constructed with plywood templates cut and secured to the bed topography which prevented any flow passage through the structure. Structures were constructed with securely placed angular stone ranging from approximately 0.25 ft to 0.50 ft along the intermediate axis. Structure top width was not determined as an influential parameter in the performed research, and the crest width was uniformly established at one-foot which allowed for adequate passage for construction equipment at prototype. Structure tips were angled at 1V:1H and was rounded to meet with the sides of the structures which were angled to achieve a bottom width of 4 ft. Figure 27 depicts an installed structure, constructed during testing by Darrow (2004), with plywood template and rock properties illustrated. Crest height was established at 0.77 ft and 0.78 ft in the Type I and Type III bend, respectively, for spur-dike structures which corresponded to design discharge flow depth. Vanes constructed by Schmidt (2005) varied the crest height along the crest axis and tied into the bank above any water-surface elevation evaluated. Specific data locations were ascribed for the collection and analysis of induced hydraulic trends within the channel for all structure geometries and configuration layouts.

**Figure 27.** Constructed instream structure in trapezoidal physical model

## 3.4. Data-collection locations

Flow depth, velocity, and boundary-shear stress data were collected across a planimetric distribution of data-collections for each configuration. Heintz (2002) established the initial planimetric data-collection location distribution as illustrated in Figure 28. Data-collection locations were allocated to cross sections, the outer-bank, the inner-bank, and to the structure tip. Three points were distributed across the cross sections with one point at the channel center, a point at the outer-bank channel toe, and one point at the inner-bank channel toe. Outer-bank points were distributed along the channel toe one-foot upstream and downstream of each structure and at the halfway along the arc between the crest centerline. A tip point was located one-foot from the structure tip, and inner-bank points were located along the axis of the radius of curvature and structure key-in at the inner-bank toe. From analysis and observations of the flow patterns within the structure fields, Heintz (2002) indicated that significant circulation cells may

exist between the structures requiring increased data-collection location density to resolve hydraulic characteristics.

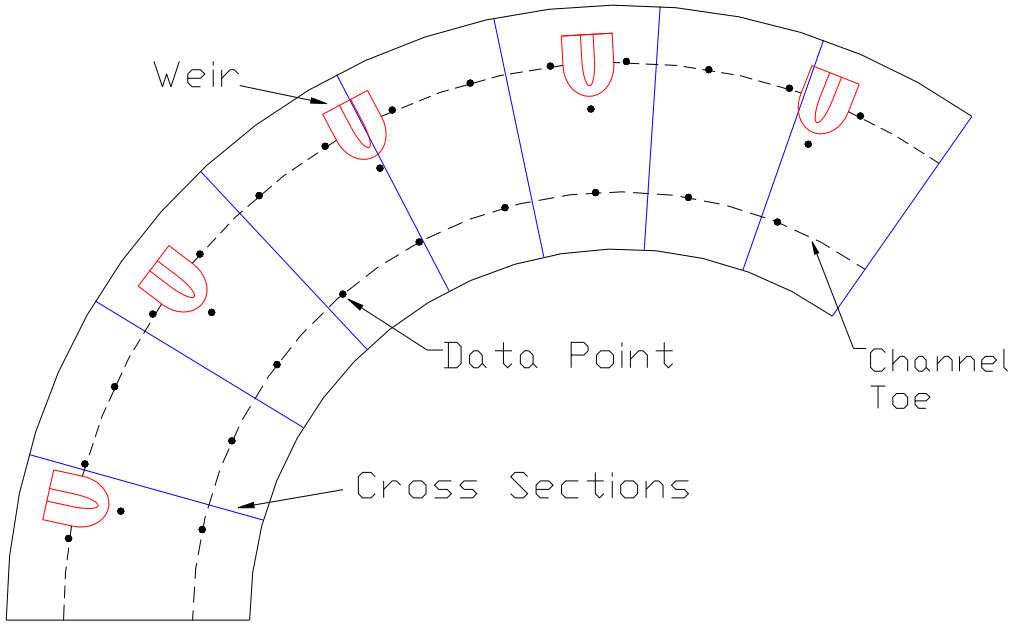


**Figure 28.** Structure data points from Heintz (2002)

Following recommendations from Heintz (2002) for increased mapping of recirculation between the structures, Darrow (2004) and Schmidt (2005) incorporated eddy-mapping data-collection locations. Data resolution along the outside of the bank within the structure field was increased for tests W04 through W22 as displayed in Figure 29. Distributions of the eddy-mapping data were centered along cross sections set at 1/8, 3/8, 5/8, and 7/8 radial distance increments between the outer-bank key-in of each structure crest. Five points were spaced along each cross section including one point halfway up the bank, one-quarter up the bank, at the channel toe, and two points within the channel. For the Type I bend, the two channel points were located 0.5 ft and 1.5 ft into the channel and for the Type III bend, points were located at

0.3 ft and 0.9 ft into the channel. An example of data-collection locations for the eddy-mapping and structure points is provided in Figure 29. For all tests, flow depth was recorded, three-dimensional velocity was collected at 60% flow depth from the water-surface elevation, and boundary shear stress was measured.

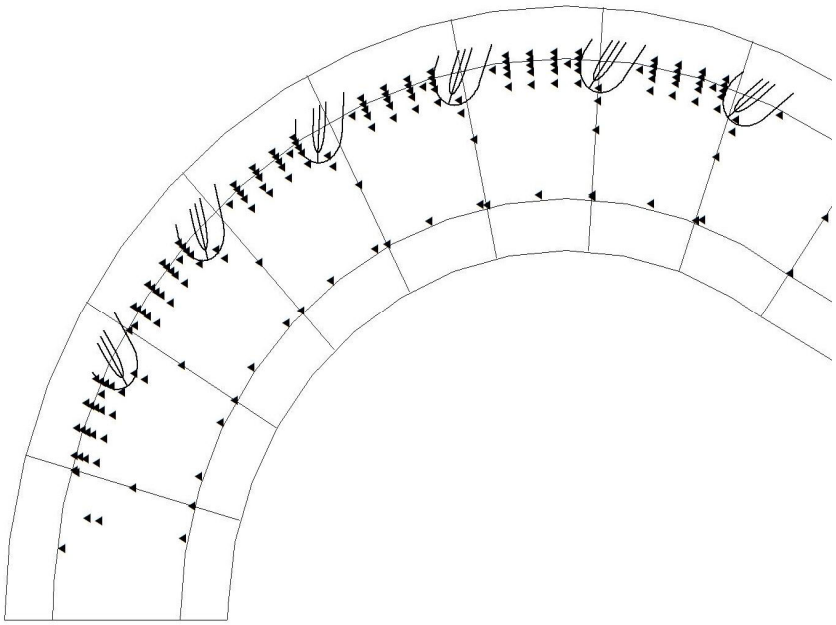

**Figure 29.** Full data-collection point distribution for structure field in upstream bend

## 3.5. Compiled research dataset

A comprehensive summary of available velocity, boundary shear stress, and flow depths recorded for all evaluated structure configurations is presented in Appendix A1. Velocity data and flow depth data were recorded with high quality for the entire dataset; however, the boundary shear-stress data were only available for select configurations. Configurations W01 to W11, as detailed in Appendix A1, received boundary shear-stress data collection for all tests. Configurations W12 through W22 did not have Preston tube responses for inclusion to the

research dataset. Therefore, the analysis dataset contains 130 independent data for velocity investigation and 66 independent data for boundary shear stress.

## 3.6. Physical modeling summary

A two-bend, trapezoidal physical model was constructed as a representation of a section of the Middle Rio Grande River at CSU. The model hosted 130 combinations of channel bend, instream structure geometry, and volumetric flow rate as reported by Heintz (2002), Darrow (2004), and Schmidt (2005). Flow depth, velocity, and boundary shear-stress data were collected throughout the structure configurations and a large dataset was compiled. The model construction, structure geometries, structure construction, model instrumentation, data collection locations, and collected data available for analyses were summarized. Collected data from the research is more plentiful than the cumulative information from the literature and serves well as a foundation for development of a concise and cogent methodology for the quantification of induced hydraulics from instream structure installation for field installation design.

# 4. Predictive model development

Data collected from the physical model at CSU were compiled, processed, and organized into a workable dataset for analysis of the hydraulic trends associated with transverse instream structures. This section provides the quantification of such hydraulic trends and the development of a predictive methodology for the design of instream structures. Planimetric velocity and boundary shear stress data are interpolated, displayed, and examined. Data are segmented into various channel regions through different approaches, including the outer-bank, centerline, and inner-bank. Maximum and average velocity and shear-stress values from each zone are quantified for all configurations. Data are normalized by the bend-averaged baseline conditions. Dimensionless parameter groupings are created which represent physically identifiable traits of the structure configurations and bend geometries. Groupings are organized into a mathematical expression and regression analyses are performed to create a set of equations which describe induced instream structure hydraulics. Equations are tailored for error reduction in parameter prediction and for ease of determination of parameters from natural field data. Variable responses are constrained during regression analyses to adhere to hydraulic intuition and minimization of error propagation.

## 4.1. Parameter normalization

Velocity and boundary shear-stress data were divided by normalization values for comparisons within the dataset and for extrapolation purposes. The velocity normalization condition was established as the bend-averaged baseline velocity as computed through continuity principles. This parameter is readily calculated from a one-dimensional, standard-step model or determined with adequate flow depth, discharge, and bathymetric data as Equation 6.

$$u_0 = \frac{Q}{k}\sum_{m=1}^{k} 1/A_m \quad (6)$$

where:

$u_0$ = bend-averaged normalization velocity [L/T];

$Q$ = volumetric flow rate [$L^3$/T];

$k$ = number of cross sections; and

$m$ = cross-sectional index.

The shear-stress normalization conditions were calculated as functions of the bend-averaged friction slope and hydraulic radius using Equation 7.

$$\tau_0 = \gamma \overline{R}\overline{S_F} \quad (7)$$

where:

$\tau_0$ = normalization boundary shear stress [F/$L^2$];

$\gamma$ = specific gravity of water [F/$L^3$];

$R$ = hydraulic radius [L]; and

$S_F$ = slope of total mechanical energy head in flow direction.

Each channel bend and volumetric flow rate had a unique normalization condition for velocity and shear stress. Flow area and hydraulic radius were calculated at each cross section using average flow depths reported from Heintz (2002). Bend-averaged friction slope was found using a best-fit line along each channel bend to the sum of the water-surface elevation and velocity head at each cross-section. Table 5, Table 6, and Table 7 provide data from Heintz

(2002) and the calculated velocity and energy at each model cross-section for the 8 cfs, 12 cfs, and 16 cfs conditions, respectively. Figure 30, Figure 31, and Figure 32 depict the energy head best-fit line for the 8 cfs, 12 cfs, and 16 cfs conditions, respectively. Table 8 summarizes the calculated normalization values for the velocity and boundary shear stress. Cross-sections 1 through 8, numbered upstream to downstream, were used for the upstream bend, and Cross-sections 10 through 18 were used for the downstream bend in normalization condition determination.

**Table 5.** Calculated normalization parameters for 8 cfs

| XS | *Distance Downstream* | *Bed Elevation* | *Measured Depth* | *Hydraulic Depth* | *Velocity* | *Energy* |
|---|---|---|---|---|---|---|
| - | ft | ft | ft | ft | ft/s | ft |
| 1 | 10.57 | 97.240 | 0.597 | 0.512 | 1.120 | 97.857 |
| 2 | 21.13 | 97.228 | 0.590 | 0.507 | 1.136 | 97.838 |
| 3 | 31.70 | 97.220 | 0.584 | 0.502 | 1.149 | 97.825 |
| 4 | 42.27 | 97.212 | 0.592 | 0.508 | 1.131 | 97.824 |
| 5 | 52.84 | 97.208 | 0.603 | 0.517 | 1.108 | 97.830 |
| 6 | 63.40 | 97.196 | 0.607 | 0.520 | 1.099 | 97.822 |
| 7 | 73.97 | 97.187 | 0.617 | 0.527 | 1.079 | 97.822 |
| 8 | 84.54 | 97.186 | 0.615 | 0.526 | 1.083 | 97.819 |
| 10 | 105.37 | 97.162 | 0.599 | 0.480 | 1.713 | 97.807 |
| 11 | 115.85 | 97.148 | 0.605 | 0.484 | 1.692 | 97.797 |
| 12 | 126.34 | 97.144 | 0.602 | 0.482 | 1.702 | 97.791 |
| 13 | 136.82 | 97.144 | 0.597 | 0.479 | 1.720 | 97.787 |
| 14 | 147.30 | 97.125 | 0.603 | 0.483 | 1.699 | 97.773 |
| 15 | 157.79 | 97.129 | 0.596 | 0.478 | 1.724 | 97.771 |
| 16 | 168.27 | 97.101 | 0.622 | 0.496 | 1.635 | 97.765 |
| 17 | 178.76 | 97.092 | 0.620 | 0.494 | 1.642 | 97.754 |

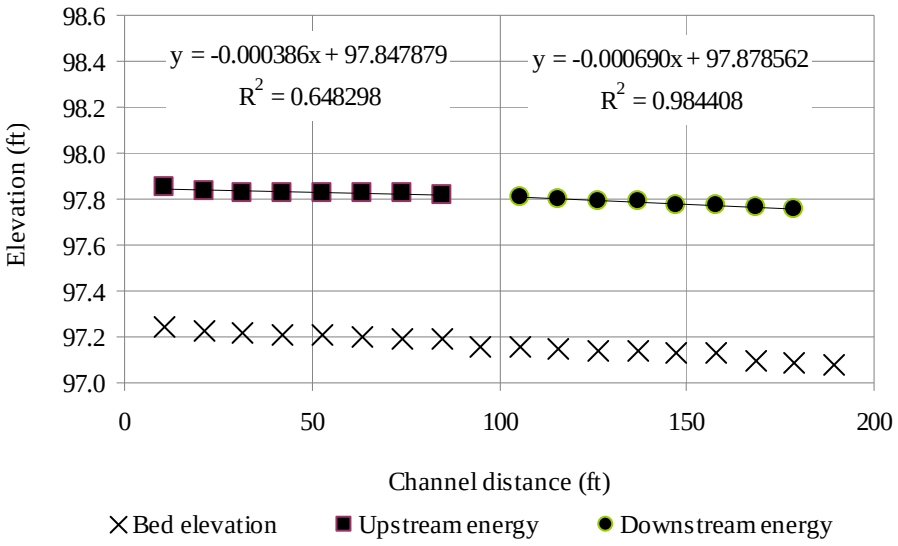


**Figure 30.** Calculation of bend-averaged friction slope for 8 cfs

**Table 6.** Calculated normalization parameters for 12 cfs

| XS | *Distance Downstream* | *Bed Elevation* | *Measured Depth* | *Hydraulic Depth* | *Velocity* | *Energy* |
|---|---|---|---|---|---|---|
| - | ft | ft | ft | ft | ft/s | ft |
| 1 | 10.57 | 97.240 | 0.764 | 0.635 | 1.260 | 98.029 |
| 2 | 21.13 | 97.228 | 0.749 | 0.624 | 1.290 | 98.003 |
| 3 | 31.70 | 97.220 | 0.753 | 0.627 | 1.282 | 97.999 |
| 4 | 42.27 | 97.212 | 0.761 | 0.632 | 1.266 | 97.998 |
| 5 | 52.84 | 97.208 | 0.766 | 0.636 | 1.256 | 97.999 |
| 6 | 63.40 | 97.196 | 0.765 | 0.635 | 1.258 | 97.986 |
| 7 | 73.97 | 97.187 | 0.778 | 0.645 | 1.234 | 97.989 |
| 8 | 84.54 | 97.186 | 0.753 | 0.627 | 1.282 | 97.965 |
| 10 | 105.37 | 97.162 | 0.752 | 0.581 | 1.933 | 97.972 |
| 11 | 115.85 | 97.148 | 0.756 | 0.584 | 1.920 | 97.961 |
| 12 | 126.34 | 97.144 | 0.752 | 0.581 | 1.933 | 97.954 |
| 13 | 136.82 | 97.144 | 0.747 | 0.578 | 1.949 | 97.950 |
| 14 | 147.30 | 97.125 | 0.761 | 0.587 | 1.904 | 97.942 |
| 15 | 157.79 | 97.129 | 0.753 | 0.582 | 1.930 | 97.940 |
| 16 | 168.27 | 97.101 | 0.777 | 0.597 | 1.854 | 97.931 |
| 17 | 178.76 | 97.092 | 0.777 | 0.597 | 1.854 | 97.922 |
| 18 | 189.24 | 97.080 | 0.770 | 0.589 | 1.875 | 97.905 |

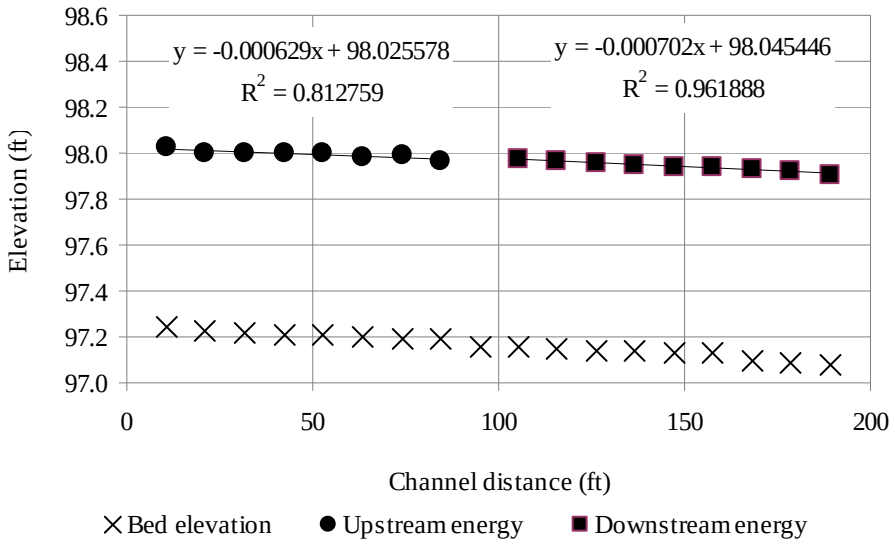


**Figure 31.** Calculation of bend-averaged friction slope for 12 cfs

**Table 7.** Calculated normalization parameters for 16 cfs

| XS | *Distance Downstream* | *Bed Elevation* | *Measured Depth* | *Hydraulic Depth* | *Velocity* | *Energy* |
|---|---|---|---|---|---|---|
| - | ft | ft | ft | ft | ft/s | ft |
| 1 | 10.57 | 97.240 | 0.896 | 0.727 | 1.389 | 98.170 |
| 2 | 21.13 | 97.228 | 0.900 | 0.730 | 1.381 | 98.160 |
| 3 | 31.70 | 97.220 | 0.900 | 0.730 | 1.381 | 98.150 |
| 4 | 42.27 | 97.212 | 0.897 | 0.728 | 1.387 | 98.140 |
| 5 | 52.84 | 97.208 | 0.899 | 0.730 | 1.383 | 98.140 |
| 6 | 63.40 | 97.196 | 0.912 | 0.738 | 1.359 | 98.139 |
| 7 | 73.97 | 97.187 | 0.925 | 0.747 | 1.336 | 98.138 |
| 8 | 84.54 | 97.186 | 0.910 | 0.737 | 1.363 | 98.129 |
| 10 | 105.37 | 97.162 | 0.892 | 0.665 | 2.067 | 98.116 |
| 11 | 115.85 | 97.148 | 0.890 | 0.664 | 2.074 | 98.107 |
| 12 | 126.34 | 97.144 | 0.890 | 0.664 | 2.074 | 98.097 |
| 13 | 136.82 | 97.144 | 0.882 | 0.659 | 2.098 | 98.098 |
| 14 | 147.30 | 97.125 | 0.891 | 0.664 | 2.070 | 98.087 |
| 15 | 157.79 | 97.129 | 0.886 | 0.661 | 2.086 | 98.088 |
| 16 | 168.27 | 97.101 | 0.912 | 0.677 | 2.008 | 98.073 |
| 17 | 178.76 | 97.092 | 0.912 | 0.677 | 2.008 | 98.063 |

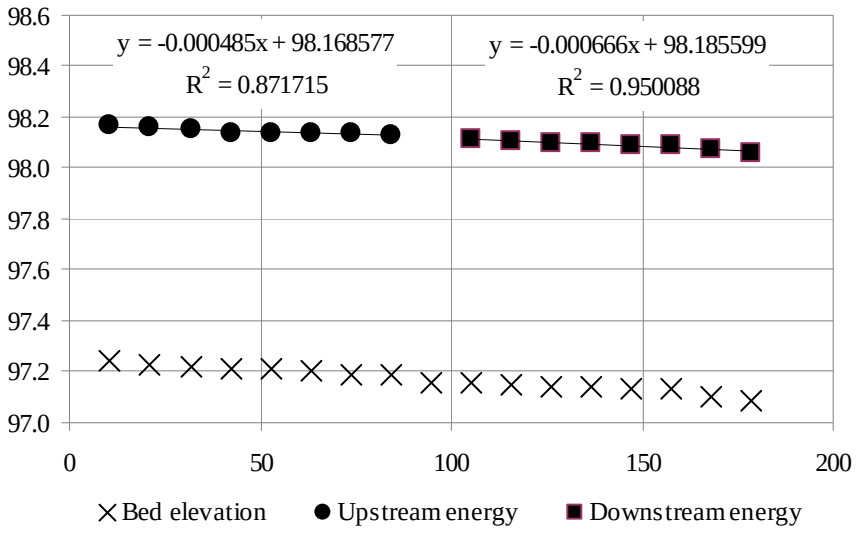


**Figure 32.** Calculation of bend-averaged friction slope for 16 cfs

**Table 8.** Normalization conditions for velocity and shear stress

| Configuration<br>- | $\tau_0$<br>*lb/ft²* | $u_0$<br>*ft/s* |
|---|---|---|
| Type I - 8 cfs | 0.0124 | 1.116 |
| Type I - 12 cfs | 0.0248 | 1.249 |
| Type I - 16 cfs | 0.0222 | 1.363 |
| Type III - 8 cfs | 0.0207 | 1.713 |
| Type III - 12 cfs | 0.0255 | 1.845 |
| Type III - 16 cfs | 0.0279 | 2.043 |

## 4.2. Velocity distributions

Velocity data collected at 60% flow depth were organized, processed, and compiled into a database for field visualization and comparisons. Data were spatially interpolated to the approximate planimetric flow extents using inverse distance weighting techniques and a four-point roaming neighborhood. Interpolated velocity fields were divided by the bend-averaged normalization condition for the bend and volumetric flow rate from Table 8 which allowed for relative comparisons to other configurations.

Figure 33, Figure 34, and Figure 35 present representative velocity distributions of W01 from Heintz (2002), W04 from Darrow (2004), and W13 from Schmidt (2005), respectively. Information regarding the configuration geometries is provided in Appendix A1. For all configurations, it was found that velocity was reduced within the structure field and increased at the channel center and inner-banks. Representative velocity plots illustrate differences between the velocity fields as functions of the geometric parameters. Reduced velocity at the outer-bank was confined within the structure field extents. Outer-bank effects were apparent for W04 where the gradient between the slowed and increased conveyance zones was captured with the structure dataset. Artificial extensions of the reduced flow field are depicted for W01 and W13 due to interpolation error. Data resolution was insufficient to capture the gradient for these configurations.

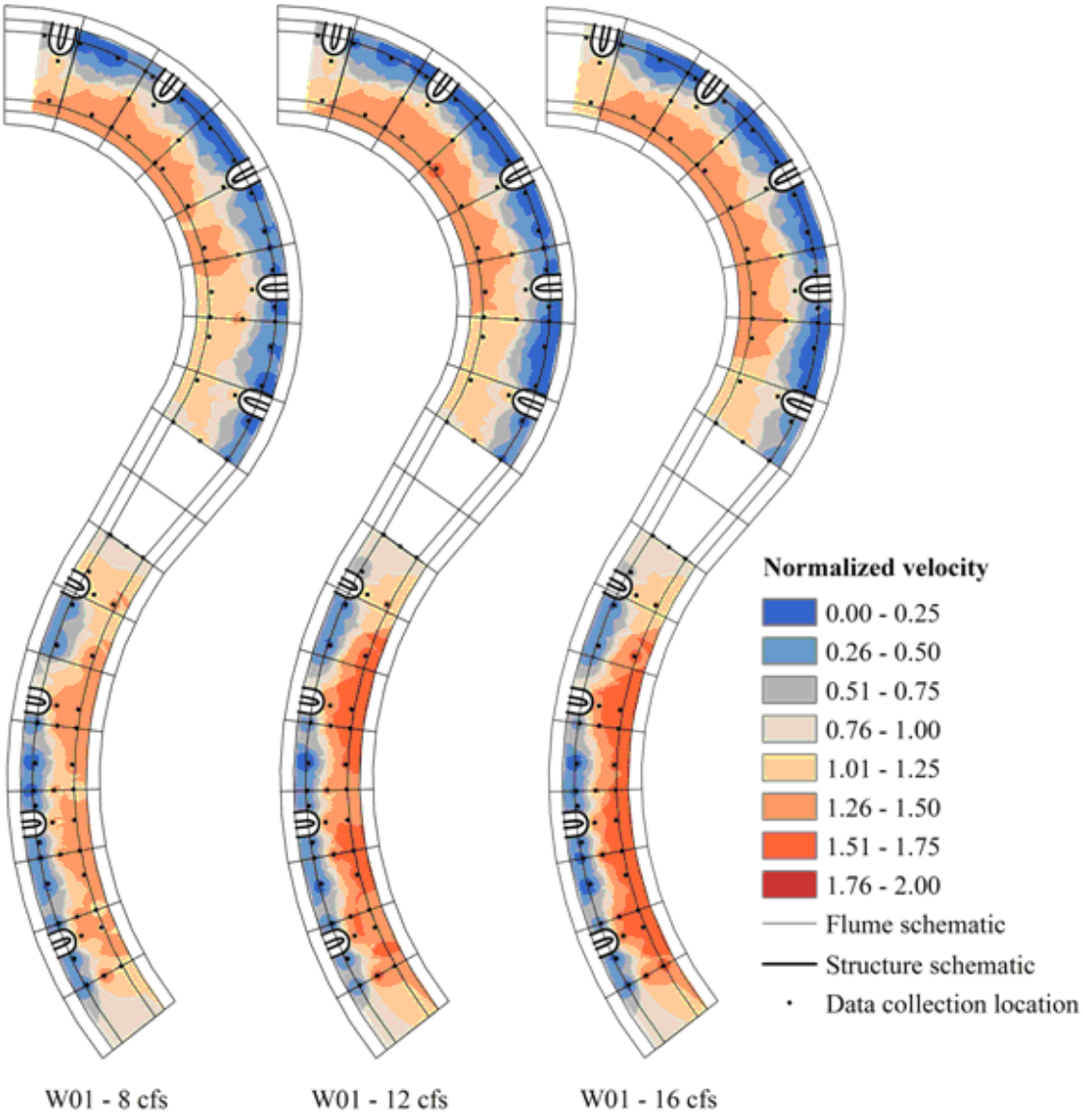


**Figure 33.** Normalized velocity for configuration W01; flow direction down-page

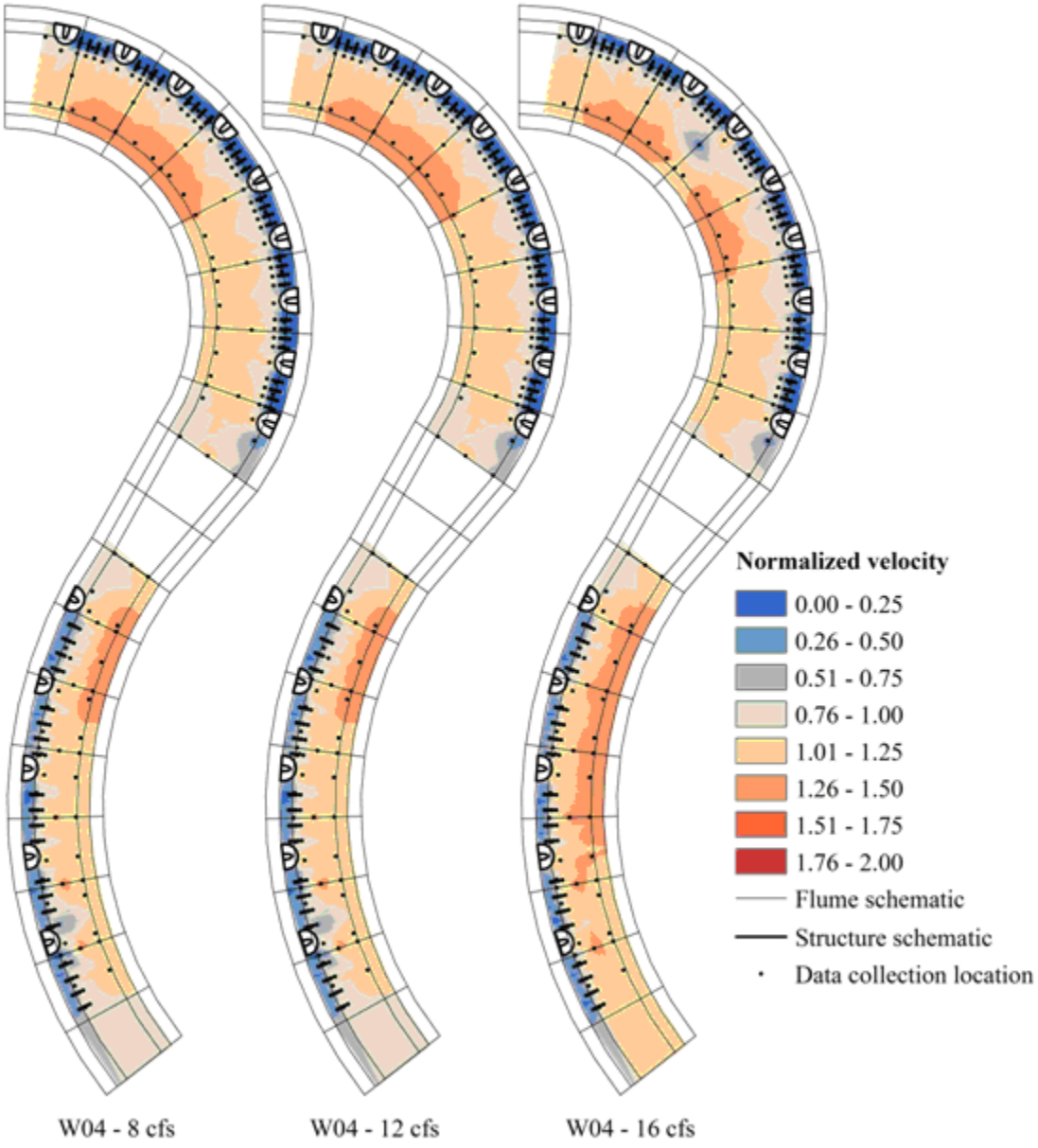


**Figure 34.** Normalized velocity for configuration W04

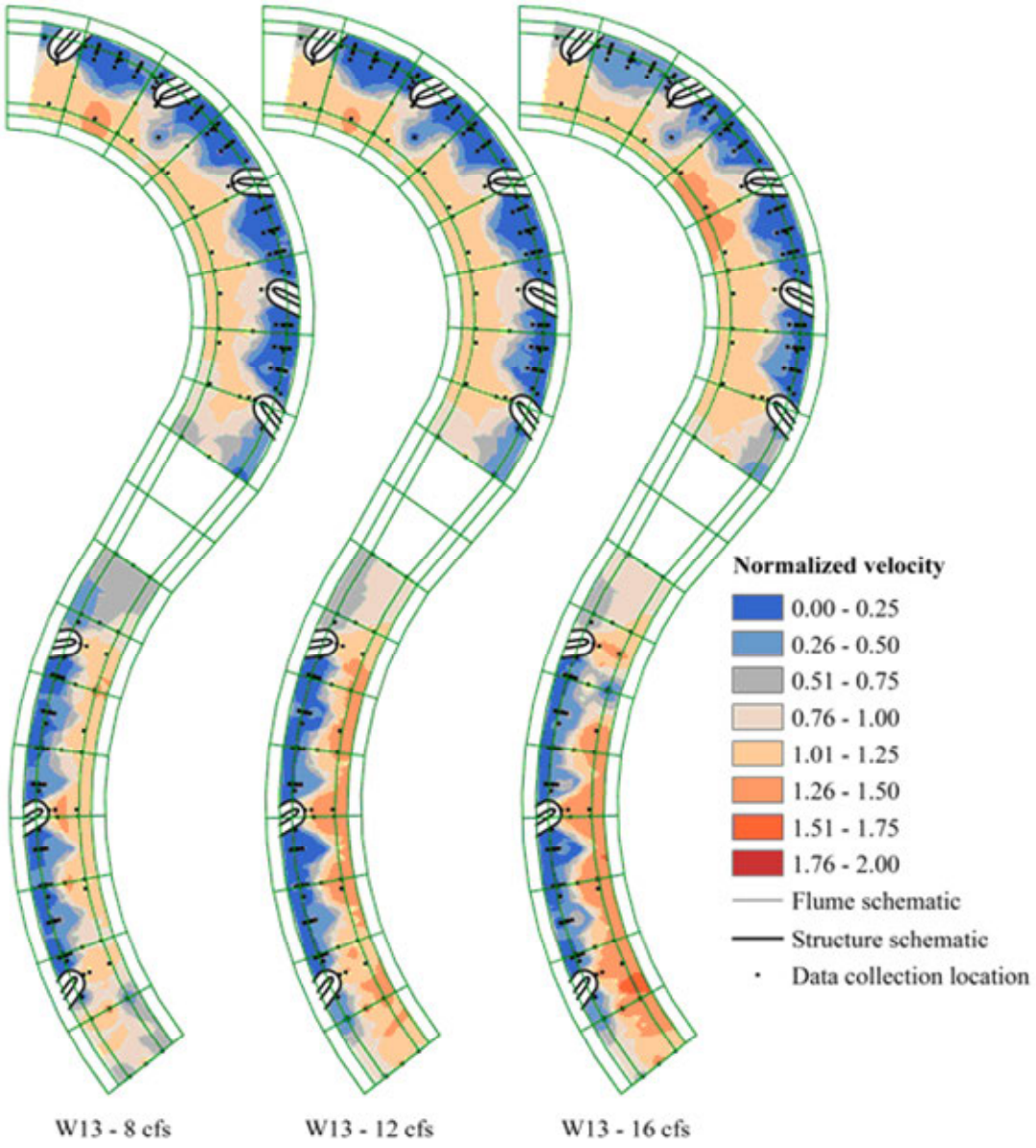


**Figure 35.** Normalized velocity for configuration W13

## 4.3. Boundary shear-stress distributions

Pressure differentials were collected with the Preston tube between the static and dynamic heads at the channel bottom for the same data-collection locations as the velocity dataset. Instrumentation output was converted to a boundary shear stress through Equation 5, and values were compiled and organized for visualization. An inverse-distance weighted interpolation technique with a four-point neighborhood and weighting power of 2.5 was used to display boundary shear-stress trends within the trapezoidal model. Interpolated boundary shear-stress distributions were normalized by the conditions reported in Table 8 for comparisons to other configurations.

Figure 36, Figure 37, and Figure 38 depict normalized boundary shear-stress distributions for the W01 configuration from Heintz (2002), the W04 configuration from Darrow (2004), and the W10 configuration from Schimdt (2005), respectively. A general trend of increased boundary shear stress near the channel center and inner-bank and a reduced zone at the outer-bank is noted for the configurations displayed. Areas of reduced shear-stress were typically confined within the structure field. Displayed trends of shear-stress reduction extending past the structure field boundary are typically artifacts of the interpolation method and spatially sparse data. Variability in the range of values was more pronounced for the shear-stress data than for the velocity data which is attributed to instrumentation sensitivity and operation. Normalized values exhibited trends uniformly low, as depicted in the W01 upstream bend, and uniformly high as in the case of the 8 cfs W04 downstream bend. Downstream normalized values for any configuration and discharge combination were generally higher than the upstream bend counterpart, which may indicate a potential discrepancy in computed normalization conditions.

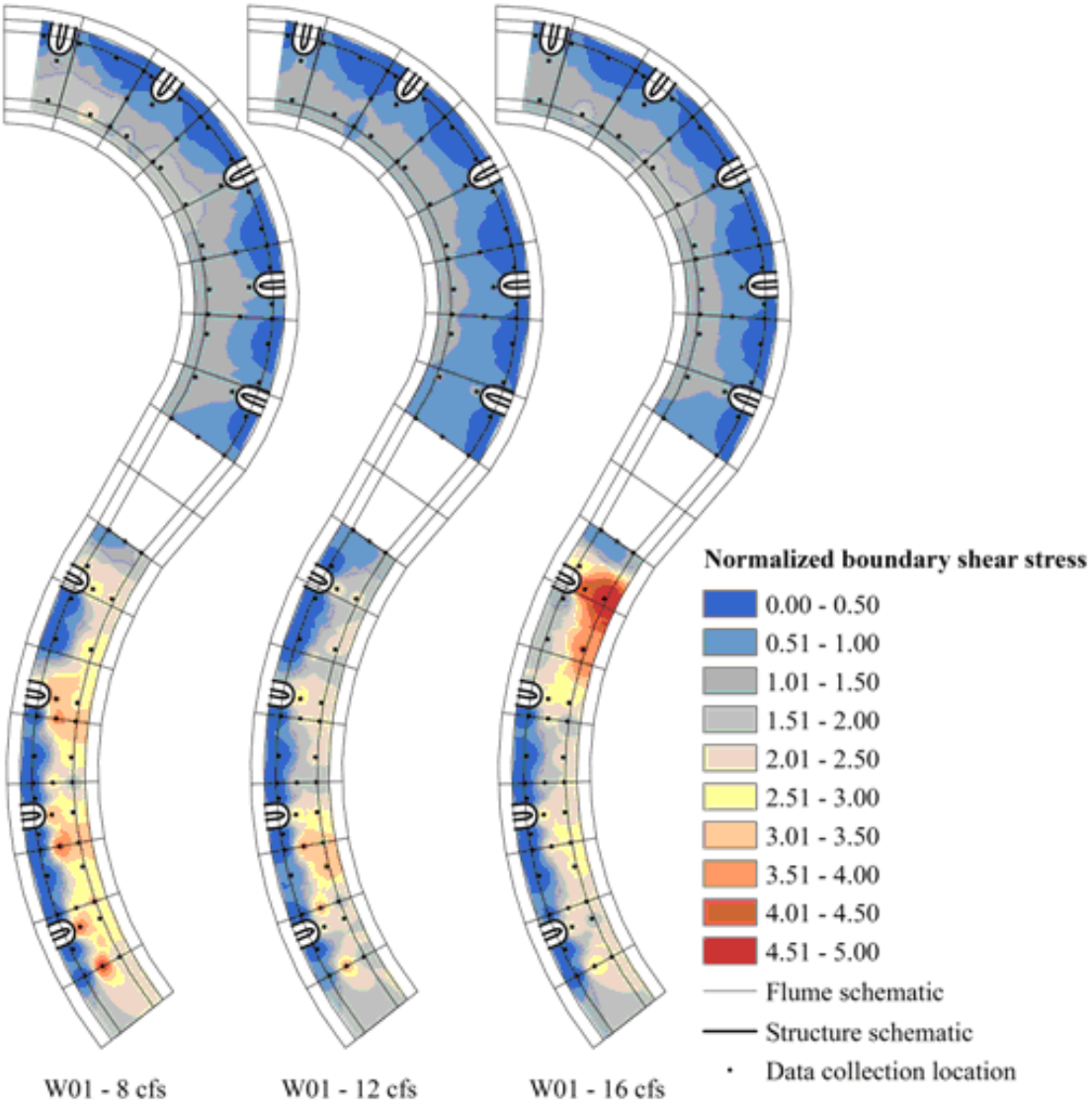


**Figure 36.** Normalized boundary shear stress for configuration W01

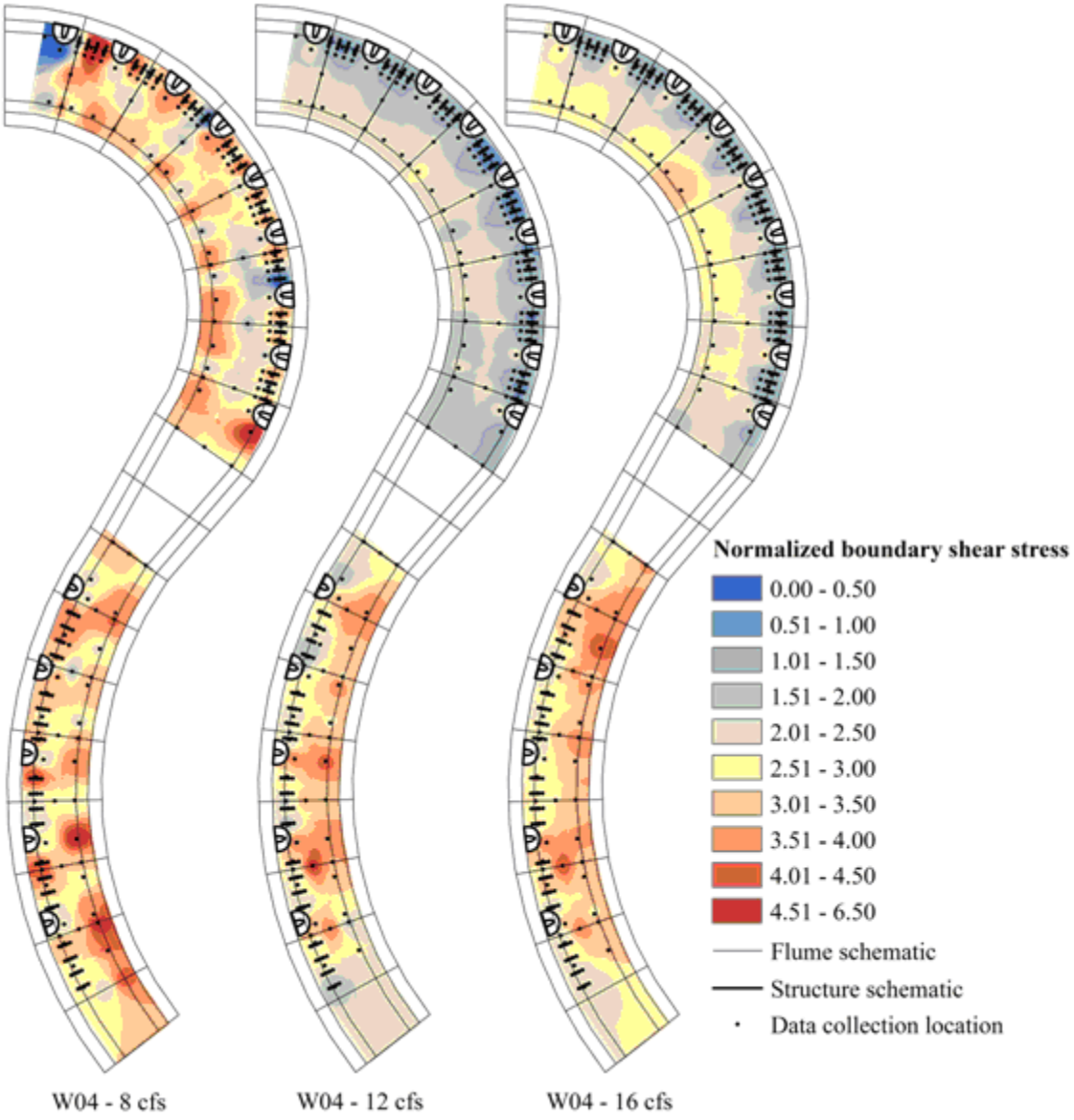


**Figure 37.** Normalized boundary shear stress for configuration W04

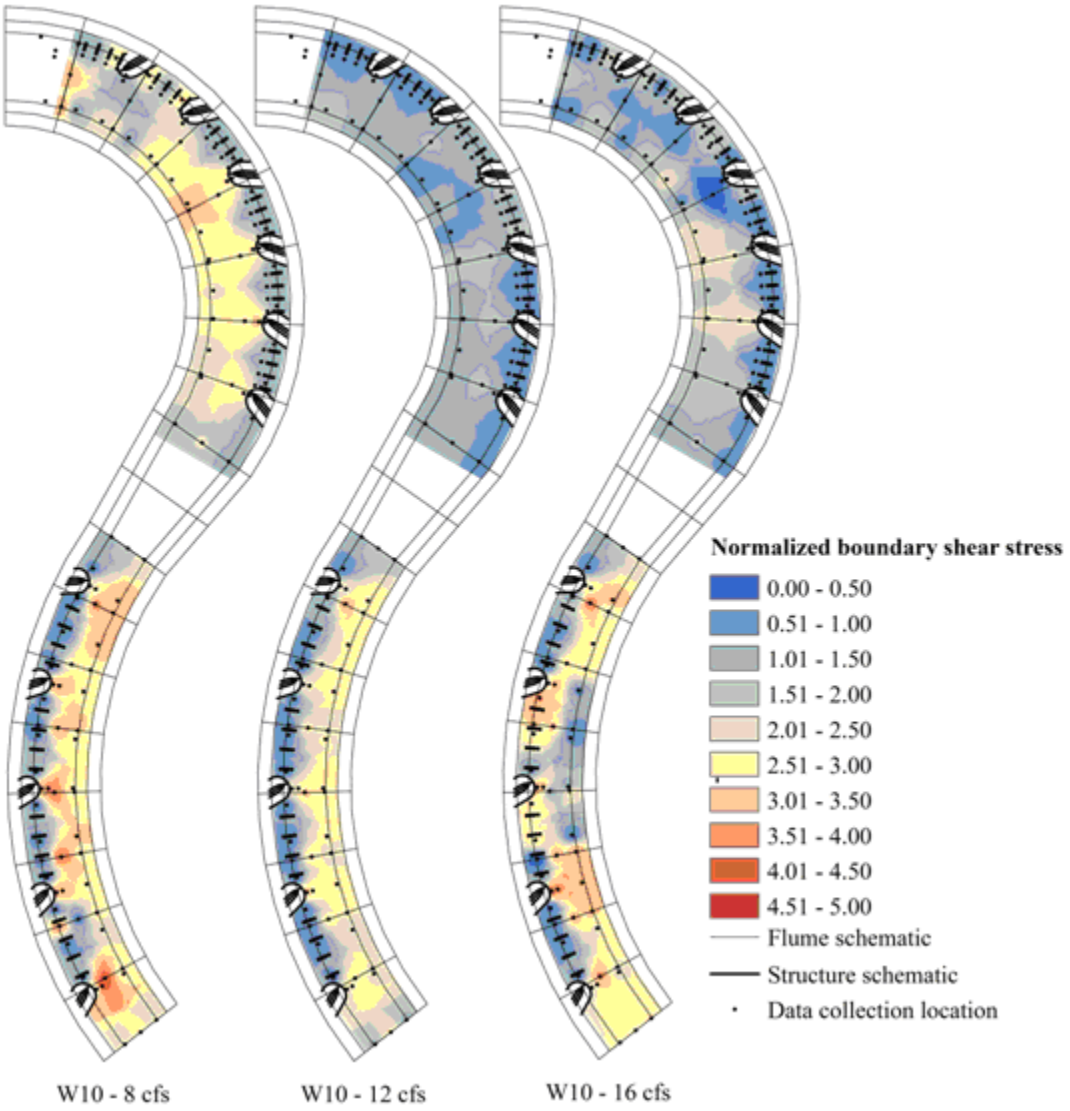


**Figure 38.** Normalized boundary shear stress for configuration W10

## 4.4. Quantification of induced structure hydraulics

Velocity and boundary shear-stress patterns were shown to be affected by the installation of transverse instream structures in the physical model through diversion of channel conveyance away from the outer-bank to the channel center and inner-bank. Studies of Heintz (2002), Darrow (2004), and Schmidt (2005) focused upon maximum velocity conditions at the outer-bank, centerline, and inner-bank. While maximum hydraulics are important for design criteria

and represent the most extreme conditions within a specific hydraulic configuration, this selection methodology does not encompass all available hydraulic information collected during the physical model. Using only one point within a full structure field diminishes potential information gained from the collected data. Large emphasis is placed on the precision of an identified maximum point and if that single point truly represented the maximum field velocity. A more robust methodology for hydraulic quantifications supplements maximum values with region-average hydraulics. As such, Equation 8 was proposed as the average velocity ratio and Equation 9 as the average shear ratio.

$$AVR_i = \frac{u_{AVG-i}}{u_0} \tag{8}$$

where:

$AVR_i$ = normalized average velocity at location $i$;

$i$ = location index = [$O$ (outer-bank), $I$ (inner-bank), $C$ (centerline)]; and

$u_{AVG-i}$ = array average of mean-flow resultant velocity at location $i$ [L/T].

$$A\tau R_i = \frac{\tau_{AVG-i}}{\tau_0} \tag{9}$$

where:

$A\tau R_i$ = normalized boundary shear stress at location $i$; and

$\tau_{AVG}$ = array average of shear-stress measurements at location $i$ [F/L$^2$].

Average velocity values used in the numerator of Equation 8 were calculated from the mean-flow resultant ADV velocities at 60% flow depth at data-collection locations within the specified

outer-bank, inner-bank, or centerline locations. Average shear-stress values for the numerator of Equation 9 were determined from the time-averaged Preston-tube data converted using Equation 5 within each channel location. Determination of the channel locations was examined to ascertain the most effective representation of induced structure hydraulics.

Quantification of specific values of the numerator in the normalized hydraulic relationships required the definition of the set of points allocated to each location: outer-bank, inner-bank, and centerline. Point allocation to the three locations was examined through two approaches. Distinct zones of structure influence are apparent within the channel and have been described with a region-influenced approach by Scurlock et al. (2013a) and Scurlock et al. (2013b) or by a point-based approach by Heintz (2002), Darrow (2004), and Schmidt (2005). The regional analysis identified data points that fell within areas of instream structure influence including the reduced outer-bank zone within the structure field and the increased conveyance zone located at the channel center and inner-bank. Point-based analysis used established data locations at specific channel coordinates, regardless of induced hydraulic patterns. Data-collection points were distributed along the outer-bank toe, inner-bank toe, and centerline arc set parallel to the curvature of the channel. Other point-based locations for instream structures may be the structure crest tip or the submerged crest itself.

Regional delineation may have advantages over point-based locations in determination of instream-structure field hydraulics as it allows for the full realization of hydraulic patterns and applies adeptly to channels where determination of channel toe and centerline locations are difficult. Point-based data collection was performed independent of the induced hydraulics, did not fully utilize the available dataset, and may have spuriously represented hydraulics within the structure field. Limiting data for quantification to the outer-bank channel toe may not fully

capture the region of velocity reduction at the outer-bank. In such a case, the efficacy of a structure configuration to reduce outer-bank erosional forces would falsely appear diminished. It is noted that in the majority of structure velocity fields, the points at the channel toe were contained within the reduced outer-bank velocity zone. Point-based analysis may provide an advantage over regional analysis in determining induced hydraulic effects specifically at the outer-bank toe, a region identified with incipient bank retreat processes by Simon et. al (2000) and Knighton (1998), or when data are not sufficient to define the outer-bank reduced zone.

Specifications of each data segmentation approach, regional or point-based, for quantitative prediction methodology development were first examined for the velocity dataset. Velocity data resolution of the inner-bank areas of the flume resulted in the inner-bank area determined as the data taken along the channel inner-toe, consistent with the inner-bank location-based analysis, yet typically with a slightly larger data array. The centerline zone ranged from the spatial velocity gradient to the inner-bank toe. Centerline data resolution was similar for the regional and point-based methods, with the regional containing slightly more points. For the regional approach, data were identified within the reduced velocity zone at the outer-bank and centerline by locating the spatial velocity gradient between the reduced and increased conveyance zones. Points falling to the outer-bank of the gradient were designated as outer-bank points, and to the inner-bank were designated centerline. Points within the gradient were not allocated to either zone. Differences between the two methodologies are the most pronounced at the outer-bank. Data within the outer-bank vicinity before the transition to the shifted conveyance area were determined as the outer-bank region zone. Figure 39 illustrates the full dataset of the 12 cfs, upstream W04 configuration with the regional outer-bank, inner-bank, and centerline datasets identified.

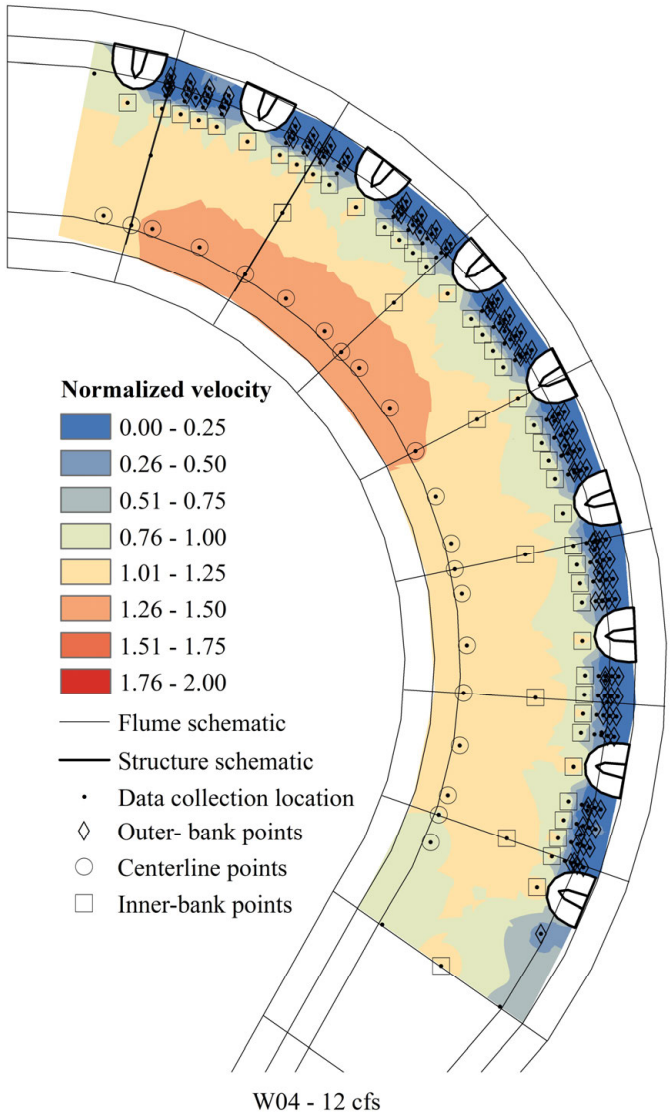


**Figure 39.** Regional analysis for upstream W04, 12 $ft^3/s$

Regional and point-based identification process was performed for all 130 independent configurations evaluated within the physical model. Data were tabulated and maximum and average velocity values at the outer-bank, inner-bank, and centerline were determined for both methodologies. Maximum and average velocities were then normalized according to the proper discharge and channel-bend value from Table 8 and distributions of *MVR* and *AVR* were

generated. Figure 40 illustrates calculated histograms for the normalized velocity ratios using the regional and point-based schemes. It was found that the outer-bank distribution of normalized maximum velocity was restricted to a more limited band for the regional approach than for the point-based analysis. Outer-bank point-based normalized velocities exhibited more values at lower velocity reduction and were distributed with a left skew compared to the regional analysis. For the outer-bank *MVR* calculated with the regional approach, 84.6% of the 130 data fell within the range of 0.3 to 0.6, while 66.2% fell within that range for the point-based approach. Higher point-based values for the outer-bank velocity ratios are attributed to points located within, or to the inside of, the spatial velocity gradient. There was no discernible difference between the inner-bank and centerline ratios for the two methodologies, reinforcing the fact that the datasets were nearly identical.

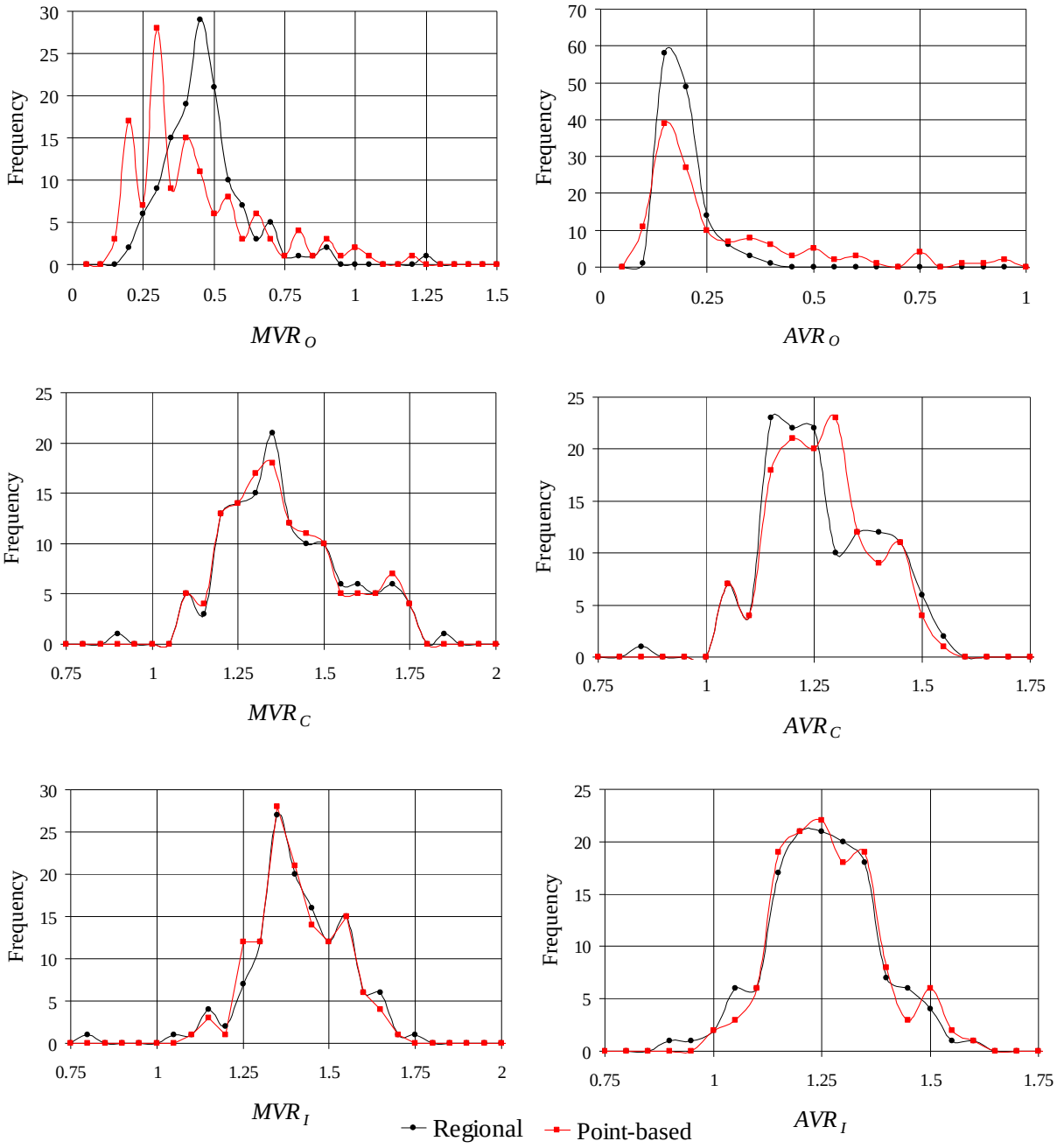


**Figure 40.** Regional and point-based analysis data distribution

Boundary shear-stress data were also examined with both regional and point-based analysis methods. It was found that the spatial gradient in shear-stress was located to the inside of the channel toe in nearly all instances, with exceptions being erratic distributions where high

zones extended to the outer-bank. The 8-$ft^3$/s distribution of W04 and 16-$ft^3$/s distribution of W10, illustrated in Figure 37 and Figure 38, respectively, represent instances where differentiation of the outer-bank zone through a clearly defined spatial shear-stress gradient is complex and somewhat subjective. The regional approach for shear-stress is further complicated by the Preston tube calibration methods. Equation 5 was developed by Heintz (2002) in a straight and flat-bottomed flume, which is potentially compromised when applied to the angled surface located to the outer-bank of the channel toe. Utilization of a point-based selection strategy for the shear-stress distributions allows for a more straightforward and definitive approach in the quantification of the shear-stress conditions. Maximum and average shear-stress values were obtained for each configuration where shear-stress data were available and are presented Appendix A2. Values were divided by the appropriate normalization condition from Table 8 to generate $M\tau R$ and $A\tau R$.

Compiled velocity and shear-stress data used as the basis for research analyses performed to fulfill project objectives, populated with regional velocities and point-based boundary shear-stresses, are presented in Appendix A2. Data represent maximum and average induced instream structure hydraulics at specific channel locations from a variety of configuration geometries and flow conditions. Evaluation of specific hydraulic effects of the structure configurations, channel geometries, and flow conditions requires development of a mathematical tool calibrated with collected physical model data.

## 4.5. Predictive model development

Velocity and boundary shear-stress effects from instream structure installation were quantified and normalized for maximum and average conditions at different regions of influence within channel bends. Description of the effects with the variables of the structures, channel, and

flow conditions required development of a mathematical approach calibrated to the collected physical model data. A properly calibrated tool may be used to predict hydraulic conditions for a variety of configurations not evaluated within the physical model through interpolation. Different approaches for the generation of a mathematical tool were considered, geometric parameters of the structures and channel bends were organized, and calibration procedures were performed to tailor a predictive design approach to the instream structure dataset.

Hydraulic mathematical models are generated through theoretical or empirical means. Theoretical models stem from the governing conservation equations for mass, momentum, and energy and strive to describe flow hydraulics through direct physical understanding of system processes. Theoretical equations are typically developed through analytical means, then compared with physical model data for calibration and validation. For complex, turbulent, open-channel flows associated with transverse instream structures, theoretical equation development for comprehensive description of hydraulics has not been shown as tractable for a single structure, let alone a structure series. Studies from the literature have indicated numerical modeling schemes using tailored versions of the Reynolds-averaged-Navier-Stokes (RANS) equations are the most theoretically derived approaches for instream structure modeling. Sinha and Marelius (2000), Abad et al. (2008), Scott et al. (2001), Han et al. (2011), Nagata et al. (2005), Haltigin et al. (2007), McCoy et al. (2007) and others have performed RANS numerical simulations as theoretical approximations of instream structure hydraulics. Numerical simulations reportedly achieve prediction of observed hydraulics with adequate accuracy; however, the models are not readily implemented by a typical practicing engineer and are cumbersome for design alternatives. Empirical method development circumvents these shortcomings by calibrating a simple, easily solved mathematical model to a collected dataset.

Purely empirical methods utilize a specified dataset and tailor coefficients to all independent parameters altered within the dataset without an understanding of the physical processes. In the most fundamental empirical model, the dependent parameter is set as a function of all independent parameters with associated weighting coefficients. The function model is either linear, where the dependent parameter is described by an offset and the addition of each independent variable multiplied by a regression weight, or nonlinear, where the dependent parameter is described by any combination of regression weights and independent parameters in at least one non-additive operation (Weisberg, 2013). Strength of any developed empirical model relies upon the influential variables chosen and the collected dataset. Poor structure of the chosen variables may produce spuriously accurate predictions, colinearity, inaccurate variable response, or inability for the mathematical model to achieve the intended purpose. With greater size and stronger validity of the analysis dataset, the prediction of the dependent parameter through empirical methods will gain in accuracy. Properly developed empirical prediction methodologies may be rapidly used to investigate a hypothetical configuration response and for maximization or minimization of desired configuration characteristics while meeting design objectives.

For the purposes of this research to quantify induced hydraulic trends in channel bends, an empirical methodology was chosen to best meet research objectives. Hydraulic and physical intuition were instrumental in the selection of parameters and formulation of dimensionless parameter groupings. Dimensionless groupings have been endorsed in the creation of empirical mathematical models across a variety of disciplines due to scalability and unit system independence (D'Agostino and Ferro, 2004; Leinster, 2004; Vignaux and Scott, 1999; Johnson, 1972). Care was taken to ensure parameters may be readily determined from natural channel

field data and apply well to design procedures. Chosen dimensionless parameters included a channel curvature ratio, a spacing ratio, a lateral contraction ratio, a submergence ratio, a planimetric angle ratio, and an area contraction ratio. Rationale behind the formation of each parameter and expected response on the maximum and average hydraulic ratios is described in detail.

### 4.5.1. Channel curvature ratio

Meandering channel $R_C$ and $T_W$ are fundamental descriptors of the channel geometry and sinuosity. A ratio of the two parameters, $R_C/T_W$, has been identified as a important calculation in the description of meandering rivers and reported values of approximately 1.5 to 4.5 are common (Garcia, 2008). Channel curvature has been linked to bank migration rates by Nanson and Hickin (1986), Biedenharn et al. (1989), and Thorne (1991). Figure 41 illustrates the migration rate observed for 18 Canadian rivers by Nanson and Hickin (1986) with a maximum rate located near $R_C/T_W$ values of approximately 3. Variability of the migration rate with the curvature ratio indicates that channel response to instream structure installations quantified through outer-bank erosivity is likely significant. Values of the channel curvature ratio were 2.02 and 4.39 for the Type I and Type III channel bends, respectively. Assuming the results of Nanson and Hickin (1986) apply to trapezoidal channels, it is speculated that a given structure configuration geometry may perform to a higher degree of efficacy, quantified by reduction of hydraulic forces at the outer-bank, to a more significant level for the Type I bend than for the Type III bend considering the Type I ratio of 2.02 is closer to maximum erosion ratio value of 3 than the Type III. The Type I bend would have greater erosive potential without structures, and therefore greater potential for reduction with a configuration installed. However, there is substantial scatter in the reported migration rate results, and any induced hydraulic trend with $R_C/T_W$ is a

possibility given the laboratory database. The channel curvature ratio was the only parameter used for model development that accounted for channel-bend geometry.

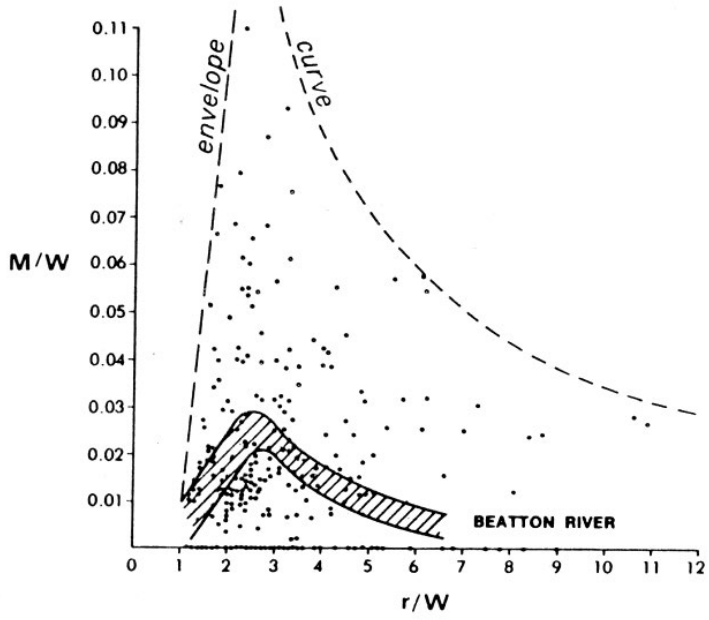


**Figure 41.** Migration rate as a function of $R_C/T_W$ from Nanson and Hickin (1986)

### 4.5.2. Spacing ratio

The distance between the structures in a configuration, $L_{ARC}$, has implications in design such that it is desired to have the downstream structure in the series located within the hydraulic shadow of the upstream structure. McCoy et al. (2007) suggested that this distance for velocity effects is as close as two times the structure crest length downstream and Scurlock et al. (2013a) reported values from approximately 2.5 to 5.5 of structure crest lengths. Design guidelines address spacing as a function directly as a function of $T_W$, or indirectly as a function of the structure length described by $T_W$ (Maryland, 2000; Johnson et al., 2001; Lagasse et al., 2009). Normalizing the spacing ratio by the channel top width makes the parameter dimensionless and applies to a variety of channel types. Spur-dike design guidelines from Lagasse et al. (2009)

suggest a maximum structure length of $T_W/5$ and spacing of $3.27L$, resulting in a spacing, $L_{ARC}/T_W = 0.65$. Ranges of $L_{ARC}/T_W$ within the laboratory were from 0.55 to 3.09.

The spacing ratio is predicted to have an interrelated effect with other structure configuration parameters. In the case of two configurations with sufficiently different spacing ratios, yet identical in other geometry characteristics and installed in the same channel bend, it is expected that the smaller the spacing ratio, the more outer-bank reduction in erosivity. In such a case, an increase in $L_{ARC}/T_W$ would be directly related to outer-bank ratios, and inversely related to inner-bank and centerline ratios. However, spacing effects on hydraulics have shown dependence to structure length which influences the region of hydraulic influence downstream of the structure. For a given length of structure, there is likely a lower threshold of the spacing ratio where no effects on the hydraulics are produced; they are already reduced from baseline conditions as much as possible.

### 4.5.3. Lateral contraction ratio

Crest length of the structure extending from the bank into the channel is fundamental to the hydraulics of the flow field. All design guidelines found from the literature for transverse instream structure designated criteria for the structure length. Focusing on the planimetric length of the weir crest projected perpendicular to the flow direction, a lateral contraction ratio may be developed by normalizing the length by the channel top width. Lateral contraction ratios, $L_{W\text{-}PROJ}/T_W$, ranged from 0.11 to 0.37 evaluated within the laboratory. Values of $L_{W\text{-}PROJ}$ of a given structure configuration were dependent upon the flow level in the physical model considering the outer-bank slope of the channel. Variable water surface and influence on $L_{W\text{-}PROJ}$ is illustrated within the trapezoidal model in Figure 25. Water-surface elevations below the structure crest

elevation produce a segment of the structure that is exposed and non-influential to the hydraulic field. A simple correction to the values of $L_{W\text{-}PROJ}$ was applied as $Z\Delta z$; where $Z$ = ratio of horizontal to vertical side slope of trapezoidal channel.

### 4.5.4. Submergence ratio

Instream structure nomenclature is largely dependent upon the relative flow depth to the structure crest elevation. Bendway-weirs structures are designed to have crest submergence, spur-dike crests are exposed, and vanes possess crests angled downwards into the flow. As indicated by Abad et al. (2008), Bhuiyan et al. (2010), Jamieson et al. (2013), Scurlock et al. (2013a), and Scurlock et al. (2013b), the degree of crest submergence may substantially affect hydraulic patterns within the channel. Submerged crests are reported to exhibit plunging flow, localized hydraulic drops, disrupted secondary currents, and outer-bank erosive force increase. Crests which are not submerged behave the same hydraulically at any level; there is no hydraulic difference between a spur-dike at an increment of design discharge to one evaluated at design discharge. A submergence ratio, $D_R$, was developed to account for flow levels above the crest elevation as $D_B/(D_B - \Delta z)$; where $D_B$ is the baseline flow depth. The submergence ratio is unity for all values where the crest is not submerged and greater than unity for overtopping flows. Representation of the ratio as a function of $\Delta z$ instead of the weir crest height was chosen for field applications; it is easier to determine the water-surface elevation and the crest elevation than the difference to a datum for field engineers. Ratio values for evaluated spur-dikes ranged from 1.00 to 1.18. Vane ratios ranged from 1.14 to 6.98. Higher submergence ratios for vanes are indicative of the slope to the channel bottom at the end of the crest. Evaluated structures within the physical model were submerged, yet did not meet classical design criteria of bendway weirs as detailed in Table 1.

Response of channel hydraulics to crest submergence is complex due to the nature of flow acceleration, eddy formation, and secondary current disruption. Bendway weirs are designed for crest submergence and have been shown by Scurlock et al. (2013a) and Scurlock et al. (2013b) to be effective at outer-bank hydraulic reduction within a physical model and by Rhoads (2003) in field installations. Submergence is not necessarily related to increased outer-bank forces within the reduced velocity core, especially if measures are taken to protect the structure at the bank key-in (Lyn and Cunningham, 2010). For spur-dikes, it is hypothesized that overtopping flows would have a deleterious effect on the inter-structure eddy formation and hydraulic reduction

### 4.5.5. Planimetric angle ratio

Orientation of a structure crest relative to the bankline tangent affects local hydraulics in a variety of ways. For non-submerged structures, the planimetric crest angle influences how the flow is accelerated and conveyed around the structure body. Downstream-angled structures will deflect streamlines in the direction parallel to the structure axis away from the outer-bank, structures with no angle will not result in effect, and non-submerged upstream-angled structures may redirect flow into the outer-bank and cause stronger recirculation zones within the spur-dike structure field. It follows that downstream-angled structures may reduce eddy turbulence structures within a configuration field; however, when submergence occurs, the beneficial alignment may become detrimental to outer-bank protection. Submerged structure crests redirect flow perpendicular to the structure axis. Downstream-angled submerged structure crests will influence flow to be redirected to the outer-bank and increase outer-bank erosion between the structures. Upstream-angled submerged structures, as in the recommendations for the design of bendway-weirs (Lagasse et al., 2009, McCullah and Gray, 2005), redirect flows over the crest to

the center channel in a plunging jet motion. The angle of the structure for submerged cases is much more significant than for non-submerged cases.

Structures evaluated within the physical model were set perpendicular to the bankline tangent ($\theta = 90^o$), or angled upstream to the flow direction ($\theta \leq 90^o$). Values ranged from $90^o$ to $60^o$. All structure types were angled upstream, which did not allow for the examination of downstream planimetric angle effects on the hydraulic fields. Angles were expressed in radians and divided by the perpendicular angle case of $\pi/2$ to create a ratio of upstream angle, $2\theta/\pi$, which ranged from unity to 2/3 in the physical model. It was expected that for non-submerged structures, the angle ratio would not significantly affect the hydraulic fields, and for submerged structures, decreasing the ratio would result in more deflection of conveyance to the channel center and away from the outer-bank.

### 4.5.6. Area contraction ratio

Structures within the trapezoidal physical model were designed using percentage area blocked constraints for baseline flow conditions. Values at the design discharge included 10.75%, 19.4%, and 27.0% (Heintz, 2002). Structure area blockage was delineated by either the crest elevation or by the flow depth, whichever was lower, and the flume boundaries. Calculated structure area can be divided by the baseline flow area for the evaluated discharge to produce a dimensionless ratio of area contraction, $A^* = A_W/A$.

Area contraction is a function of variables included in other dimensionless ratios including $L_{W\text{-}PROJ}$, $D_B$, and $\Delta z$, yet also accounts for information not included in the ratios such as the crest toe tie in. Assuming that the minimum $L_{W\text{-}PROJ}$ crosses the outer-bank channel toe, $A^*$ can be expressed as Equation 10.

$$A^* = \frac{(D_B - \Delta z)[L_{W-PROJ} + 0.5(D_B - \Delta z)(Z_W - Z)]}{D_B(T_W - D_B Z)} \quad (10)$$

where:

$Z$ = ratio of horizontal to vertical distance at outer-bank slope; and

$Z_W$ = ratio of horizontal to vertical distance on projected weir crest tip tie-in.

Linear response with the projected crest length and nonlinear response with the baseline flow depth and depth ratio was observed for $A^*$. As with the lateral contraction ratio, it is expected that an increase in flow blockage would reduce outer-bank velocity, producing a negative effect on the outer-bank hydraulic ratios and a positive effect on the inner-bank and centerline ratios. Due to $A^*$ reliance upon the other dimensionless variables, a joint hydraulic response is expected for the prediction of channel hydraulics. For instance, lateral contraction response may indicate that a smaller crest would result in reduced outer-bank velocity when coupled with a stronger $A^*$ response for increased velocity. Cumulative effects of both parameters on velocity at the outer-bank would be an indirect function of $L_{W\text{-}PROJ}$ in this case.

### 4.5.7. Predictive mathematical model

Dimensional analysis theory suggests the conglomeration of identified dimensionless variables into a power equation. Such representation has scaling and self-similarity benefits as detailed by Barrenblatt (1996) and possesses advantages over a linear representation. Dimensionless terms representing channel and structure geometries were organized into a single mathematical expression as Equation 11.

$$VR_{i\,s}\big|_{M,Avg};\tau R_i\big|_{M,Avg} = a_1(A^*)^{a_2}\left(\frac{L_{ARC}}{T_W}\right)^{a_3}\left(\frac{R_C}{T_W}\right)^{a_4}\left(\frac{L_{W-PROJ}}{T_W}\right)^{a_5}\left(\frac{D_B}{D_B-\Delta z}\right)^{a_6}\left(\frac{2\theta}{\pi}\right)^{a_7} \quad (11)$$

where:

*s* = structure type index (*s* = all-structures, spur-dike, vane);

*M* = maximum value; and

*Avg* = average value.

Evaluated structures from the trapezoidal physical model included upstream-angled spur-dikes, submerged spur-dikes, and vanes. Submerged spur-dikes possessed a submergence ratio up to 1.18, while for the structures to be classified as bendway weirs according to design criteria, $D_R$ should be within the range [2,3]. (Lagasse et al., 2009). Including submerged spur-dikes within the design spur-dike dataset allows for realization of flow conditions which exceed the design discharge by 33.3%. For the velocity mathematical model, three structure type equations were created including an all-structure equation, a spur-dike equation, and a vane equation. Shear-stress data were limited to spur-dike structures only and one equation was created to describe hydraulic conditions. Maximum and average hydraulic conditions at the outer-bank, centerline, and inner-bank were implemented to the format of Equation 11 and regression procedures were used to tailor the coefficients to the collected datasets. A total of twenty-four equations were developed for the quantification and prediction of induced instream structure hydraulics.

## 4.6. Model optimization

Application of Equation 11 as a hydraulic prediction tool required optimization of the parameter weights to each data subset through regression procedures. Both linear and non-linear

regression procedures were used to identify the underlying trends in the prediction methods. Methods chosen were based on primary influential parameter identification, outlier removal, and prediction of essential response of normalized hydraulics to independent parameters. Final equations are applicable for field design, possess physically intuitive variable response, and reduce error from inaccurate parameter estimations.

Backwards, multivariate linear regression was performed at a level of 0.05 to refine Equation 11 to the most influential predictive parameters. Weisburg (2013) describes multivariate linear regression methods in detail. Multivariate linear regression was performed on the log-transformed full equation model, resulting in prediction estimates for each of the regression coefficients with associated standard error, *t* statistic, and *p* statistic. Standard error of the coefficient is a measure of the deviation in the coefficient across the full dataset and gauges the precision of the regression coefficient. The *t* statistic is the predicted coefficient divided by the standard error and the *p* statistic is the comparison of the *t* statistic to the Student's *t* distribution. Values of *p* less than or equal to 0.05 indicate that there is a 95% confidence that the independent variable is significant in the prediction of the dependent variable. Small *p* values do not necessarily indicate that the independent variable has a large impact on the dependent variable, only that the variable is significant for prediction within the specified mathematical model. Significant independent variables may have small regression coefficients. After the full model of Equation 11 was evaluated, the independent variable with the highest *p* score was identified and eliminated, creating a new equation model. The process was iterated on the truncated equation model until all remaining variables were determined as significant. Backwards regression procedures were conducted for the full dataset for each hydraulic ratio to formulate underlying core mathematical models.

Data collected from the physical model were observed to contain outlier data in some instances. Such data were attributed to turbulent structures or boundary interference for the velocity data and to instrumentation calibration errors for the boundary shear-stress data. Outlier data were found to significantly disrupt the prediction of the remainder of the model, most notably with the boundary shear-stress data. To account for the lack of prediction accuracy in the non-outlier data, a systematic approach was taken for all datasets for outlier identification and removal, and for regression optimization.

Squared error was calculated for all predictions from the paired regression models from the backwards linear regression procedure and the standard deviation of the error was determined. Data falling outside of two standard deviations of squared error, representing the data at the highest 2.3% of a normal error distribution, were identified as outliers and removed from further analysis. Approximately 5% to 15% of the data were removed from outlier analysis. Nonlinear regression was performed with coefficient constraints on the remainder of the dataset as it was found to produce a higher adjusted $R^2$ than with linear regression procedures. Calibration of regression parameters was conducted using the Generalized Reduced Gradient (GRG2) optimization code by minimizing the sum of the square error between observed and predicted values (Ladson and Warren, 1978).

For boundary shear-stress data at the outer-bank, a portion of the data had very small to negligible values. These values may have been real or artifacts of instrumentation error; regardless, the low shear-stress at these points skewed predictive equations to not apply well to non-zero values. Any outer-bank boundary shear-stress ratio value less than 0.1 was discarded from the analysis dataset in order to better describe the remaining data as a function of the identified independent parameters.

Coefficients were constrained for reduction of measurement error amplification and the intercept was limited for measurement precision requirements. A degree of uncertainty is typically associated with laboratory or field measurements of hydraulic parameters. Calibrated laboratory instrumentation may have error typically on the order of 5% of the measured value, and field assumptions for parameter determination can result in errors that are much larger. Structuring power-type regression equations for the reduction of measurement error propagation is possible using restraints on coefficient ranges. Figure 42 illustrates the prediction error in the dependent parameter as a function of measurement error in the independent variable and parameter coefficient. Error in the independent parameter is reduced for values less than unity and greater than approximately -1.5 and increased outside of that range. Ideally, all coefficients would be limited to the range [-1.5,1] to confidently minimize error augmentation; however, over-constraining values weakens the optimized regression fit and predictive power of the model.

Parameters were constrained to [-2,2] unless the resulting drop in adjusted $R^2$ was greater than 0.25, in which case the equation was not constrained. Regression intercepts establish the number of significant digits required for measurement precision. A lower limiting value of 0.01 was chosen to allow for the equations to apply to field scenarios without over-constraining the natural regression procedure.

For conservative design purposes, offset values were generated as two standard deviations of the error distribution away from the root mean square deviation of the truncated dataset. Offsets accounted for 97.7% of the data utilized for the equation development and provide a designer a mathematically grounded safety factor. Regression coefficients, error

statistics, observed and predicted plots, and equation offsets were determined for all twenty-four hydraulic prediction relationships represented by Equation 11.

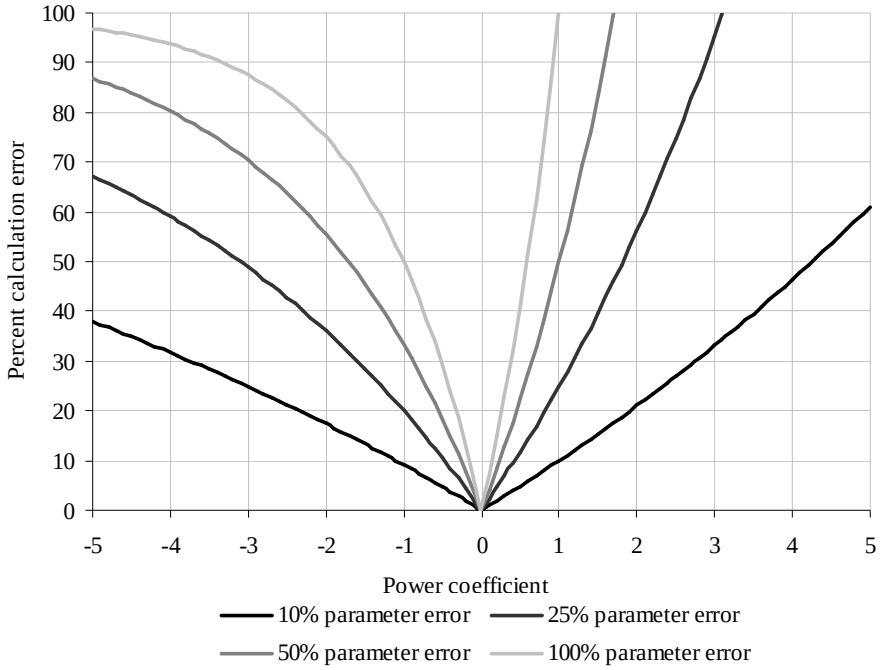


**Figure 42.** Parameter estimation error propagation in power-type prediction equations

## 4.7. Predictive mathematical models

Results of the regression analyses performed are described in detail. Equation coefficients for the all-structure, spur-dike, and vane velocity equations, and for the spur-dike boundary shear-stress equations are presented in tabular format with adjusted $R^2$, root-mean-square-deviation (*RMSD*), and offset values provided. Observed and predicted hydraulic ratios for outer-bank, centerline, and inner-bank are plotted with excluded outliers, line of perfect agreement, and calculated prediction offsets identified.

### 4.7.1. Velocity relationships

Regression analyses were performed on Equation 11 for the all-structure velocity dataset, spur-dike velocity dataset, and vane velocity dataset. Table 9 presents regression coefficients and statistics and Figure 43 provides the observed and predicted velocity ratios (black circle) with identified outlier data (red circle), perfect agreement line (black line), and offset line (hatched line) for the all-structure velocity equations. Values from Table 9 correspond to the regression weights of Equation 11. For example, evaluation of the $MVR_O$ ratio would yield; $MVR_O = 0.047A^{*-1.770}(L_{ARC}/T_W)^{0.770}(R_C/T_W)^{-0.232}(L_{W\text{-}PROJ}/T_W)^{0.572}$, where exponents of zero remove the parameter influence from the relationship. Values from Table 9, and subsequent tables, are referred to as the ratio equation set for a given structure type which includes all calculated ratios for the structure subset.

Overall, ratios were predicted to a high degree of accuracy, with maximum ratios predicted better than average ratios. Average values were more tightly grouped and had less of a distribution than the maximum values, especially for the outer-bank where 85% of the data were scattered between 0.1 and 0.2. The scatter within a narrow range resulted in more difficult prediction of *AVR* by a mathematical model than for the broader *MVR* distributions. The *RMSD* may be interpreted as the mean absolute percent error in channel velocity estimation, expressed in hundredths, as predicted values are normalized. Channel velocity is defined as the velocity ratio multiplied by the normalization factor. The *RMSD* for the all-structure equation set and was at or below 8% (0.08) for all ratios with a mean value of 7%. The spacing ratio was found to be significant for the outer-bank ratios only. Planimetric angle was found to be significant and positive for all ratios except $MVR_O$ and the lateral contraction ratio was significant for all ratios except $MVR_C$. Offset values were on the order of 15% (0.15) of the channel velocity estimation.

**Table 9.** $R^2$ and regression coefficients for Equation 11; all-structure velocity ratios

| Ratio | $R^2$ *Adj.* | *RMSD* | Intercept | *A** | $L_{ARC}/T_W$ | $R_C/T_W$ | $L_{W\text{-}PROJ}/T_W$ | $D_R$ | $2\theta/\pi$ | *offset* |
|---|---|---|---|---|---|---|---|---|---|---|
| $MVR_O$ | 0.835 | 0.084 | 0.047 | -1.770 | 0.770 | -0.232 | 0.572 | 0 | 0 | 0.148 |
| $MVR_I$ | 0.545 | 0.079 | 2.030 | 0 | 0 | 0 | 0.220 | -0.075 | 0.137 | 0.147 |
| $MVR_C$ | 0.580 | 0.098 | 1.497 | 0.159 | 0 | 0.143 | 0 | 0 | 0.101 | 0.317 |
| $AVR_O$ | 0.485 | 0.030 | 0.061 | 0 | 0.268 | 0 | -0.593 | 0.237 | 0.264 | 0.058 |
| $AVR_I$ | 0.432 | 0.080 | 1.743 | 0 | 0 | 0 | 0.211 | -0.047 | 0.087 | 0.150 |
| $AVR_C$ | 0.761 | 0.057 | 1.322 | 0.071 | 0 | 0.155 | 0.095 | 0 | 0.086 | 0.102 |

Table 10 details the results of the regression analysis for the spur-dike velocity dataset. Figure 44 illustrates the observed and predicted normalized values, the outliers excluded from analysis, perfect agreement lines, and offset lines. Normalized velocity maximum and average trends were predicted well, with adjusted $R^2$ values of 0.8 and above for all ratios except $AVR_O$. Observed data for $AVR_O$ were distributed with 89% of values scattered between 0.1 and 0.2, resulting in difficulties in mathematical model prediction. All values were predicted to a higher degree of accuracy for the isolated spur-dike equations than for the all-structure equations. Spacing ratios were statistically significant for the outer-bank predictions only, while the planimetric angle was found to be significant for the inner-bank and centerline only. Lateral contraction ratio was significant for all ratios except $AVR_C$ and the area contraction ratio was significant for outer-bank and centerline ratios. Crest submergence ratio was determined as significant for all values except $MVR_O$ and $AVR_C$. *RMSD* was the greatest for the $MVR_O$ at 8% and the mean for all ratios was 5%. Offset values varied between 5% and 15%, with a mean of 9%.

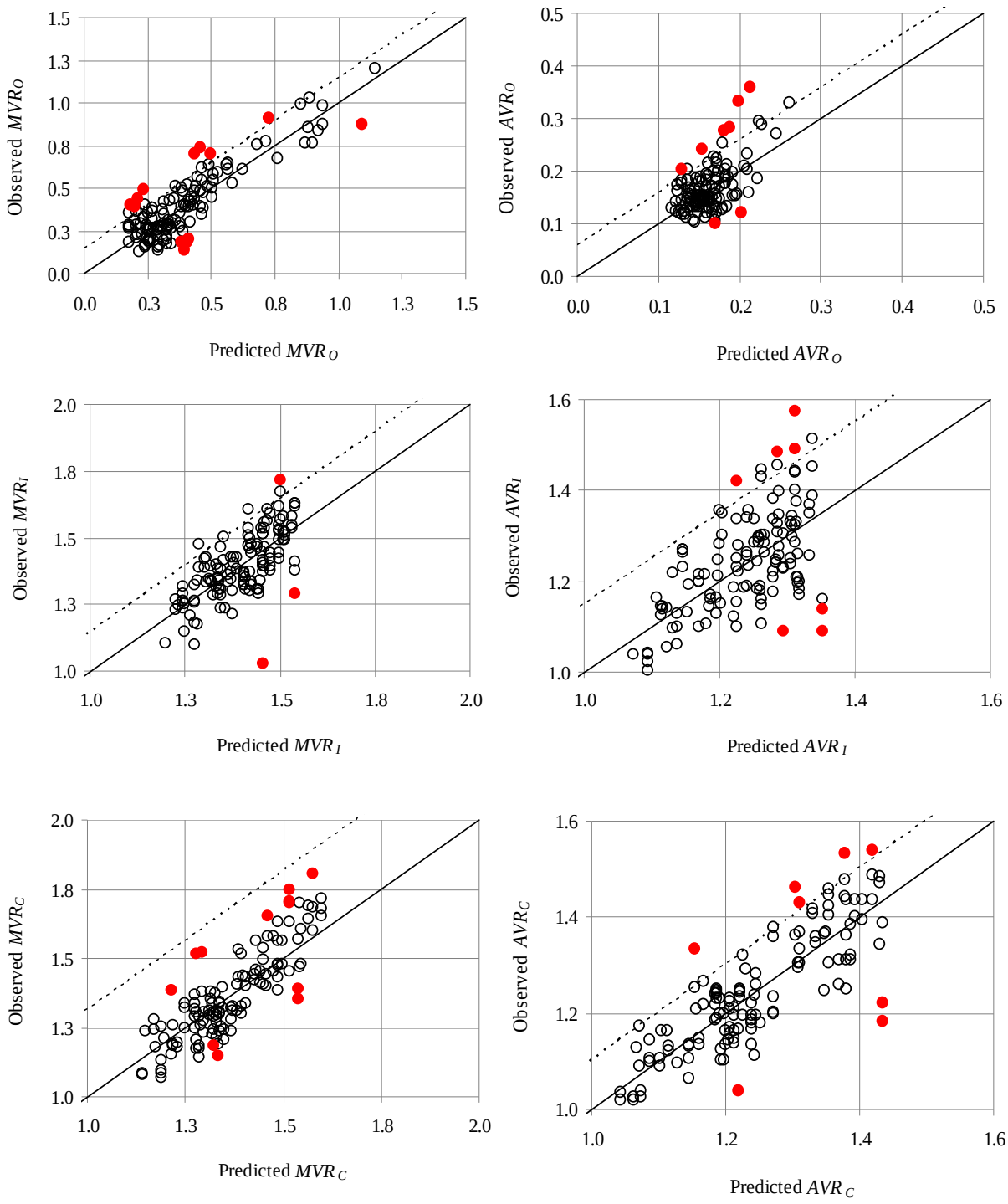


**Figure 43.** Velocity ratios for all-structure dataset

**Table 10.** $R^2$ and regression coefficients for Equation 11; spur-dike velocity ratios

| Ratio | $R^2$ *Adj.* | *RMSD* | *Intercept* | *A** | $L_{ARC}/T_W$ | $R_C/T_W$ | $L_{W\text{-}PROJ}/T_W$ | $D_R$ | $2\theta/\pi$ | *offset* |
|---|---|---|---|---|---|---|---|---|---|---|
| $MVR_O$ | 0.837 | 0.081 | 0.078 | -2.000 | 0.487 | 0 | 1.294 | 0 | 0 | 0.146 |
| $MVR_I$ | 0.791 | 0.056 | 2.124 | 0 | 0 | 0 | 0.244 | 0.158 | 0.187 | 0.096 |
| $MVR_C$ | 0.906 | 0.053 | 1.393 | 0.193 | 0 | 0.228 | -0.138 | 0.509 | 0.213 | 0.099 |
| $AVR_O$ | 0.664 | 0.025 | 0.121 | -1.684 | 0.725 | -0.408 | 1.335 | -2.000 | 0 | 0.046 |
| $AVR_I$ | 0.800 | 0.052 | 1.717 | 0 | 0 | 0.057 | 0.259 | 0.478 | 0.129 | 0.089 |
| $AVR_C$ | 0.814 | 0.057 | 1.312 | 0.155 | 0 | 0.173 | 0 | 0 | 0.170 | 0.110 |

Table 11 provides the regression results for the vane velocity dataset. Figure 45 illustrates observed and predicted normalized values, outliers excluded from analysis, perfect agreement lines, and offset lines. Predicted values from the isolated vane dataset were on the order of, or predicted better than, the all-structure equations. Spacing ratios were determined to be significant for the inner-bank ratios only, planimetric angle insignificant for all ratios, the area contraction significant for all ratios except $AVR_C$, and the channel curvature ratio universally significant. Lateral contraction was determined significant only for $AVR_O$. The only ratio which was unconstrained due to significant loss of adjusted $R^2$ was $AVR_O$ which exhibited coefficients outside of the ranges specified for error propagation minimization. Data were clustered at the lower ranges of $AVR_O$; 87% the data fell within the range of 0.1 to 0.2. Values of *RMSD* indicate less than 10% average error was associated with prediction of vane velocity ratios and the mean prediction error across all ratios was calculated at 5%. Offset values ranged from 4% to 17%, with a mean of 9%.

**Table 11.** $R^2$ and regression coefficients for Equation 11; vane velocity ratios

| Ratio | $R^2$ *Adj.* | *RMSD* | *Intercept* | *A** | $L_{ARC}/T_W$ | $R_C/T_W$ | $L_{W\text{-}PROJ}/T_W$ | $D_R$ | $2\theta/\pi$ | *offset* |
|---|---|---|---|---|---|---|---|---|---|---|
| $MVR_O$ | 0.833 | 0.087 | 0.010 | -1.316 | 0 | 0.769 | 0 | 0.325 | 0 | 0.165 |
| $MVR_I$ | 0.739 | 0.036 | 1.027 | 0.076 | -0.170 | 0.256 | 0 | 0.094 | 0 | 0.062 |
| $MVR_C$ | 0.895 | 0.048 | 1.300 | 0.093 | 0 | 0.143 | 0 | 0 | 0 | 0.090 |
| $AVR_O$ | 0.910 | 0.020 | 0.010 | -4.175 | 0 | 0.329 | 3.956 | 0 | 0 | 0.041 |
| $AVR_I$ | 0.529 | 0.052 | 0.654 | 0.150 | -0.213 | 0.375 | 0 | 0.151 | 0 | 0.091 |
| $AVR_C$ | 0.742 | 0.047 | 0.916 | 0 | 0 | 0.187 | 0 | 0.056 | 0 | 0.096 |

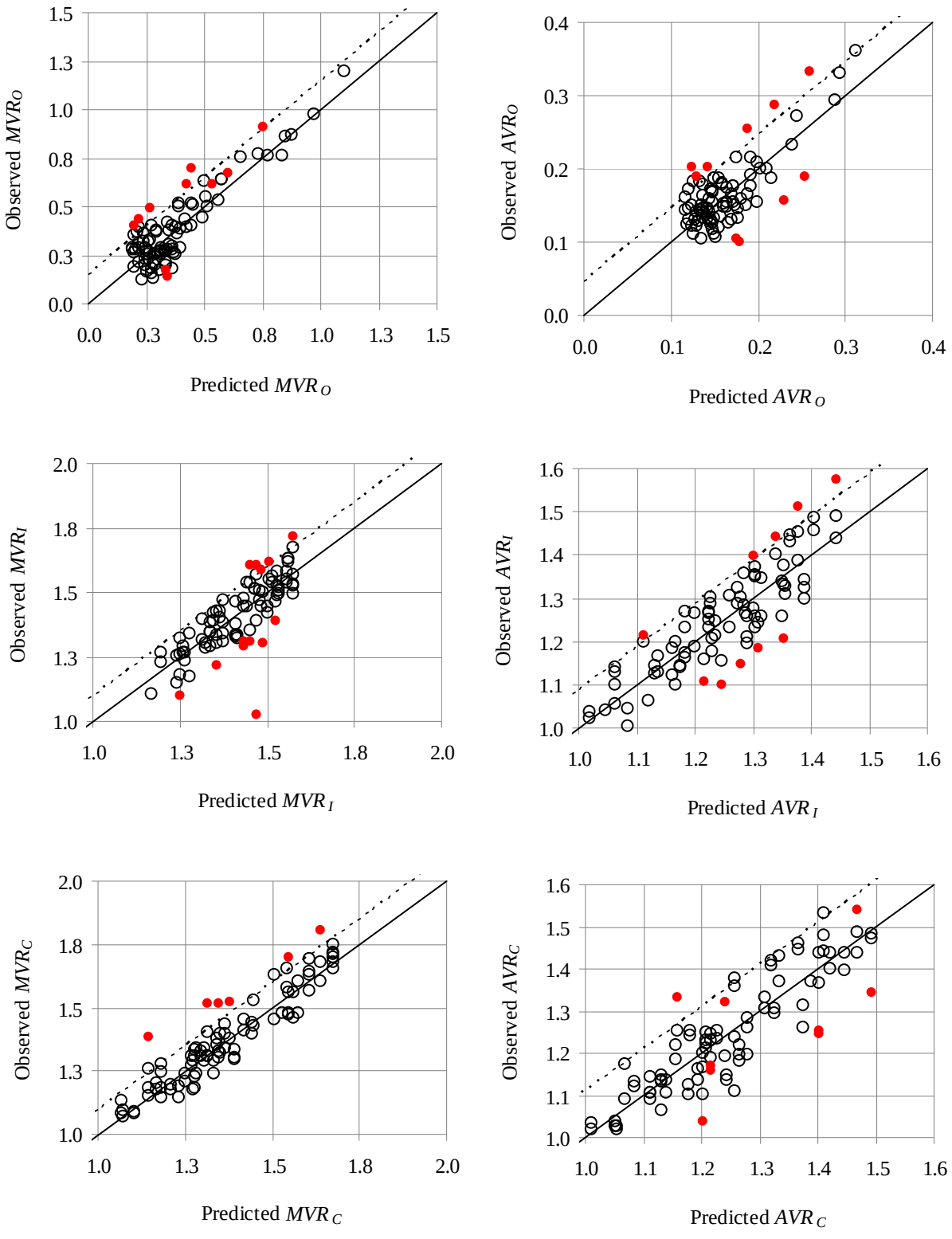


**Figure 44.** Velocity ratios for spur-dike dataset

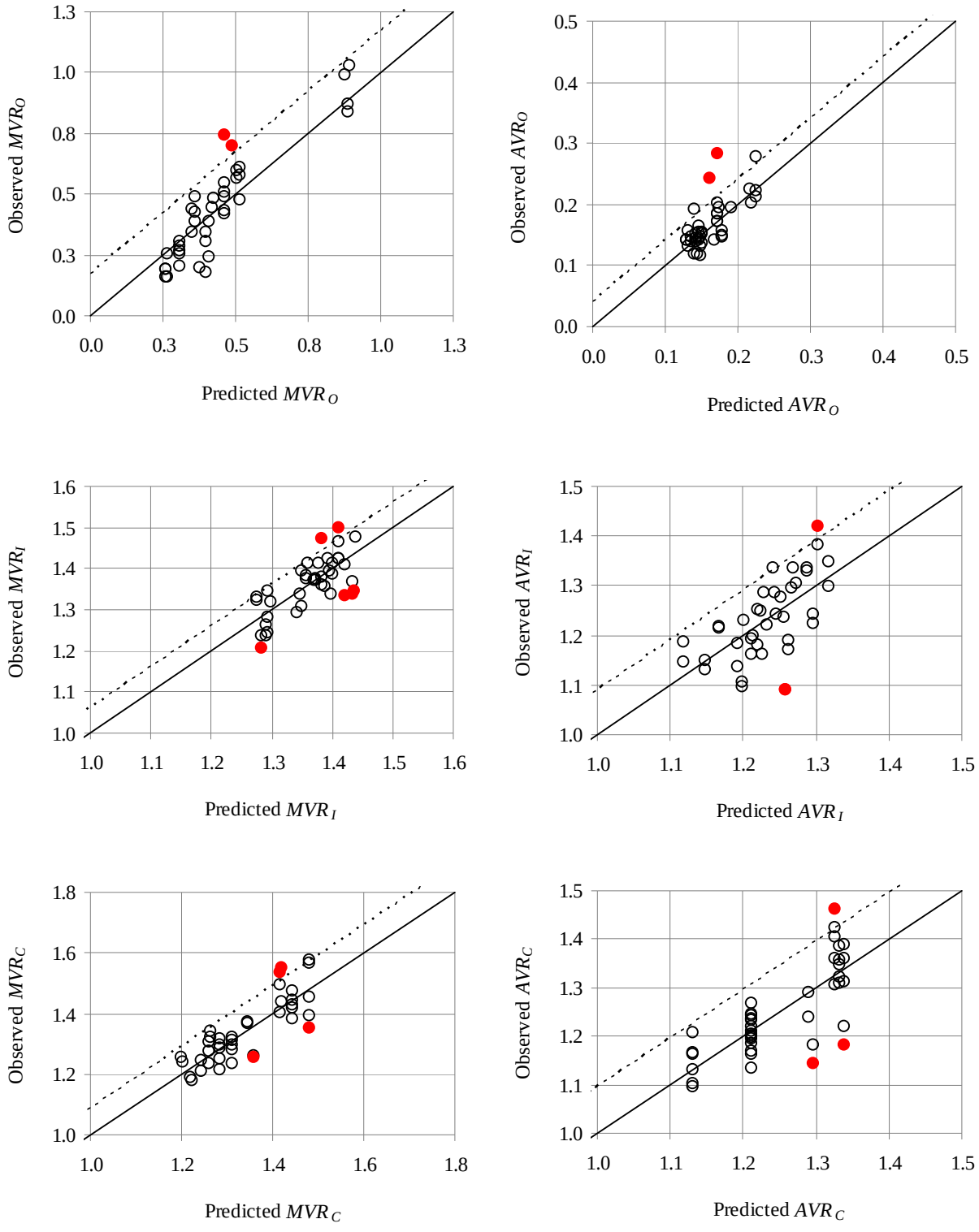


**Figure 45.** Velocity ratios for vane dataset

### 4.7.2. Boundary shear-stress relationships

Boundary shear-stress data were analyzed using regression procedures on Equation 11. Table 12 provides the regression results for the spur-dike boundary shear-stress dataset. Figure 46 provides observed and predicted normalized values, outliers excluded from analysis, perfect agreement lines, and offset lines. Boundary shear-stress ratios for spur-dikes were predicted to a lesser degree of accuracy than for the spur-dike velocity ratios by the order of $R^2$ of 0.1 and *RMSD* of 0.3. The spacing ratio and planimetric angle ratio were not found significant for any shear-stress ratio. Structure submergence was found as statistically significant for the shifted-conveyance zone, but not the outer-bank. Lateral contraction was significant for all shear-stress ratios except $M\tau R_O$ and the area contraction ratio was significant for all ratios except for $A\tau R_O$. Values of *RMSD* were much higher than for the predictive velocity ratios, were on the order of 30% error, and ranged up to 53% error for $M\tau R_O$. Offsets were similarly large, with a maximum of 111% and mean of 71% of the predicted channel velocity.

**Table 12.** $R^2$ and regression coefficients for Equation 11; spur-dike boundary shear-stress ratios

| Ratio | $R^2$ *Adj.* | *RMSD* | *Intercept* | *A** | $L_{ARC}/T_W$ | $R_C/T_W$ | $L_{W\text{-}PROJ}/T_W$ | $D_R$ | $2\theta/\pi$ | *offset* |
|---|---|---|---|---|---|---|---|---|---|---|
| $M\tau R_O$ | 0.591 | 0.527 | 0.100 | -1.313 | 0 | 0 | 0 | 0 | 0 | 1.113 |
| $M\tau R_I$ | 0.685 | 0.307 | 0.591 | 0.991 | 0 | 0.379 | -1.614 | 1.6085 | 0 | 0.640 |
| $M\tau R_C$ | 0.838 | 0.385 | 0.442 | 1.163 | 0 | 0.768 | -1.702 | 1.25847 | 0 | 0.705 |
| $A\tau R_O$ | 0.553 | 0.304 | 0.100 | 0 | 0 | 0.349 | -1.065 | 0 | 0 | 0.591 |
| $A\tau R_I$ | 0.674 | 0.296 | 0.526 | 0.960 | 0 | 0.483 | -1.443 | 1.6839 | 0 | 0.583 |
| $A\tau R_C$ | 0.746 | 0.334 | 0.479 | 0.926 | 0 | 0.597 | -1.401 | 1.33805 | 0 | 0.644 |

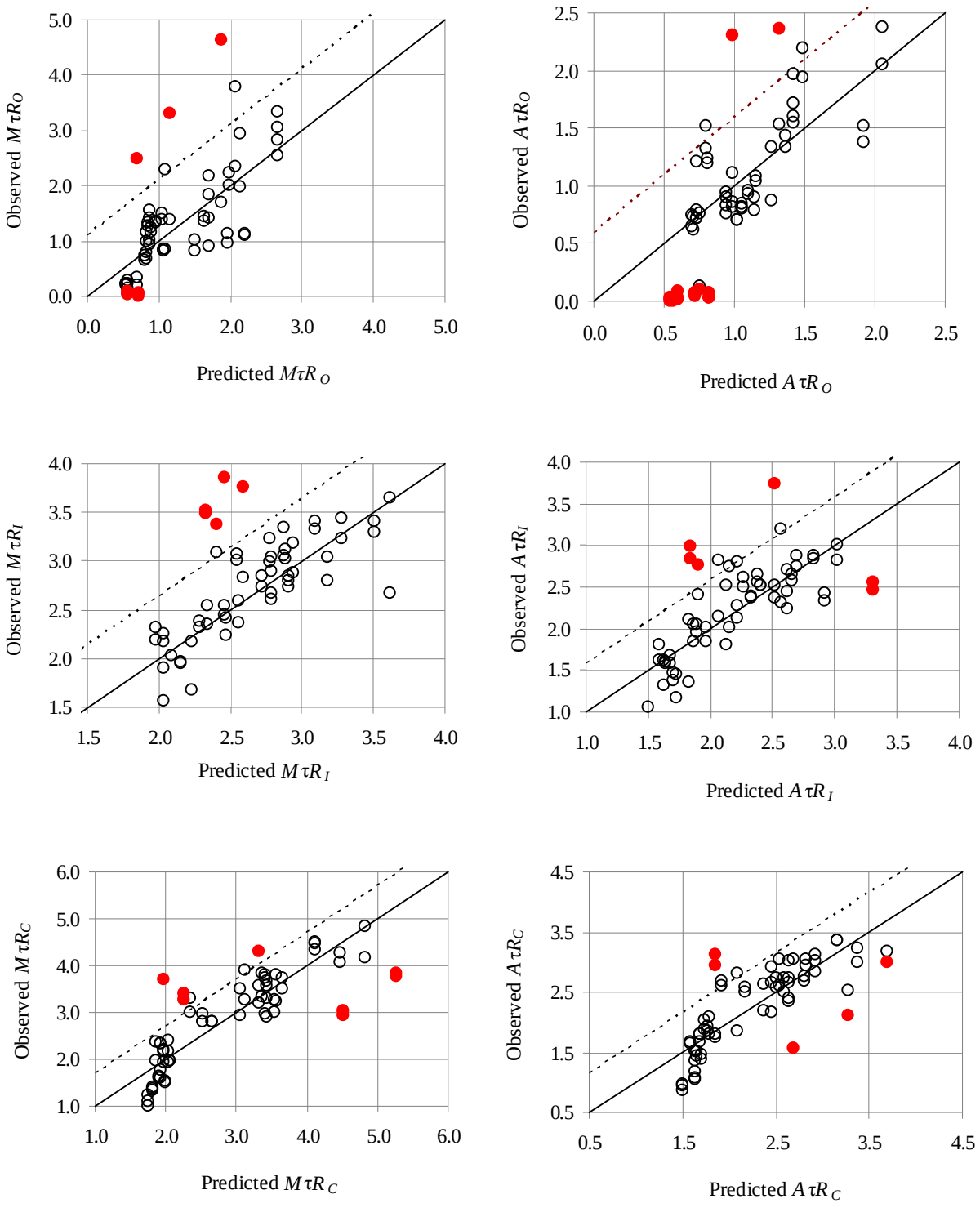


**Figure 46.** Spur-dike ratios for spur-dike dataset

## 4.8. Parameter response and sensitivity

Equations were shown to approximate hydraulics within the model to a statistically significant level for all hydraulic ratios as indicated by positive $R^2$ values generally above 0.5. Performed statistics and generated plots do not provide comprehensive insight into ratio dependence upon parameter adjustments. It is difficult to fully predict the equation response due to alteration of independent, non-dimensional parameters, especially considering developed equations contained interrelated dimensionless parameters, such as $A^*$, the lateral contraction ratio, and the submergence ratio. Parameters without joint interaction affect the ratio according to the regression exponent of the dimensionless ratio. Joint parameters affect the dependent ratio as a combination of regression exponents and with the underlying interrelating function. Physical expectations of individual parameter alteration on the hydraulic ratio may be evaluated through a sensitivity analysis of the regression results. To visualize the effects of parameter alteration, variables were altered through and past the laboratory data ranges while all other parameters were held static. Responses of each hydraulic ratio to individual parameter alteration were determined, sensitivity of the equations to parameter alteration is discussed, and implications for extrapolation past laboratory ranges are presented.

### 4.8.1. Laboratory data ranges

Six independent design variables were identified which were fundamental for the dimensionless ratios of Equation 11. For each velocity and shear-stress ratio, $L_{W\text{-}PROJ}$, $L_{ARC}$, $R_C$, $\Delta z$, $T_W$, and $\theta$ were altered and the effects of the resulting altered dimensionless grouping on the hydraulic ratios were calculated. Equation 10 was used as the relating mathematical expression for $A^*$, $L_{W\text{-}PROJ}$, and $\Delta z$. Median laboratory data were calculated and were incorporated as static

inputs for all variables except the parameter under examination. The dynamic variable was altered incrementally, starting below the minimum laboratory value and extending beyond the maximum value. Table 13 provides the median value and range of laboratory values for each parameter altered for the velocity and shear-stress ratios.

**Table 13.** Static median values and ranges of laboratory data

| *All-data* | Median | Minimum | Maximum |
|---|---|---|---|
| $L_{W\text{-}PROJ}$ [ft] | 3.10 | 1.06 | 5.14 |
| $L_{ARC}$ [ft] | 19.07 | 8.54 | 29.60 |
| $T_W$ [ft] | 12.61 | 9.59 | 15.63 |
| $R_C$ [ft] | 52.29 | 38.75 | 65.83 |
| $h_W$ [ft] | 0.46 | 0.13 | 0.78 |
| $D_B$ [ft] | 0.75 | 0.60 | 0.91 |
| $A^*$ | 0.19 | 0.11 | 0.27 |
| $L_{W\text{-}PROJ}/T_W$ | 0.24 | 0.11 | 0.37 |
| $L_{ARC}/T_W$ | 1.82 | 0.55 | 3.09 |
| $R_C/T_W$ | 4.67 | 2.48 | 6.86 |
| $D_R$ | 3.99 | 1.00 | 6.98 |
| $2\theta/\pi$ | 0.83 | 0.67 | 1.00 |

| *Spur-dike* | Median | Minimum | Maximum |
|---|---|---|---|
| $L_{W\text{-}PROJ}$ [ft] | 2.59 | 1.06 | 4.13 |
| $L_{ARC}$ [ft] | 19.07 | 8.54 | 29.60 |
| $T_W$ [ft] | 12.61 | 9.59 | 15.63 |
| $R_C$ [ft] | 52.29 | 38.75 | 65.83 |
| $h_W$ [ft] | 0.78 | 0.77 | 0.78 |
| $D_B$ [ft] | 0.75 | 0.60 | 0.91 |
| $A^*$ | 0.19 | 0.11 | 0.27 |
| $L_{W\text{-}PROJ}/T_W$ | 0.20 | 0.11 | 0.28 |
| $L_{ARC}/T_W$ | 1.82 | 0.55 | 3.09 |
| $R_C/T_W$ | 4.67 | 2.48 | 6.86 |
| $D_R$ | 1.09 | 1.00 | 1.18 |
| $2\theta/\pi$ | 0.83 | 0.67 | 1.00 |

| *Vane* | Median | Minimum | Maximum |
|---|---|---|---|
| $L_{W\text{-}PROJ}$ [ft] | 3.40 | 1.66 | 5.14 |
| $L_{ARC}$ [ft] | 15.30 | 8.54 | 22.06 |
| $T_W$ [ft] | 12.61 | 9.59 | 15.63 |
| $R_C$ [ft] | 52.29 | 38.75 | 65.83 |
| $h_W$ [ft] | 0.41 | 0.13 | 0.69 |

| *Vane* | Median | Minimum | Maximum |
|---|---|---|---|
| $D_B$ [ft] | 0.75 | 0.60 | 0.91 |
| $A^*$ | 0.15 | 0.11 | 0.19 |
| $L_{W\text{-}PROJ}/T_W$ | 0.26 | 0.15 | 0.37 |
| $L_{ARC}/T_W$ | 1.42 | 0.55 | 2.30 |
| $R_C/T_W$ | 4.67 | 2.48 | 6.86 |
| $D_R$ | 4.06 | 1.14 | 6.98 |
| $2\theta/\pi$ | 0.83 | 0.67 | 1.00 |

### 4.8.2. Summarized parameter response

Regression equations performed on the all-structure, spur-dike, and vane velocity and boundary shear-stress datasets were examined to calculate physical parameter response and sensitivity. Each database subset contained six normalized predictions with unique regression coefficients. For each structure subset and ratio, the six identified physical parameters were altered to investigate response and sensitivity. Equation response to each parameter alteration was plotted as a function of the containing dimensionless parameter. Plots and descriptions of the ratio responses are provided in Appendix A3. A general summary of important trends in parameter response and sensitivity are addressed.

The compiled ratio sensitivities to parameter alteration revealed recurring trends regarding hydraulics associated with instream structure installation and predictive methodology behavior. Ratio responses typically adhered to expectations of hydraulics as reported within the literature. Maximum ratios were always predicted higher than average ratios and conservation principles were observed through opposite response at the reduced and increased conveyance zones. Combined effects on the hydraulic ratios of each adjusted parameter were compared to the expected physical trends during model development and rationale pertaining to how well the hydraulics responded to physical intuition is provided.

The channel curvature ratio was hypothesized to exhibit higher erosion reduction at the outer-bank for values of $R_C/T_W$ closer to the maximum observed values of approximately 3 from Nanson and Hickin (1986). For all outer-bank ratios except the vane velocity dataset, response to curvature ratio alteration was minimal, growing slightly for $A\tau R_O$, and decreasing slightly for the all-structure velocity $MVR_O$ and spur-dike $AVR_O$. This increase, coupled with the negligible or insignificant decreasing effects, may illustrate that tighter channel-bends may experience channel-wide reduced hydraulics due to instream structure installation. Effects are influenced by the limited variance for $R_C/T_W$ within the laboratory dataset and may have been influenced by normalization condition dependence upon volumetric flow rate, which is directly linked to $T_W$.

Results from McCoy et al. (2007) and Scurlock et al. (2013a) indicated that a spacing threshold may exist as a function of the leeward zone of structure influence, such that spacing ratios exceeding the threshold may not fully reduce outer-bank hydraulics. McCoy et al. (2007) and Scurlock et al. (2013a) indicated a return to undisturbed flow conditions at a maximum spacing of two and five times the structure length, respectively. A corresponding increase in the shifted-conveyance hydraulics was expected for smaller spacing ratios due to continuity, yet effects were also likely threshold dependent. Slight increase in velocities were noted at the outer-bank with increased spacing for the all-structure and spur-dike datasets, with all shifted-conveyance ratios not significantly affected. Vane velocity equations depicted inner-bank velocity decay with increased structure spacing as more conveyance was carried to the outer-bank and negligible response for all other ratios. Shear-stress was not significantly affected by the structure spacing ratio. Increased spacing ratios reduced structure efficacy for spur-dikes at the outer-bank and decreased the inner-bank vane velocity for the ranges of ratios evaluated in the laboratory.

Lateral contraction of the instream structures was hypothesized to strongly impact the induced hydraulic fields, with increased values reducing outer-bank hydraulics and increasing hydraulics in the shifted-conveyance zone. Increasing the lateral contraction ratio through $L_{W\text{-}PROJ}$ was shown to be significant for all hydraulic ratios. At the outer-bank zone, increase in $L_{W\text{-}PROJ}$ reduced the velocity or boundary shear-stress in a rapidly decaying fashion. Outer-bank ratios decayed rapidly from a vertical asymptote below the minimum laboratory data range and moved through the laboratory range to relatively constant extrapolation. Smaller values of $L_{W\text{-}PROJ}/T_W$ (less than approximately 0.2) were found to result in high sensitivity in ratio response. Shifted-conveyance ratios had different responses for the velocity and shear-stress parameters. For all shifted-conveyance velocity ratios, increased $L_{W\text{-}PROJ}$ had a direct relationship with velocity increase and was shown to extrapolate smoothly outside of laboratory bounds. Spur-dike boundary shear-stress shifted-conveyance ratios grew in value from the lower laboratory range to a maximum near $L_{W\text{-}PROJ}/T_W$ of 0.15, then decayed with increasing $L_{W\text{-}PROJ.}$ Shear-stress ratio response was unexpected, indicating that increased structure length resulted in higher boundary shear-stress.

Submergence of instream structures has been indicated through a variety of numerical, field, and laboratory studies to significantly affect secondary channel currents and outer-bank velocity conveyance to the crest key-in with the bankline. Submergence effects have been noted as highly complex and yet to be fully realized. Expectations from the literature review suggested that conveyance diverted to the outer-bank from structure submergence would result in erosive increase within the structure field and a decrease in the shifted-conveyance zone due to continuity principles (Jamieson et al., 2013, Scurlock et al. 2013a). Ratio response to altered submergence was the most complex of all parameter interactions. Vane velocity equations

generally respond to purported physical expectations, yet the outer-bank velocity ratios were highly sensitive to the velocity ranges and produced unreasonable values moving past 2.75, well within the laboratory maximum of 6.98. Similar results were found for the all-structure velocity dataset; shifted-conveyance ratios were negatively impacted by increasing submergence, velocities at the outer-bank were increased, yet a sensitive reaction was observed for the $MVR_{O.}$ Spur-dike velocity ratios did not exhibit this vertical asymptote within laboratory bounds. Discretion should be advised in application of the velocity equations to vanes outside of submergence ratios of 2.75, or spur-dikes outside of 1.18. Both spur-dike ratios, velocity and boundary shear-stress, exhibited general positive reactions across the full channel to submergence. Response at the shifted-conveyance zone was slight, but generally positive, which was not physically expected. It is hypothesized that increased hydraulics at the shifted-conveyance zone may have been attributed to the interference of the plunging jet flow over the submerged crest with the inter-structure eddy zone, reducing turbulence and allowing for more conveyance downstream.

Planimetric angle response was expected to have minimal effect for non-submerged structures and to have a positive effect for the redirection of flows to the shifted-conveyance zone during submerged conditions. Vanes and boundary-shear stress ratios were not affected by planimetric angle adjustment. A small, gradual positive effect was noted for the shifted-conveyance zone for spur-dikes only which is in contrast to the physical expectations; 90º structures produced higher shifted conveyance than upstream-angled structures. Acceleration effects around the structure tip coupled with potentially increased volumetric storage within upstream-angled configurations may explain the response; however, true reasons merit further investigation.

Channel $T_W$ serves as a primary factor in all dimensionless parameters with the exception of the planimetric angle ratio. As such, its impacts on the hydraulic ratios represent a measure of cumulative equation response. All hydraulic ratios exhibited response to $T_W$ alteration; increased $T_W$ produced an increase in outer-bank hydraulics and a decrease in shifted-conveyance hydraulics. Shear-stress ratios responded to a more significant degree than the velocity ratios to perturbation of $T_W$, primarily due to the larger range of predicted ratios and instrumentation accuracy. Response mimics that of $L_{W\text{-}PROJ}$ to the largest degree, with illustrated vertical asymptotic tendencies towards the lower limit of the laboratory ranges for the outer-bank ratios. This lends credence to the significance of $L_{W\text{-}PROJ}$ in the prediction of induced channel-bend hydraulics. Continuity between the outer-bank and shifted-conveyance zones and physically correct equation response to changes in $T_W$ provides a significant level of validity to the formulated mathematical prediction models.

## 4.9. Model development summary

Mean-flow velocity and boundary shear-stress data collected from the CSU physical modeling research of Heintz (2002), Darrow (2004), and Schmidt (2005) were organized for visualization, segmented into regions, and normalized by bend-averaged baseline hydraulic values. Three different regions of influence were identified as the outer-bank, centerline, and inner-bank, which were defined by regions of hydraulic influence or point-based methodologies. Maximum and averaged normalized values were described as a function of dimensionless geometric properties of the channel and structure configurations such that equations were scale independent. Consideration was given to the physical meaning of each dimensionless parameter and to implications for field implementation during model development.

Regression analyses were conducted to tailor the developed functional relationship to specific expressions for the maximum and average outer-bank, centerline, and inner-bank velocity and boundary shear-stress ratios. Equations quantified velocity and shear-stress trends for the spur-dike structures and quantified velocity for the independent vane and combined structure dataset. A set of twenty-four equations were developed for the quantification of induced structure hydraulics as summarized by Table 9, Table 10, Table 11, and Table 12. Equation coefficients and error metrics were tabulated and observed vs. predicted plots were generated. Generally, the velocity equations performed to a higher degree of accuracy than the shear-stress equations, and the structure specific velocity equations performed better than the all-structure equations. Velocity and shear-stress equations quantified laboratory data with mean error on the order of 5% and 30%, respectively. Predictive mathematical models were analyzed using parameter response and sensitivity analysis. Reaction of the equations provided key insights to physical parameter response, application ranges, and extrapolation viability. The developed models were shown to apply well to the laboratory data; however, further analysis of the developed methodologies is necessary to reveal equation applicability to natural topographies and as a design optimization tool.

# 5. Developed methodology analyses and design application

Mathematical prediction methods for the quantification of induced instream structure hydraulics were developed and tailored to a robust physical model dataset. Results indicated a high level of equation functionality and performance in quantifying hydraulic trends within the model. Equations were developed to minimize parameter estimation error, provide ease of measurement within the field, and to readily apply to natural topographies. Full evaluation of the predicted methods requires application to data collected in natural topography instream structure configurations. This section evaluates developed models with extraneous data from the literature, applies developed models to a hypothetical design scenario, and discusses implications for usage in natural channel instream structure design.

## 5.1. Equation application to natural-channel topography

Application of the developed methodologies to natural channel topographies was accomplished through identification of studies within the literature which reported sufficient data to substantiate approximation of each term in Equation 11. Developed velocity equations were applied to extraneous datasets only. Data reported from the literature centered primarily on specific structure or configuration hydraulics and did not place emphasis on reporting maximum field velocities or documenting specific geometric parameters needed to evaluate the design methodologies. Literature detailing instream structures with required detail included Lyn and Cunningham (2010), Bui (2011), Thornton et al. (2011), Scurlock et al. (2013a), and Scurlock et al. (2013b). Comparison studies span two physical model flumes and one field site and had a cumulative of twenty unique instream structure configurations for equation evaluation.

Research conducted by Thornton et al. (2011), Scurlock et al. (2013a), and Scurlock et al. (2013b) collected sufficient data that determination of each term from Equation 11 was accomplished by a query of reported datasets. Field data from Bui (2011) and laboratory data from Lyn and Cunningham (2010) required additional analysis to determine necessary parameters.

Bui (2011) field structure geometries and baseline cross sections were extracted from construction schematics reported by BIO-WEST (2006) and channel curvature was taken from aerial photography (Google, 2007). A HEC-RAS model (USACE, 2010) was created, set with normal depth conditions at seepage-adjusted discharges for the measurement conditions of Bui (2011), and calibrated to the reported water surface elevations to extract bend-averaged cross-sectional baseline velocity required for the computation of *MVR* and *AVR*. Point velocities from Bui (2011) were designated regions based upon their relative location to the structure field; points within the structure field were designated within the outer-bank region and points off the structure crest were set at the centerline region.

Lyn and Cunningham (2010) reported geometries of evaluated structure configurations and the channel-bend, and provided planimetric interpolations of velocity fields. Inlet velocity was reported and used as a surrogate for the bend-averaged baseline velocity. Induced structure velocities were selected from velocity field interpolations with visual region identification and were subjective due to the full dataset not reported. Lyn and Cunningham (2010) and the field data from Bui (2011) did not report sufficient data to compute all velocity ratios.

Table 14 presents the determined dimensionless ratios for Equation 11 from the literature studies and the laboratory ranges. The majority of structures found from the literature were bendway weirs which coincided with traditional design overtopping conditions. Studies which

evaluated structures specifically tested in the trapezoidal physical model included Thornton et al. (2011) and Scurlock et al. (2013b). Dimensionless parameters typically fall within the ranges of laboratory data. Exceptions were found in the channel-curvature ratio for selected tests from Thornton et al. (2011), Scurlock et al. (2013a), and Scurlock et al. (2013b) and the BW05 configuration lateral contraction ratio from Scurlock et al. (2013b).

**Table 14.** Parameters determined for method evaluation from the literature

| Study | Configuration | Str. Class | $A^*$ | $L_{ARC}/T_W$ | $R_C/T_W$ | $L_{W\text{-}PROJ}/T_W$ | $D_R$ | $2\theta/\pi$ |
|---|---|---|---|---|---|---|---|---|
| Lyn and Cunningham (2010) | H050-V22-T24A,B | bendway weir | 0.119 | 0.920 | 3.332 | 0.241 | 2.000 | 0.833 |
| | H050-V22-T48 | bendway weir | 0.119 | 0.920 | 3.332 | 0.241 | 2.000 | 0.833 |
| | H050-V25-T12A,B | bendway weir | 0.119 | 0.920 | 3.332 | 0.241 | 2.000 | 0.833 |
| | H075-V22-T48 | bendway weir | 0.105 | 0.920 | 3.332 | 0.241 | 1.333 | 0.833 |
| | H100-V22-T48 | spur-dike | 0.105 | 0.920 | 3.332 | 0.241 | 1.000 | 0.833 |
| Bui (2011) | 2,237 cfs | bendway weir | 0.128 | 0.373 | 3.358 | 0.124 | 1.587 | 0.778 |
| | 2,971 cfs | bendway weir | 0.107 | 0.339 | 3.054 | 0.113 | 1.498 | 0.778 |
| | 2,944 cfs | bendway weir | 0.108 | 0.341 | 3.068 | 0.114 | 1.500 | 0.778 |
| Thornton et al. (2011) | NW01 | spur-dike | 0.108 | 1.570 | 8.154 | 0.194 | 1.000 | 1.000 |
| | NW02 | spur-dike | 0.194 | 1.021 | 3.613 | 0.250 | 1.000 | 0.667 |
| | NW03 | spur-dike | 0.108 | 1.489 | 8.154 | 0.298 | 1.000 | 0.667 |
| | NW04 | spur-dike | 0.194 | 1.077 | 3.613 | 0.171 | 1.000 | 1.000 |
| Scurlock et al. (2013a) | BW01 | bendway weir | 0.159 | 1.203 | 8.273 | 0.351 | 1.734 | 1.000 |
| | BW02 | bendway weir | 0.169 | 0.861 | 4.100 | 0.234 | 1.644 | 0.667 |
| | BW03 | bendway weir | 0.256 | 1.003 | 7.864 | 0.368 | 1.549 | 0.667 |
| | BW04 | bendway weir | 0.222 | 0.986 | 3.793 | 0.237 | 1.490 | 1.000 |
| Scurlock et al. (2013b) | BW05 | bendway weir | 0.152 | 1.003 | 7.864 | 0.383 | 1.752 | 0.667 |
| | BW06 | bendway weir | 0.194 | 0.986 | 3.793 | 0.250 | 1.681 | 1.000 |
| | SD05 | spur-dike | 0.194 | 1.003 | 7.864 | 0.261 | 1.000 | 0.667 |
| | V05 | vane | 0.162 | 1.003 | 7.864 | 0.261 | 1.169 | 0.667 |
| Current research | Maximum | variable | 0.270 | 3.085 | 6.862 | 0.373 | 6.984 | 1.000 |
| | Minimum | variable | 0.108 | 0.547 | 2.479 | 0.110 | 1.000 | 0.667 |
| | Median | variable | 0.189 | 1.816 | 4.670 | 0.242 | 3.992 | 0.833 |

Table 15 provides the determined velocity ratios for each comparison study. It is noted that many studies illustrated maximum velocity ratios at the outer-bank which exceeded unity.

Outer-bank velocity zones were found within configurations that increased velocities higher than the baseline bend-average. These studies include H050-V22-T24A,B from Lyn and Cunningham (2010), NW01 and NW02 from Thornton et al. (2011), and BW02 from Scurlock et al. (2013a). The configuration from Lyn and Cunningham (2010) was the only study found to exhibit an $AVR_O$ greater than unity due to significant conveyance directed to the outer-bank key-in of the evaluated bendway weirs.

**Table 15.** Computed velocity ratios for comparison

| Study | Configuration | $MVR_O$ - | $MVR_I$ - | $MVR_C$ - | $AVR_O$ - | $AVR_I$ - | $AVR_C$ - |
|---|---|---|---|---|---|---|---|
| Lyn and Cunningham (2010) | H050-V22-T24A,B | 1.364 | 1.250 | 1.364 | 1.151 | 1.136 | 1.182 |
| | H050-V22-T48 | | 1.250 | 1.364 | | 1.068 | 1.364 |
| | H050-V25-T12A,B | | 1.364 | 1.477 | | 1.273 | 1.409 |
| | H075-V22-T48 | | 1.250 | 1.364 | | 1.108 | 1.250 |
| | H100-V22-T48 | | 1.250 | 1.364 | | 1.165 | 1.273 |
| Bui (2011) | 2,237 cfs | 0.229 | | 0.440 | 0.184 | | 0.431 |
| | 2,971 cfs | 0.215 | | | 0.180 | | |
| | 2,944 cfs | | | 0.309 | | | 0.290 |
| Thornton et al. (2011) | NW01 | 1.442 | 1.235 | 1.354 | 0.918 | 0.971 | 1.089 |
| | NW02 | 0.666 | 1.422 | 1.676 | 0.252 | 0.866 | 1.212 |
| | NW03 | 0.663 | 1.421 | 1.598 | 0.264 | 1.209 | 1.079 |
| | NW04 | 1.594 | 1.215 | 1.880 | 0.782 | 0.868 | 1.285 |
| Scurlock et al. (2013a) | BW01 | 0.864 | 1.829 | 1.829 | 0.554 | 1.208 | 1.208 |
| | BW02 | 1.795 | 1.948 | 1.948 | 0.458 | 1.740 | 1.740 |
| | BW03 | 0.692 | 1.690 | 1.690 | 0.411 | 1.060 | 1.060 |
| | BW04 | 0.917 | 1.990 | 1.990 | 0.303 | 1.497 | 1.497 |
| Scurlock et al. (2013b) | BW05 | 0.868 | 1.872 | 1.872 | 0.290 | 0.779 | 0.779 |
| | BW06 | 0.924 | 1.919 | 1.919 | 0.318 | 1.136 | 1.136 |
| | SD05 | 0.608 | 2.491 | 2.491 | 0.147 | 0.843 | 0.843 |
| | V05 | 0.587 | 1.837 | 1.837 | 0.190 | 0.810 | 0.810 |

Developed spur-dike and vane prediction models were applied to the structure configurations from the literature which matched respective structure classifications. Bendway-weir structures were compared to the all-structure prediction equations. Calculated results and absolute error between observed and predicted values are tabulated in Appendix A4. Figure 47 provides plotted observed and predicted value for all velocity ratios with the line of perfect agreement and offset line illustrated. The offset illustrated was for the all-structure equations

which uniformly represented the maximum offset of the three equation sets. Each literature study is plotted as a separate series on Figure 47 and it is observed that the developed models predicted natural topography instream structures to varying degrees of accuracy. Results of equation application are analyzed and discussed for each study.

The two bendway-weir studies with mobile boundaries were evaluated with the all-structure prediction equations from Table 9. As illustrated in Figure 47, Lyn and Cunningham (2010) maximum and average velocities were under-predicted at the outer-bank yet were fairly well described at the inner-bank and centerline. The outer-bank velocities reported by Lyn and Cunningham (2010) were found to be greater than the normalization conditions and represented bendway-weir specific hydraulics. Outer-bank ratios greater than unity and predicted outer-bank velocity reduction led to errors on the order of 100%. Conversely, prediction error for the inner-bank and centerline ratios was well predicted, on the order of 10%. Structure field hydraulics from Bui (2011) were very well described by the predictive velocity ratios. Outer-bank maximum values were predicted with 4% error and average values were predicted with 2% error. Centerline velocities were over-estimated by approximately 100%, representing inaccurate, but conservative equation response. Data reported from Bui (2011) indicate centerline velocities less than the normalization condition which was not observed in the laboratory and contributes to the over-prediction error. For the mobile-bed bendway-weir studies, data which were considered appropriate for comparison to physical model conditions, the shifted conveyance values of Lyn and Cunningham (2010) and outer-bank values of Bui (2011), were predicted with less than 10% error.

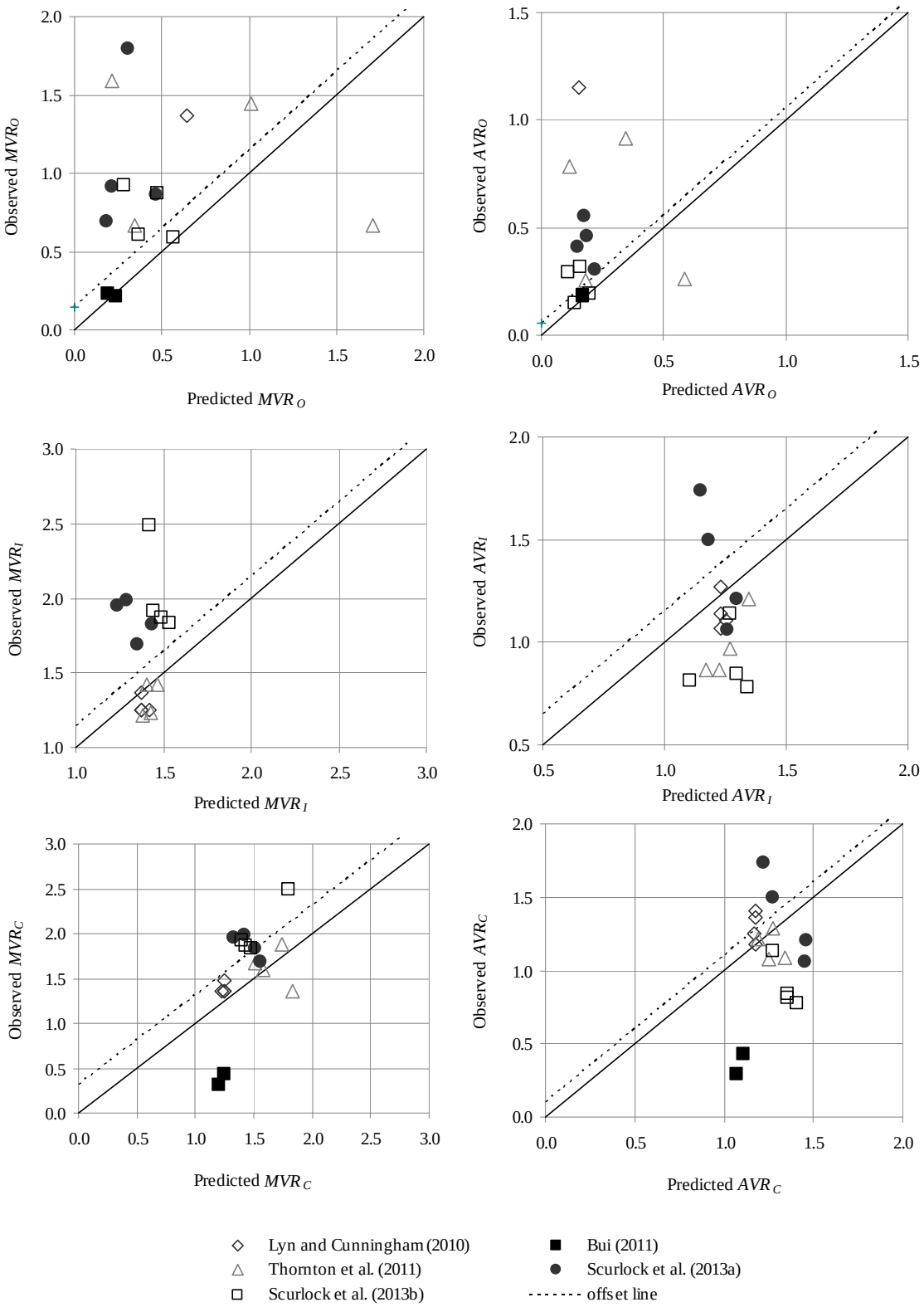


**Figure 47.** Evaluation of developed methodologies with literature data

Rigid-bed spur-dike and vane studies were the only structures found for which equations were directly developed and are summarized in Table 10 and Table 11, respectively. The spur-dikes of Thornton et al. (2011) contained two structure configurations which exhibited higher maximum velocities at the outer-bank than the baseline bend-averaged conditions. As illustrated in Figure 47, the developed methodology marginally predicted these maximums, under-predicting by upwards of 140%. Average outer-bank velocities for these configurations were similarly under-predicted, but by a lesser amount of approximately 65%. Of the two configurations which reduced outer-bank velocities below baseline conditions, one was over-predicted (NW03) and one was predicted with reasonable accuracy (NW04). NW03 exceeded the laboratory range of $R_C/T_W$ which may explain the under-prediction. NW04 maximum and average outer-bank velocities were under-predicted by 30% and 7%, respectively. Inner-bank and centerline responses were better described than the outer-bank velocity reduction.

Developed equations with applied offsets predicted velocity increase conservatively for all spur-dike configurations. For the spur-dike configuration of Scurlock et al. (2013b), outer-bank maximum and average velocities were under-predicted with 24% and 1% error, respectively. Maximum shifted conveyance velocities were under-predicted and average velocities were over-predicted on the order of 100% error. The vane configuration from Scurlock et al. (2013b) was well approximated at the outer-bank by the vane velocity equations. Maximum and average velocities were predicted with 2% and 0.5% error, respectively. Inner-bank and centerline maximum velocities were predicted with error on the order of 30%, and averages on the order of 75%.

The six rigid-bed bendway-weir configurations of Scurlock et al. (2013a) and Scurlock et al. (2013b) were predicted with the all-structure equation set of Table 9. Outer-bank velocity

maximum and average values were uniformly under-predicted on the order of 50% and 20%, respectively. Maximum velocities within the shifted-conveyance zone were similarly under-predicted, and the average velocities were scattered about the line of perfect agreement. The rigid-bed bendway weir dataset had significant prediction errors compared with the remainder of the literature comparison data and had an average prediction error of 50% for all ratios.

Overall, results from model application to natural-channel topography research from the literature were varied. However, for data corresponding to conditions evaluated within the laboratory, the developed model of Equation 11 performed to a higher degree of accuracy. Equations predicted specific hydraulics, such as the reduced outer-bank velocities for the Bernalillo field data and vane configuration, and the shifted conveyance velocities of Lyn and Cunningham (2010), with high accuracy of less than 10% error. Lack of application to specific data, such as to the Lyn and Cunningham (2010) and Thornton et al. (2011) cases of the structure configurations increasing the outer-bank velocity compared to normalization conditions, to shifted conveyance values below normalization conditions, and to values exceeding laboratory ranges, was expected due to those data not represented within the regression dataset. Rigid-bed bendway-weir data comprised the majority of the comparison database which represented a structure type and bed condition not evaluated during the trapezoidal physical model testing. Results of under-prediction of outer-bank velocities for the bendway-weirs indicates that bendway weirs reduce outer-bank velocities to a lesser extent than spur-dikes or vanes, and does not necessarily indicate shortcomings in the equation model.

The rigid-bed construction of the physical model implemented by Thornton et al. (2011), Scurlock et al. (2013a), and Scurlock et al. (2013b) possessed characteristics which emulated survey data from natural channels, yet were not a directly scaled representation. Constrained

channel geometry of the rigid-bed construction may have affected recorded velocities and results of developed methodology comparisons. Significant application errors, especially at the centerline and inner-banks, were likely the result of a lack of rigid-bed channel morphology to an equalized energy dissipation state within the channel.

The mathematical models described hydraulics within mobile-bed channels and to scenarios in which data corresponded to conditions evaluated within the physical model with a high degree of accuracy. Limitations of applications lay within extraneous structure types or rigid-bed physical model construction of comparative data sources. No comparative studies were found which were directly applicable to situations found within the trapezoidal physical model dataset. Comparison to natural-topography datasets indicated developed mathematical prediction methodologies may be rapidly applied to non-prismatic channels and used as a design tool for field installation.

## 5.2. Application of methodology for field design

The predictive model of Equation 11 was created with rapid implementation for field design as a priority. Results of the mathematical regression procedures and the application to natural channel studies showed that the methods may be used as a tool for structure installations in natural channels. Using developed methods is a significant enhancement from the anecdotal design guidelines which currently exist for the structures. A hypothetical design situation is presented and the design equations are optimized based upon hydraulic and geometric constraints. Optimization of the developed mathematical models allows for the investigation of a number of options to achieve a design objective.

Channel geometry and necessary hydraulic conditions were assumed for the case of a design example. Spur-dikes were selected for the example since laboratory structures were more similar to codified design procedures than vanes. The example channel has the same geometric properties of the Bernalillo field site from Bui (2011) with a $R_C$ of 675 ft, a $T_W$ of 220 ft, and a channel curvature ratio of 3.06, classified in the highly erodible regime by Figure 41. The outer-bank velocity was desired to be reduced to 65% of the normalization condition and economics of the project demand that a minimum amount of material is used for configuration construction. Therefore, it was desirable to have the fewest number of structures within the channel bend and the shortest structure length possible while reducing the outer-bank velocity to a desired value. Total volume used for the configuration was approximated as the product of the structure area blocked, the structure width, and the number of structures in the channel bend. Total number of structures was computed as the desired protected length divided by the structure spacing. Channel bend rotation desired for protection was set at a bend rotation of $\pi/2$, corresponding to a bend length of 1060.3 ft.

Design conditions were initially set by recommendations from Lagasse et al. (2009) as summarized in Table 2. Lagasse et al. (2009) represents an example of the codified anecdotal guidelines prevalent for instream structure design, and any anecdotal design method would have produced similar results. Structure area was calculated using the numerator of Equation 10, and channel flow area was calculated using the wide-channel approximation of $T_W D_B$. Using the specified input parameters, seven structures were required, the total rock volume was 13,104 $ft^3$, and no information regarding the hydraulic characteristics was provided. Using the developed spur-dike equation set from Table 10, calculated reduction in maximum outer-bank velocity for the detailed configuration was 75%, and average velocity reduction was 88%. While percent

reduction was met by design recommendations in Table 2, no information regarding velocity reduction associated with design geometry was available inherently within the approach.

The GRG2 optimization code was implemented on the $MVR_O$ equation from Table 10, iteratively adjusting structure length, angle, and spacing to meet at least 50% velocity reduction criteria while minimizing total volume. Further velocity reduction from 35% to 50% accounts for the 15% offset value provided for the $MVR_O$ in Table 10. Limitations were set on parameters such that dimensionless ratios did not exceed the laboratory ranges used for equation development. Table 16 provides the results of the optimization process. Optimized equations met velocity reduction criteria, reducing maximum velocities to 49% and average velocities to 23% of normalization conditions, with only four structures compared to the original seven. Volume required for construction was 4,646 $ft^3$, or only 35% of the original material required.

**Table 16.** Methodology optimization results

| Parameter | Lagasse et al. (2009) | Current research | Units |
|---|---|---|---|
| $L$ | 44.00 | 29.20 | *ft* |
| $\theta$ | 1.57 | 1.57 | *radians* |
| $L_{W\text{-}PROJ}$ | 44.00 | 29.20 | *ft* |
| $L_{ARC}$ | 143.88 | 237.09 | *ft* |
| $T_W$ | 220.00 | 220.00 | *ft* |
| $R_C$ | 675.00 | 675.00 | *ft* |
| $\Delta z$ | 0.00 | 0.00 | *ft* |
| $D_B$ | 4.00 | 4.00 | *ft* |
| $A_C$ | 880.00 | 880.00 | $ft^2$ |
| $A_W$ | 156.00 | 96.80 | $ft^2$ |
| $A^*$ | 0.18 | 0.11 | - |
| $L_{W\text{-}PROJ}/T_W$ | 0.20 | 0.13 | - |
| $L_{ARC}/T_W$ | 0.65 | 1.08 | - |
| $R_C/T_W$ | 3.07 | 3.07 | - |
| $D_R$ | 1.00 | 1.00 | - |
| $2\theta/\pi$ | 1.00 | 1.00 | - |
| $Z_W$ | 1.50 | 1.50 | - |
| $Z$ | 4.00 | 4.00 | - |
| $W$ | 12.00 | 12.00 | *ft* |
| *protection length* | 1060.29 | 1060.29 | *ft* |
| *no. structures* | 7 | 4 | - |

| Parameter | Lagasse et al. (2009) | Current research | Units |
|---|---|---|---|
| *total volume* | 13104 | 4646 | $ft^3$ |
| $MVR_O$ | 0.252 | 0.490 | - |
| $MVR_I$ | 1.435 | 1.298 | - |
| $MVR_C$ | 1.609 | 1.553 | - |
| $AVR_O$ | 0.121 | 0.225 | - |
| $AVR_I$ | 1.208 | 1.086 | - |
| $AVR_C$ | 1.220 | 1.133 | - |

Tailoring the developed methodologies for other design criteria is achieved by selecting a different hydraulic value as the state parameter. Increased shifted-conveyance velocities for navigation purposes, reduced outer-bank shear stress, or any other design application may be optimized using the developed methodologies and an appropriate minimization algorithm. Additional restraints on any parameter may be added to the optimization process if required. Developed methodology optimization has the potential for substantial cost reduction of structure installation with a measure of hydraulic quantification previously unattainable.

## 5.3. Methodology analysis summary

Developed methodologies were scrutinized in their application to natural-topography instream structure configurations and as a design tool. Parameters of the developed methods were computed from five literature sources including physical laboratory and field data. Computed velocity ratios were within order-of-magnitude ranges for all studies and many induced hydraulic patterns were described to levels of accuracy below 10%. Applied as a design tool, developed methodologies were shown to adapt well to mathematical optimization models. Optimized equations have the potential of significant cost savings for a given installation and allow for the designer to investigate the hydraulic response of various hydraulics and constraints.

# 6. Conclusions and recommendations

A summary of conducted research, study conclusions, and recommendations for further research are presented.

## 6.1. Research summary and discussion

Channel-bend hydraulics are complex and dynamic, existing in quasi-equilibrium states of perpetually changing planimetric geometry. Dynamic morphology of the channel boundaries may be deemed problematic to anthropogenic priorities if the channel encroaches upon infrastructure or valuable land holdings. Migrating river geomorphic regimes are defined with alluvial floodplains and mild topographic gradients, emphasizing desire for human inhabitation and further exacerbating problematic erosion potential. Bank protection measures have been widely implemented to mitigate outer-bank erosional processes. A shift towards transverse instream structures has gained momentum recently due to cost reduction and habitat improvement over traditional revetment protection.

Transverse instream structures are constructed from rock extending from the outer-bank of the channel to the channel center. Design guidelines were identified and summarized for three structure types. Nomenclature of the structure type is dependent upon the intended flow effects. Bendway weirs are constructed with the crest height below design flow elevation where conveyance is passed perpendicularly over the crest top into the channel center. Spur-dikes are constructed with the crest height set at design discharge and divert all conveyance at design conditions off the structure tip to the channel center. Vanes are a hybrid between the bendway-weir and spur-dike, extending from the outer-bank tie in at design discharge flow elevation and

decreasing into the channel at a negative slope. Design guidelines specify basic geometric characteristics of the structures, yet do not provide quantification of the induced hydraulics.

Research regarding hydraulic characteristics of transverse instream structures is extensive. Numerical, physical, and field data document induced hydraulics around the three types of structures in detail. Studies illuminate key findings regarding structure velocity fields, turbulence, and erosional effects, yet many studies focus on a single structure or independent structure configuration. Studies from the literature indicated that the current design procedures are lacking in quantification of induced structure hydraulics as functions of geometric parameters of the structure configurations and cited such as the impetus for conducted research. Conducted research which developed mathematical models for the quantification of hydraulics was limited to studies from CSU, which utilized a robust dataset for development of equations describing spur-dikes, submerged spur-dikes, and vanes. While developed mathematical models from the literature quantified induced hydraulics within the physical model well (Adjusted $R^2 > 0.640$), parameters included in the equations are tailored to prismatic channels and are limited for field applications. A methodology for induced hydraulic quantification in natural channels was a fundamental gap in the knowledge base for transverse instream structures.

The physical model dataset from Heintz (2002), Darrow (2004), and Schmidt (2005) was reexamined and velocity, shear-stress, and structure geometry data were compiled and tabulated. A total of 130 independent structure configurations were found which spanned two channel bends, three discharges, two structure types, and a variety of altered spacing, length, and planimetric angle orientation. Boundary shear-stress data were found to be of quality for analysis for 66 of the 130 configurations and velocity data were of high quality for all configurations. Data were segmented into three regions of hydraulic influence: the outer-bank

reduced zone, the inner-bank increased zone, and the centerline increased zone. A point-based analysis was used for shear-stress data segmentation and a regional-based analysis was used for velocity data. Spatially interpolated velocity data clearly demarcated the outer-bank reduced zone from the zone of shifted conveyance, yet shear-stress data did not exhibit easily defined regions. Maximum and average velocity and shear-stress data were determined for specific zones of hydraulic influence for each configuration and then normalized by bend-averaged baseline conditions.

A mathematical model was developed for the quantification of hydraulics within the physical model with a focus upon extrapolation to natural channel design. Influential geometric parameters altered within the physical model dataset were identified and organized into dimensionless groupings. Consideration to natural channel field measurement was given and each parameter is readily measured from rudimentary bathymetric survey and discharge data. Each grouping had a physically identifiable meaning with implications for hydraulic influence which were addressed within the literature. Dimensionless terms were organized into Equation 11 which possessed regression coefficients for tailoring of the model to the trapezoidal physical modeling dataset. Equation 11 was used as the foundation for the development of outer-bank, centerline, and inner-bank maximum and average velocity and shear-stress equations. A total of twenty-four equations were generated to describe hydraulics associated with the various structure types as summarized by Table 9, Table 10, Table 11, and Table 12.

Parameter constraints were set for reduction in measurement error propagation and applicability to field applications, and backwards linear regression was performed on the logarithmic transformation of the equation to reduce models to statistically significant parameters. Outlier data were removed based on standard deviation criteria to focus upon core

hydraulic response, and then non-linear regression optimization was used to develop finalized prediction models. Offsets were developed accounting for two standard deviations of prediction error for a factor of safety.

Models quantified hydraulics within the model to a higher degree of accuracy for the velocity data than for the shear-stress data. Prediction error for velocity was on the order of 10%, while shear-stress data were predicted error on the order of 30%. Shear-stress data were collected with a calibrated instrument for one-dimensional flow conditions in a highly three-dimensional flow environment. Instrumentation limitations, coupled with the reduced amount of available data, are most likely responsible for the lesser accuracy of the shear-stress predictive relationships when compared to the velocity equations. When comparable, hydraulics were quantified to a higher degree of accuracy for the developed models than the previous equation iteration of Schmidt (2005). Adjusted $R^2$ values were increased by approximately 0.2 for all maximum velocity ratios.

Velocity and shear-stress equations were analyzed using sensitivity analysis to determine parameter response. Generally, equations behaved according to the hydraulic expectations of parameter adjustment from the literature. Outer-bank reduction and shifted-conveyance zone responses typically responded differently, according to continuity principles, and parameter response throughout the laboratory ranges was generally smooth and extrapolated well. Exceptions included vane response to the submergence ratio and asymptotic response outside of laboratory ranges for specific parameters.

Predictive models were evaluated with field and physical model data from natural channel topographies reported from the literature. Twenty velocity data, spanning six studies,

were compared with predicted velocities from the developed equations. The majority of the studies examined bendway-weirs, a structure type not incorporated in the trapezoidal physical model dataset. Parameters of the design equations were determined without significant assumptions for each of the identified studies. Predictions of developed equations were found to be on the order of magnitude as those observed, with specific hydraulic characteristics described with high accuracy. Data not well described by the equations were not representative of hydraulics observed in the physical model. Velocities which were increased at the outer-bank and slowed at the shifted-conveyance zone after structure installation were predicted poorly.

A hypothetical field design application was examined for the optimization of the developed design methods for the reduction of configuration construction cost while achieving a desired hydraulic condition. The developed methods were compared with the current accepted design criteria. It was determined that the mathematical relationships optimize well and provide significant savings over the current design procedures. Mathematical models should apply well to field design applications at a significant benefit to the designer.

Developed methodologies have limitations grounded in the laboratory dataset used for regression analyses. Structure parameter values evaluated in the laboratory did not uniformly fall within commonly accepted design protocol ranges. Use of the current design guidelines for spur-dikes and vanes from Table 2 and Table 3, respectively, may exceed the limitations of applicability for the regression relationships. Implementing design equations outside of the laboratory ranges used for development will result in extrapolation errors and is not recommended. Performed sensitivity analysis indicated adherence to the bounds of laboratory ranges of $L_{W\text{-}PROJ}$ and $\Delta z$ is most critical for extrapolation error minimization.

Design relationships were developed from a rigid-bed, trapezoidal physical model not accounting for morphological response to structure installation. Tip scour, outer-bank deposition, outer-bank scalloping, and inner-bank erosion are probable. Inner-bank erosion Effects of morphological change will alter resulting velocity fields; however, the severity of the alterations is unknown. Outer-bank sedimentation patterns would likely further decrease the hydraulics such that the design equations represent maximum conditions. Inner-bank response could potentially include significant erosion and a planform channel shift. Localized topography should be examined by a practitioner implementing the developed relationships to gauge the likelihood of undesired channel redirection and the hydraulic threshold warranting such movement. Velocity trends were predicted well by the developed methodologies for the mobile bed data from Lyn and Cunningham (2010) and Bui (2011) when applicable.

## 6.2. Conclusions

The research conducted provided a series of important findings and conclusions to address the need for transverse instream structure design guidelines. Fundamental findings from this study are as follows:

- A mathematical model was developed for the quantification of induced instream structure hydraulics. The model was comprised of dimensionless groupings having physical meaning with variables that may be assessed from field data. Conducted research provided the first documented methodology for a design tool to quantify induced velocities and boundary shear stresses from transverse instream structure installations in natural channel field applications. Provided as Equation 11, the developed methodology is presented as follows:

$$VR_{i\,s}\big|_{M,Avg};\tau R_i\big|_{M,Avg} = a_1(A^*)^{a_2}\left(\frac{L_{ARC}}{T_W}\right)^{a_3}\left(\frac{R_C}{T_W}\right)^{a_4}\left(\frac{L_{W-PROJ}}{T_W}\right)^{a_5}\left(\frac{D_B}{D_B-\Delta z}\right)^{a_6}\left(\frac{2\theta}{\pi}\right)^{a_7} \quad (11)$$

- The developed method of Equation 11 described was tailored to normalized velocity and boundary shear-stress data from a robust dataset from a trapezoidal physical model. Twenty-four predictive relationships were developed for maximum and average hydraulics at the outer-bank, centerline, and inner-bank. Results were provided in Table 9, Table 10, Table 11, and Table 12. $R^2$ values for the maximum outer-bank ratio for velocities were greater than 0.8 for all structure types and 0.6 for spur-dike shear stresses.

- Models were shown applicable to field design. Optimized equations provided significant advantages of volume reduction and hydraulic quantification over current design recommendations.

- Equation response to parameter alteration coincided with hydraulic expectations from the literature review.

- Equations were developed from a physical model with ranges of altered parameters. Application of equations outside of the laboratory ranges is not advised.

## 6.3. Recommendations for further research

Developed mathematical models from this research provide a solid framework for the description of a variety of hydraulic parameters within instream structure fields. Expansion of the methods to other datasets would improve the functionality and applicability of the relationships for transverse instream structures.

Equations were developed from a rigid bed, prismatic model which approximated natural channel bathymetry. Data from instream structures in a mobile bed channel bend model, or from a natural channel topography, would supplement results from the prismatic model, serving to validate the regression exponents or reformulate a new set of equations. Performing additional configuration installations within a modeled natural channel allows for further evaluation. The developed mathematical model allows for the incorporation of numerical or physical model data. Documentation of channel response to instream structures installation is a valuable addition to the current research.

Specific hydraulic trends were determined as important to instream structure design, yet not accounted for in this research. Trends included acceleration around the structure tip, which may have implications for structure stability. Using the developed equation format to design mathematical prediction models for acceleration around the structure tip would aid in design of structure materials to resist hydraulic forces.

Bendway weirs were a structure classification not represented within the trapezoidal, physical model database, yet studies within the literature were found which emphasized the structure type. A sufficient database would allow for development of tailored design methods for bendway-weir structures which may be accomplished in a physical model setting.

Evaluation of the models is currently limited; only one field site was found with adequate data for prediction comparisons. Monitoring model implementations in field design applications would allow for evaluation of method efficacy in achieving design objectives. Recommended data for field collection include velocities at the structure tips, within the structure field, and at

the shifted conveyance zone. Capturing the velocity gradient between the outer-bank reduced zone and shifted-conveyance zone is important for identifying field regions of influence.

# 7. References


Abad, J.D., Rhoads, B.L., Guneralp, I., and Garcia, M.H. (2008). "Flow structure at different stages in a meander-bend with bendway weirs." *Journal of Hydraulic Engineering.* 134:8. 1052-1063.

Baird, D.C., Klump, C.C., Scurlock S.M., and Samad, M.I. (2014). "Interim bank stabilization with environmental features design guidelines." United States Bureau of Reclamation. Denver, CO.

Bathurst, J. C., Throne, C. R., and Hey, R. D. (1979). "Secondary Flow and Shear Stress at River Bends." *Journal of the Hydraulics Division-ASCE 105*. 1979, 1277-1295.

Bhuiyan, F., Hey. R., and Wormleaton, . (2010). "Bank-attached vanes for bank erosion control and restoration of river meanders." *Journal of Hydraulic Engineering.* 136(9). 583-596.

Blanckaert, K., and Graf, W.H. (2001). "Mean flow and turbulence in open-channel bend." *J. Hydraul. Engr*. 127(10), 835-847.

Barenblatt, G.I. (1996). "Scaling, self-similarity, and intermediate asymptotics: dimensional analysis and intermediate asymptotics." Cambridge University Press. New York, NY.

Biedenharn, D.S., Elliot, C.M., and Watson, C.C. (1997). "The WES stream investigation and streambank stabilization handbook." USACE. Waterways Experiment Station. Vicksburg, Mississippi.

BIO-WEST (2006). "Bernalillo Priority Site: Final Design, Final Design Drawings." Bureau of Reclamation, Albuquerque Area Office, Albuquerque, NM.

Brown, S.A. (1985). "Design of spur-type streambank stabilization structures, Final Report." Federal Highway Administration, Washington D.C. FHWA-IP-89-016.

Bui, C. (2011). "Bernalillo 2007 & 2008 Data Collection Report." Bureau of Reclamation, Albuquerque Area Office, Albuquerque, NM.

Cencetti, C. Duranti, A., Fredduzi, A., and Marchesini, I. (2004). "Narrowing and bed incision of a cobble bed river in central Italy." *Geophysical Research Abstracts*. Vol. 6. 03792.

Crosato, A. (2008). "Analysis and modeling of river meandering." *IOS Press*.

D'Agostino, V. and Ferro, V. (2004). "Scour on alluvial bed downstream of grade-control structures." *J. Hydraul. Engr.* 130(1). 24-37.

Dahle, B.P. (2009). "Evaluating shallow-flow rock structures as scour countermeasures at bridges." Brigham Young University. Dept. of Civil and Environmental Engineering. Technical Report. Prepared for Utah Dept. of Transportation Research Division.

Darrow, J.D. (2004). "Effects of bendway weir characteristics on resulting flow conditions." M. S. Thesis. Colorado State University, Department of Civil Engineering. Fort Collins, Colorado.

Derrick, D.L. (1997). "Bendway weirs redirect rivers flow to protect highway bank abutments." U.S. Army Corps of Engineers Waterways Experiment Station, Vicksburg, M.S.

Derrick, D.L., Pokrefke, T.J., Boyd, M.B., Crutchfield, J.P., and Henderson, R.R. (1994). "Design and development of bendway-weirs for the Dogtooth Bend Reach, Mississippi River." U.S. Army Corps of Engineers.

Dietrich, W. E., Smith, J. D., and Dunne, T. (1979). "Flow and Sediment Transport in a Sand Bedded Meander." *The Journal of Geology*. 87(3), 305-315.

Duan, J.G. (2009). "Mean flow and turbulence around a laboratory spur dike." *Journal of Hydraulic Engineering.*. 135(10). 803-811.

Federal Highway Administration (2009). “Bridge Scour and Stream Instability Countermeasures: Experience, Selection, and Design Guidance – Third Edition” U.S. Department of Transportation.

Fitzpatrick, F.A., Peppler, M.C., Schwar, H.E., Hoopes, J.A., and Diebel, M.W. (2013). "Monitoring channel morphology and bluff erosion at two installations of flow-deflecting vanes, north fish creek, Wisconsin, 2000-03. *Scientific Investigations Report* 2004-5272. United States Geological Survey, Virginial

Fox, J. F., Papanicolau, A.N., Hobbs, B., Kramer, C., and Kjos, L. (2005). "Fluid-sediment dynamics around a barb: An experimental case study of a hydraulic structure for the Pacific Northwest." *Can. J. Civ. Engr.* 32. 853-867.

Garcia, M.H. (2008). "Sedimentation engineering. Processes, measurements, modeling, and practice." *ASCE Manuals and Reports on Engineering Practice*. 110.

Haltigin, T.W., Biron, P.M., and Lapointe, M.F. (2007). "Predicting equilibrium scour-hole geometry near angled stream deflectors using a three-dimensional numerical flow model." *J. Hydraul. Engr.* 138(8). 983-988.

Han, S.S., Biron, P.M., and Ramamurthy, A.S. (2011). "Three-dimensional modeling of flow in sharp open-channel bends with vanes." *J. Hydraul. Research.* 49(1). 64-72.

Head, M.R. and Rechenberg, I. (1962). "The Preston tube as a means of measuring skin friction." *Journal of Fluid Mechanics*. (14).

Heintz, M.L. (2002). “Investigation of bendway weir spacing.” M. S. Thesis. Colorado State University, Department of Civil Engineering. Fort Collins, Colorado.

Ippen, A. T., Drinker, P. A., Jobin, W. R., and Noutsop, G. K. (1960). “ The distribution of boundary shear stresses in curved trapezoidal channels.” Report- Massachusetts Institute of Technology. Hydrodynamics Laboratory. Technical Report No. 43, 1-82.

Jamieson, E.C., Rennie, C.D., and Townsend, R.D. (2013). "3D flow and sediment dynamics in a laboratory channel bend with and without stream barbs." *Journal of Hydraulic Engineering.*. 139(2). 154-166.

Jia, Y., Scott, S., Xu, Y., Huang, S., and Wang, S.Y. (2005). "Three-dimensional numerical simulation and analysis of flows around a submerged weir in a channel bendway." Journal of Hydraulic Engineering. 131:8. 682-693.

Jia, Y., Wang, S. Y. Y., and Xu, Y. (2002). “Validation and application of a 2D model to channels with complex geometry.” Int. J. Comput. Eng. Sci., 3(1). 57–71.

Jia, Y., Zhu, T., and Scott, S. (2011). "Turbulent flow around submerged bendway weirs and its influence on channel navigation." Hydrodynamics - Optimizing methods and tools, Prof. Harry Schulz (Ed.), ISBN: 978-953-307-712-3, InTech.

Johnson, C.G. (1972). "Dimensional analysis and the interpretation of regression coefficients." *J. Financial and Quantitative Analysis.* 7(1). 1399-1406.

Johnson, P.A., Hey, R.D., Tessier, M., and Rosgen, D.L. (2001). "Use of vanes for control of scour at vertical wall abutments." *Journal of Hydraulic Engineering*. 127(9). 772-778.

Julien, Pierre, Y. and Duncan, Josh R. 2003. “Optimal design criteria of bendway weirs from numerical simulations and physical model studies.” Colorado State University, Department of Civil Engineering. Fort Collins, Colorado.

Knighton, D. (1998). "Fluvial forms and processes: a new perspective." *Hodder Arnold Publication*.

Ladson, L.S., and Warren, A.D. (1978). "Generalized reduced gradient software for linearly and nonlinearly constrained problems." *Design and Implementation of Optimization Software*. 335-362.

Lagasse, P.F., Clopper, P.E., Pagan-Ortiz, J.E., Zevenbergen, L.W., Arneson, L.A., Schall, J.D., and Girard, L.G. (2009). "Bridge scour and stream instability countermeasures: experience, selection, and design guidance." 3rd ed. HEC-23. Federal Highway Administration. FHWA-NHI-09-111.

Leinster, T. (2004). "A general theory of self-similarity I." *ArXiv Mathematics e-prints*.

Leopold, L.B. and Wolman, M.G. (1957). "River channel patterns: braided, meandering, and straight." *Geological survey professional paper*. 282-B. United States Department of the Interior.

Lyn, D.A. and Cunningham, R. (2010). "A laboratory study of bendway weirs as a bank erosion countermeasure." *Purdue e-Pubs. JTRP Technical Reports*. FHWA/IN/JTRP-2010/24.

Maryland Department of the Environment (2000). "Maryland's waterway construction guidelines." Water Management Administration.

Matsuura, T. and Townsend R. (2004). "Stream-barb installations for narrow channel bends - a laboratory study." *Can. J. Civ. Engr.* 31. 478-486.

McCoy, A., Constantinescu, G., and Weber, L. (2007). "Hydrodynamics of flow in a channel with two lateral submerged groynes." ASCE. World Environmental and Water Resources Congress 2007.

McCullah, J.A. and Gray, D., 2005, "Environmentally Sensitive Channel- and Bank-Protection Measures," NCHRP Report 544, Transportation Research Board, National Academies of Science, Washington, D.C.

McLelland, S.J. and Nicholas, A.P. (2000). "A new method for evaluating errors in high-frequency ADV measurements." *Hydrological processes*. (14). 351-366.

Nagata, N., Hosoda, T. Nakato, T., and Muramoto, Y. (2005). "Three-dimensional numerical model for flow and bed deformation around river hydraulic structures." *J. Hydraul. Engr.* 131(12). 1074-1087.

Nanson, G.C., and Hickin, E.J. (1986). "A statistical analysis of bank erosion and channel migration in western Canada." *Geol. Soc. Am. Bull.* 97(4). 497-504.

Ottevanger, K., Blanckaert, K., Uijttewaal, W.S.J (2011). "Processes governing the flow redistribution in sharp river bends." *Geomorphology.*

Piper, K.L,, Hoag, J.C., Allen, H.H., Durham, G., Fischenich, J.C., and Anderson, R.O. (2001). "Bioengineering as a tool for restoring ecological integrity to the Carson River." *WRAP Technical Notes Collection ERDC TN-WRAP-01-05*. USACE Research and Development Center, Vicksburg, MS.

Radspinner, R.R., Diplas, P., Lightbody, A.F., and Sotoropoulis, F. (2010). "River training and ecologic enhancement potential using in-stream structures." *Journal of Hydraulic Engineering.* 136(12). 967-980.

Rhoads, B.L. (2003), "Protocols for geomorphic characterization of meander bends in Illinois." University of Illinois at Urbana-Champaign. Urbana, IL

Richard, G. and Julien, P. (2003). "Dam impacts on and restoration of an alluvial river - Rio Grande, New Mexico." *International Journal of Sediment Research,* 18 (2), 89-96.

Rosgen, D. L. (2001). "The cross-vane, w-weir, and j-hook structures... their description, design, and application for stream stabilization and restoration." ASCE River and Wetland Restoration Conference.

Rosgen, D. L. (2006). "The cross-vane, w-weir, and j-hook structures... their description, design, and application for stream stabilization and restoration." *Wildland Hydrology, Inc.*

Schmidt, P.G. (2005). "Effects of bendway weir field geometry characteristics on channel flow conditions." M. S. Thesis. Colorado State University, Department of Civil Engineering. Fort Collins, Colorado.

Schumm, S.A. and Brakenridge, G.R. (1987). "River responses." *The Geology of North America.* Vol. K-3. 221-240.

Scottt, S. H., Jai, Y., Wang, S.S.Y, and Xu, Y. (2001) "Analysis of near-field hydrodynamics of submerged weirs." United States Army Corps of Engineers. ERDC/EHL CHETN-VII-1.

Scurlock, S.M., Thornton, C.I., and Abt, S.R. (2013a). "Middle Rio Grande physical modeling - Evaluation of bendway-weir structures in the native-topography model." In review. Colorado State University, Department of Civil Engineering. Fort Collins, CO.

Scurlock, S.M., Thornton, C.I., and Abt, S.R. (2013b). "Middle Rio Grande physical modeling - Reevaluations and comparisons of instream structures within the native-topography channel." In review. Colorado State University, Department of Civil Engineering. Fort Collins, CO.

Sellin, R.H.J., Ervine, D.A., and WIlletts, B.B. (1993). "Behaviour of meandering two-stage channels." *Proc. Inst. Civ. Eng., Waters. Maritime Enrg.*, 101, 99-111.

Shields, F.D., Knight, S.S., and Cooper, C.M. (1998). "Addition of spurs to stone toe protection for warmwater fish rehabilitation." *J. Am. Water Res. Assoc.* 34. 1427-1436.

Shields, F.D., Knight, S.S., and Cooper, C.M. (2000). "Warmwater stream bank protection and fish habitat: a comparative study." *Environ. Management.* 26(3). 317-328.

Simon, A., Curini, A., Darby, S.E., and Langendoen, E.J. (2000). "Band and near-bank processes in an incised channel." *Geomorphology*. 35. 193-217.

Sinha, S.K., and Marelius, F. (2000). "Analysis of flow past submerged vanes." *J. Hydraul. Res.* 38(1). 65-71.

Smith, S.P., and Wittler, R.J. (1998). "Bendway weirs and highway protection in Colorado: A case study on the Blue River." International Water Resources Engineering. 465-470.

SonTek (1999). "SonTek ADV: Acoustic Doppler Velocimeters." SonTek. San Diego, CA.

*Source*: "Middle Rio Grande River." 35°18'44.49" N and 106°33'32.75" W. *Google Earth*. February 25, 2007.

*Source*: "Middle Rio Grande River." 35°18'44.49" N and 106°33'32.75" W. *Google Earth.* March 21, 2012.

Strom, K. B., and Papanicolaou, A. N. (2007). "ADV Measurements around a Cluster Microform in a Shallow Mountain Stream." *Journal of Hydraulic Engineering*. 133(12), 1379-1389.

Surian, N. and Rinaldi, M. (2003). "Morphological response to river engineering and management in alluvial channels in Italy." *Geomorphology*. 50. 307-326.

Voulgaris, G., and Trowbridge, J.H. (1998). "Evaluation of the Acoustic Doppler Velocimeter (ADV) for turbulence measurements." *J. Atmos. and Oceanic Tech.* 15. 272-289.

Thorne, C.R. (1978). "Process of bank erosion in river channels." Ph.D. thesis, University of East Anglia, Norwich, UK.

Thorne, C.R. (1991). "Bank erosion and meander migration of the Red and Mississippi Rivers, USA." *IAHS Publication*. Wallingford, England.

Thornton, C.I., Cox, A.L, Ursic, M.E., and Youngblood, N.A. (2011). "Data report for completed bendway-weir configurations within the native topography model." Colorado State University, Department of Civil Engineering. Fort Collins, CO.

United States Department of Agriculture (2005). "Design of stream barbs." *Technical Note No. 23*.

Vignaux, G.A. and Scott, J.L. (1999). "Simplifying regression models using dimensional analysis." *Austral. and New Zealand J. Statist.* 41(1). 31-41.

Wahl, T.L. (2000). "Analyzing ADV data using WinADV." *ASCE. Water Resources 2000.*

Wardman, B.G. and Papanicolaou, A.N. (2006). "Flow around submerged barbs in the Raccoon River Iowa." *ASCE. World Environmental and Water Resources Congress 2006*.

Weisberg, S. (2013). "Applied linear regression, 3rd ed." *Wiley Publishing*.

# Appendix

## A1. Data used for analysis

**Table 17.** Instream structure tests and associated geometric parameters

| Study | ID | Bend | $Q$ | φ | θ | $L_{W\text{-}PROJ}$ | $L_{ARC}$ | $T_W$ | $R_C$ | $h_W$ | $D_B$ | $A^*$ |
|---|---|---|---|---|---|---|---|---|---|---|---|---|
| - | - | - | $ft^3/s$ | ° | ° | ft | ft | ft | ft | ft | ft | - |
| Heintz (2002) | W01 | US | 8 | 0 | 90 | 3.62 | 16.88 | 13.76 | 38.75 | 0.77 | 0.60 | 26.60 |
| Heintz (2002) | W01 | US | 12 | 0 | 90 | 4.13 | 16.88 | 14.79 | 38.75 | 0.77 | 0.77 | 26.90 |
| Heintz (2002) | W01 | US | 16 | 0 | 90 | 4.13 | 16.88 | 15.63 | 38.75 | 0.77 | 0.91 | 22.00 |
| Heintz (2002) | W01 | DS | 8 | 0 | 90 | 2.50 | 20.90 | 9.59 | 65.83 | 0.78 | 0.60 | 26.70 |
| Heintz (2002) | W01 | DS | 12 | 0 | 90 | 3.04 | 20.90 | 10.68 | 65.83 | 0.78 | 0.78 | 27.10 |
| Heintz (2002) | W01 | DS | 16 | 0 | 90 | 3.04 | 20.90 | 11.40 | 65.83 | 0.78 | 0.90 | 22.50 |
| Heintz (2002) | W02 | US | 8 | 0 | 90 | 3.62 | 21.08 | 13.76 | 38.75 | 0.77 | 0.60 | 26.60 |
| Heintz (2002) | W02 | US | 12 | 0 | 90 | 4.13 | 21.08 | 14.79 | 38.75 | 0.77 | 0.77 | 26.90 |
| Heintz (2002) | W02 | US | 16 | 0 | 90 | 4.13 | 21.08 | 15.63 | 38.75 | 0.77 | 0.91 | 22.00 |
| Heintz (2002) | W02 | DS | 8 | 0 | 90 | 2.50 | 29.60 | 9.59 | 65.83 | 0.78 | 0.60 | 26.70 |
| Heintz (2002) | W02 | DS | 12 | 0 | 90 | 3.04 | 29.60 | 10.68 | 65.83 | 0.78 | 0.78 | 27.10 |
| Heintz (2002) | W02 | DS | 16 | 0 | 90 | 3.04 | 29.60 | 11.40 | 65.83 | 0.78 | 0.90 | 22.50 |
| Heintz (2002) | W03 | US | 8 | 0 | 90 | 3.62 | 14.03 | 13.76 | 38.75 | 0.77 | 0.60 | 26.60 |
| Heintz (2002) | W03 | US | 12 | 0 | 90 | 4.13 | 14.03 | 14.79 | 38.75 | 0.77 | 0.77 | 26.90 |
| Heintz (2002) | W03 | US | 16 | 0 | 90 | 4.13 | 14.03 | 15.63 | 38.75 | 0.77 | 0.91 | 22.00 |
| Heintz (2002) | W03 | DS | 8 | 0 | 90 | 2.50 | 16.74 | 9.59 | 65.83 | 0.78 | 0.60 | 26.70 |
| Heintz (2002) | W03 | DS | 12 | 0 | 90 | 3.04 | 16.74 | 10.68 | 65.83 | 0.78 | 0.78 | 27.10 |
| Heintz (2002) | W03 | DS | 16 | 0 | 90 | 3.04 | 16.74 | 11.40 | 65.83 | 0.78 | 0.90 | 22.50 |
| Darrow (2004) | W04 | US | 8 | 0 | 90 | 1.71 | 8.54 | 13.76 | 38.75 | 0.77 | 0.60 | 10.70 |
| Darrow (2004) | W04 | US | 12 | 0 | 90 | 2.22 | 8.54 | 14.79 | 38.75 | 0.77 | 0.77 | 11.60 |
| Darrow (2004) | W04 | US | 16 | 0 | 90 | 2.22 | 8.54 | 15.63 | 38.75 | 0.77 | 0.91 | 9.50 |
| Darrow (2004) | W04 | DS | 8 | 0 | 90 | 1.06 | 12.99 | 9.59 | 65.83 | 0.78 | 0.60 | 8.20 |
| Darrow (2004) | W04 | DS | 12 | 0 | 90 | 1.60 | 12.99 | 10.68 | 65.83 | 0.78 | 0.78 | 9.90 |
| Darrow (2004) | W04 | DS | 16 | 0 | 90 | 1.60 | 12.99 | 11.40 | 65.83 | 0.78 | 0.90 | 8.20 |
| Darrow (2004) | W05 | US | 8 | 0 | 90 | 1.71 | 10.30 | 13.76 | 38.75 | 0.77 | 0.60 | 10.70 |
| Darrow (2004) | W05 | US | 12 | 0 | 90 | 2.22 | 10.30 | 14.79 | 38.75 | 0.77 | 0.77 | 11.60 |
| Darrow (2004) | W05 | US | 16 | 0 | 90 | 2.22 | 10.30 | 15.63 | 38.75 | 0.77 | 0.91 | 9.50 |
| Darrow (2004) | W05 | DS | 8 | 0 | 90 | 1.06 | 16.78 | 9.59 | 65.83 | 0.78 | 0.60 | 8.20 |
| Darrow (2004) | W05 | DS | 12 | 0 | 90 | 1.60 | 16.78 | 10.68 | 65.83 | 0.78 | 0.78 | 9.90 |
| Darrow (2004) | W05 | DS | 16 | 0 | 90 | 1.60 | 16.78 | 11.40 | 65.83 | 0.78 | 0.90 | 8.20 |
| Darrow (2004) | W06 | US | 8 | 0 | 90 | 2.74 | 11.49 | 13.76 | 38.75 | 0.77 | 0.60 | 19.30 |
| Darrow (2004) | W06 | US | 12 | 0 | 90 | 3.25 | 11.49 | 14.79 | 38.75 | 0.77 | 0.77 | 19.90 |
| Darrow (2004) | W06 | US | 16 | 0 | 90 | 3.25 | 11.49 | 15.63 | 38.75 | 0.77 | 0.91 | 16.30 |
| Darrow (2004) | W06 | DS | 8 | 0 | 90 | 1.81 | 17.07 | 9.59 | 65.83 | 0.78 | 0.60 | 17.80 |
| Darrow (2004) | W06 | DS | 12 | 0 | 90 | 2.35 | 17.07 | 10.68 | 65.83 | 0.78 | 0.78 | 18.80 |
| Darrow (2004) | W06 | DS | 16 | 0 | 90 | 2.35 | 17.07 | 11.40 | 65.83 | 0.78 | 0.90 | 15.60 |
| Darrow (2004) | W07 | US | 8 | 0 | 90 | 2.74 | 13.85 | 13.76 | 38.75 | 0.77 | 0.60 | 19.30 |
| Darrow (2004) | W07 | US | 12 | 0 | 90 | 3.25 | 13.85 | 14.79 | 38.75 | 0.77 | 0.77 | 19.90 |
| Darrow (2004) | W07 | US | 16 | 0 | 90 | 3.25 | 13.85 | 15.63 | 38.75 | 0.77 | 0.91 | 16.30 |
| Darrow (2004) | W07 | DS | 8 | 0 | 90 | 1.81 | 22.06 | 9.59 | 65.83 | 0.78 | 0.60 | 17.80 |

| Study | ID | Bend | $Q$ | φ | θ | $L_{W\text{-}PROJ}$ | $L_{ARC}$ | $T_W$ | $R_C$ | $h_W$ | $D_B$ | $A^*$ |
|---|---|---|---|---|---|---|---|---|---|---|---|---|
| - | - | - | ft³/s | ° | ° | ft | ft | ft | ft | ft | ft | - |
| Darrow (2004) | W07 | DS | 12 | 0 | 90 | 2.35 | 22.06 | 10.68 | 65.83 | 0.78 | 0.78 | 18.80 |
| Darrow (2004) | W07 | DS | 16 | 0 | 90 | 2.35 | 22.06 | 11.40 | 65.83 | 0.78 | 0.90 | 15.60 |
| Darrow (2004) | W08 | US | 8 | 0 | 60 | 1.78 | 8.54 | 13.76 | 38.75 | 0.77 | 0.60 | 11.90 |
| Darrow (2004) | W08 | US | 12 | 0 | 60 | 2.30 | 8.54 | 14.79 | 38.75 | 0.77 | 0.77 | 12.70 |
| Darrow (2004) | W08 | US | 16 | 0 | 60 | 2.30 | 8.54 | 15.63 | 38.75 | 0.77 | 0.91 | 10.40 |
| Darrow (2004) | W08 | DS | 8 | 0 | 60 | 1.13 | 12.99 | 9.59 | 65.83 | 0.78 | 0.60 | 10.30 |
| Darrow (2004) | W08 | DS | 12 | 0 | 60 | 1.67 | 12.99 | 10.68 | 65.83 | 0.78 | 0.78 | 11.60 |
| Darrow (2004) | W08 | DS | 16 | 0 | 60 | 1.67 | 12.99 | 11.40 | 65.83 | 0.78 | 0.90 | 9.70 |
| Darrow (2004) | W09 | US | 8 | 0 | 60 | 1.78 | 10.30 | 13.76 | 38.75 | 0.77 | 0.60 | 11.90 |
| Darrow (2004) | W09 | US | 12 | 0 | 60 | 2.30 | 10.30 | 14.79 | 38.75 | 0.77 | 0.77 | 12.70 |
| Schmidt (2005) | W09 | US | 16 | 0 | 60 | 2.30 | 10.30 | 15.63 | 38.75 | 0.77 | 0.91 | 10.40 |
| Darrow (2004) | W09 | DS | 8 | 0 | 60 | 1.13 | 16.78 | 9.59 | 65.83 | 0.78 | 0.60 | 10.30 |
| Darrow (2004) | W09 | DS | 12 | 0 | 60 | 1.67 | 16.78 | 10.68 | 65.83 | 0.78 | 0.78 | 11.60 |
| Darrow (2004) | W09 | DS | 16 | 0 | 60 | 1.67 | 16.78 | 11.40 | 65.83 | 0.78 | 0.90 | 9.70 |
| Schmidt (2005) | W10 | US | 8 | 0 | 60 | 2.71 | 11.18 | 13.76 | 38.75 | 0.77 | 0.60 | 19.70 |
| Schmidt (2005) | W10 | US | 12 | 0 | 60 | 3.23 | 11.18 | 14.79 | 38.75 | 0.77 | 0.77 | 20.20 |
| Schmidt (2005) | W10 | US | 16 | 0 | 60 | 3.23 | 11.18 | 15.63 | 38.75 | 0.77 | 0.91 | 16.50 |
| Schmidt (2005) | W10 | DS | 8 | 0 | 60 | 1.82 | 16.49 | 9.59 | 65.83 | 0.78 | 0.60 | 19.30 |
| Schmidt (2005) | W10 | DS | 12 | 0 | 60 | 2.37 | 16.49 | 10.68 | 65.83 | 0.78 | 0.78 | 20.00 |
| Schmidt (2005) | W10 | DS | 16 | 0 | 60 | 2.37 | 16.49 | 11.40 | 65.83 | 0.78 | 0.90 | 16.60 |
| Schmidt (2005) | W11 | US | 8 | 0 | 60 | 2.71 | 13.48 | 13.76 | 38.75 | 0.77 | 0.60 | 19.70 |
| Schmidt (2005) | W11 | US | 12 | 0 | 60 | 3.23 | 13.48 | 14.79 | 38.75 | 0.77 | 0.77 | 20.20 |
| Schmidt (2005) | W11 | US | 16 | 0 | 60 | 3.23 | 13.48 | 15.63 | 38.75 | 0.77 | 0.91 | 16.50 |
| Schmidt (2005) | W11 | DS | 8 | 0 | 60 | 1.82 | 21.30 | 9.59 | 65.83 | 0.78 | 0.60 | 19.30 |
| Schmidt (2005) | W11 | DS | 12 | 0 | 60 | 2.37 | 21.30 | 10.68 | 65.83 | 0.78 | 0.78 | 20.00 |
| Schmidt (2005) | W11 | DS | 16 | 0 | 60 | 2.37 | 21.30 | 11.40 | 65.83 | 0.78 | 0.90 | 16.60 |
| Schmidt (2005) | W12 | US | 8 | 0 | 60 | 3.52 | 13.70 | 13.76 | 38.75 | 0.77 | 0.60 | 26.50 |
| Schmidt (2005) | W12 | US | 12 | 0 | 60 | 4.04 | 13.70 | 14.79 | 38.75 | 0.77 | 0.77 | 26.60 |
| Schmidt (2005) | W12 | US | 16 | 0 | 60 | 4.04 | 13.70 | 15.63 | 38.75 | 0.77 | 0.91 | 21.80 |
| Schmidt (2005) | W12 | DS | 8 | 0 | 60 | 2.45 | 20.28 | 9.59 | 65.83 | 0.78 | 0.60 | 27.70 |
| Schmidt (2005) | W12 | DS | 12 | 0 | 60 | 2.99 | 20.28 | 10.68 | 65.83 | 0.78 | 0.78 | 27.50 |
| Schmidt (2005) | W12 | DS | 16 | 0 | 60 | 2.99 | 20.28 | 11.40 | 65.83 | 0.78 | 0.90 | 22.80 |
| Schmidt (2005) | W13 | US | 8 | 0 | 60 | 3.52 | 16.52 | 13.76 | 38.75 | 0.77 | 0.60 | 26.50 |
| Schmidt (2005) | W13 | US | 12 | 0 | 60 | 4.04 | 16.52 | 14.79 | 38.75 | 0.77 | 0.77 | 26.60 |
| Schmidt (2005) | W13 | US | 16 | 0 | 60 | 4.04 | 16.52 | 15.63 | 38.75 | 0.77 | 0.91 | 21.80 |
| Schmidt (2005) | W13 | DS | 8 | 0 | 60 | 2.45 | 26.19 | 9.59 | 65.83 | 0.78 | 0.60 | 27.70 |
| Schmidt (2005) | W13 | DS | 12 | 0 | 60 | 2.99 | 26.19 | 10.68 | 65.83 | 0.78 | 0.78 | 27.50 |
| Schmidt (2005) | W13 | DS | 16 | 0 | 60 | 2.99 | 26.19 | 11.40 | 65.83 | 0.78 | 0.90 | 22.80 |
| Schmidt (2005) | W14 | US | 8 | 0 | 75 | 3.62 | 13.95 | 13.76 | 38.75 | 0.77 | 0.60 | 26.80 |
| Schmidt (2005) | W14 | US | 12 | 0 | 75 | 4.13 | 13.95 | 14.79 | 38.75 | 0.77 | 0.77 | 27.10 |
| Schmidt (2005) | W14 | US | 16 | 0 | 75 | 4.13 | 13.95 | 15.63 | 38.75 | 0.77 | 0.91 | 22.20 |
| Schmidt (2005) | W14 | DS | 8 | 0 | 75 | 2.45 | 20.43 | 9.59 | 65.83 | 0.78 | 0.60 | 26.40 |
| Schmidt (2005) | W14 | DS | 12 | 0 | 75 | 2.99 | 20.43 | 10.68 | 65.83 | 0.78 | 0.78 | 26.80 |
| Schmidt (2005) | W14 | DS | 16 | 0 | 75 | 2.99 | 20.43 | 11.40 | 65.83 | 0.78 | 0.90 | 22.20 |
| Schmidt (2005) | W15 | US | 8 | 0 | 75 | 3.62 | 16.82 | 13.76 | 38.75 | 0.77 | 0.60 | 26.80 |
| Schmidt (2005) | W15 | US | 12 | 0 | 75 | 4.13 | 16.82 | 14.79 | 38.75 | 0.77 | 0.77 | 27.10 |
| Schmidt (2005) | W15 | US | 16 | 0 | 75 | 4.13 | 16.82 | 15.63 | 38.75 | 0.77 | 0.91 | 22.20 |
| Schmidt (2005) | W15 | DS | 8 | 0 | 75 | 2.45 | 26.39 | 9.59 | 65.83 | 0.78 | 0.60 | 26.40 |

| Study | ID | Bend | $Q$ | φ | θ | $L_{W\text{-}PROJ}$ | $L_{ARC}$ | $T_W$ | $R_C$ | $h_W$ | $D_B$ | $A^*$ |
|---|---|---|---|---|---|---|---|---|---|---|---|---|
| - | - | - | ft³/s | ° | ° | ft | ft | ft | ft | ft | ft | - |
| Schmidt (2005) | W15 | DS | 12 | 0 | 75 | 2.99 | 26.39 | 10.68 | 65.83 | 0.78 | 0.78 | 26.80 |
| Schmidt (2005) | W15 | DS | 16 | 0 | 75 | 2.99 | 26.39 | 11.40 | 65.83 | 0.78 | 0.90 | 22.20 |
| Schmidt (2005) | W16 | US | 8 | 10 | 90 | 5.14 | 15.03 | 13.76 | 38.75 | 0.13 | 0.60 | 22.50 |
| Schmidt (2005) | W16 | US | 12 | 10 | 90 | 5.14 | 15.03 | 14.79 | 38.75 | 0.13 | 0.77 | 19.90 |
| Schmidt (2005) | W16 | US | 16 | 10 | 90 | 5.14 | 15.03 | 15.63 | 38.75 | 0.13 | 0.91 | 17.80 |
| Schmidt (2005) | W16 | DS | 8 | 10 | 90 | 3.11 | 19.23 | 9.59 | 65.83 | 0.42 | 0.60 | 21.20 |
| Schmidt (2005) | W16 | DS | 12 | 10 | 90 | 3.11 | 19.23 | 10.68 | 65.83 | 0.42 | 0.78 | 18.80 |
| Schmidt (2005) | W16 | DS | 16 | 10 | 90 | 3.11 | 19.23 | 11.40 | 65.83 | 0.42 | 0.90 | 17.00 |
| Schmidt (2005) | W17 | US | 8 | 10 | 90 | 5.14 | 11.49 | 13.76 | 38.75 | 0.13 | 0.60 | 22.50 |
| Schmidt (2005) | W17 | US | 12 | 10 | 90 | 5.14 | 11.49 | 14.79 | 38.75 | 0.13 | 0.77 | 19.90 |
| Schmidt (2005) | W17 | US | 16 | 10 | 90 | 5.14 | 11.49 | 15.63 | 38.75 | 0.13 | 0.91 | 17.80 |
| Schmidt (2005) | W17 | DS | 8 | 10 | 90 | 3.11 | 17.07 | 9.59 | 65.83 | 0.42 | 0.60 | 21.20 |
| Schmidt (2005) | W17 | DS | 12 | 10 | 90 | 3.11 | 17.07 | 10.68 | 65.83 | 0.42 | 0.78 | 18.80 |
| Schmidt (2005) | W17 | DS | 16 | 10 | 90 | 3.11 | 17.07 | 11.40 | 65.83 | 0.42 | 0.90 | 17.00 |
| Schmidt (2005) | W18 | US | 8 | 10 | 60 | 4.91 | 11.49 | 13.76 | 38.75 | 0.13 | 0.60 | 22.10 |
| Schmidt (2005) | W18 | US | 12 | 10 | 60 | 4.91 | 11.49 | 14.79 | 38.75 | 0.13 | 0.77 | 19.90 |
| Schmidt (2005) | W18 | US | 16 | 10 | 60 | 4.91 | 11.49 | 15.63 | 38.75 | 0.13 | 0.91 | 18.20 |
| Schmidt (2005) | W18 | DS | 8 | 10 | 60 | 3.00 | 17.07 | 9.59 | 65.83 | 0.42 | 0.60 | 20.80 |
| Schmidt (2005) | W18 | DS | 12 | 10 | 60 | 3.00 | 17.07 | 10.68 | 65.83 | 0.42 | 0.78 | 18.80 |
| Schmidt (2005) | W18 | DS | 16 | 10 | 60 | 3.00 | 17.07 | 11.40 | 65.83 | 0.42 | 0.90 | 17.30 |
| Schmidt (2005) | W19 | US | 8 | 10 | 90 | 5.14 | 13.85 | 13.76 | 38.75 | 0.13 | 0.60 | 22.50 |
| Schmidt (2005) | W19 | US | 12 | 10 | 90 | 5.14 | 13.85 | 14.79 | 38.75 | 0.13 | 0.77 | 19.90 |
| Schmidt (2005) | W19 | US | 16 | 10 | 90 | 5.14 | 13.85 | 15.63 | 38.75 | 0.13 | 0.91 | 17.80 |
| Schmidt (2005) | W19 | DS | 8 | 10 | 90 | 3.11 | 22.06 | 9.59 | 65.83 | 0.42 | 0.60 | 21.20 |
| Schmidt (2005) | W19 | DS | 12 | 10 | 90 | 3.11 | 22.06 | 10.68 | 65.83 | 0.42 | 0.78 | 18.80 |
| Schmidt (2005) | W19 | DS | 16 | 10 | 90 | 3.11 | 22.06 | 11.40 | 65.83 | 0.42 | 0.90 | 17.00 |
| Schmidt (2005) | W20 | US | 8 | 10 | 60 | 4.91 | 13.48 | 13.76 | 38.75 | 0.13 | 0.60 | 22.10 |
| Schmidt (2005) | W20 | US | 12 | 10 | 60 | 4.91 | 13.48 | 14.79 | 38.75 | 0.13 | 0.77 | 19.90 |
| Schmidt (2005) | W20 | US | 16 | 10 | 60 | 4.91 | 13.48 | 15.63 | 38.75 | 0.13 | 0.91 | 18.20 |
| Schmidt (2005) | W20 | DS | 8 | 10 | 60 | 3.00 | 21.30 | 9.59 | 65.83 | 0.42 | 0.60 | 20.80 |
| Schmidt (2005) | W20 | DS | 12 | 10 | 60 | 3.00 | 21.30 | 10.68 | 65.83 | 0.42 | 0.78 | 18.80 |
| Schmidt (2005) | W20 | DS | 16 | 10 | 60 | 3.00 | 21.30 | 11.40 | 65.83 | 0.42 | 0.90 | 17.30 |
| Schmidt (2005) | W21 | US | 8 | 10 | 90 | 2.88 | 8.54 | 13.76 | 38.75 | 0.44 | 0.60 | 12.60 |
| Schmidt (2005) | W21 | US | 12 | 10 | 90 | 2.88 | 8.54 | 14.79 | 38.75 | 0.44 | 0.77 | 11.60 |
| Schmidt (2005) | W21 | US | 16 | 10 | 90 | 2.88 | 8.54 | 15.63 | 38.75 | 0.44 | 0.91 | 10.40 |
| Schmidt (2005) | W21 | DS | 12 | 10 | 90 | 1.72 | 16.78 | 10.68 | 65.83 | 0.69 | 0.78 | 9.80 |
| Schmidt (2005) | W21 | DS | 16 | 10 | 90 | 1.72 | 16.78 | 11.40 | 65.83 | 0.69 | 0.90 | 9.70 |
| Schmidt (2005) | W22 | US | 8 | 10 | 60 | 2.79 | 8.54 | 13.76 | 38.75 | 0.44 | 0.60 | 12.50 |
| Schmidt (2005) | W22 | US | 12 | 10 | 60 | 2.79 | 8.54 | 14.79 | 38.75 | 0.44 | 0.77 | 11.70 |
| Schmidt (2005) | W22 | US | 16 | 10 | 60 | 2.79 | 8.54 | 15.63 | 38.75 | 0.44 | 0.91 | 10.80 |
| Schmidt (2005) | W22 | DS | 12 | 10 | 60 | 1.66 | 16.78 | 10.68 | 65.83 | 0.69 | 0.78 | 9.80 |
| Schmidt (2005) | W22 | DS | 16 | 10 | 60 | 1.66 | 16.78 | 11.40 | 65.83 | 0.69 | 0.90 | 9.80 |

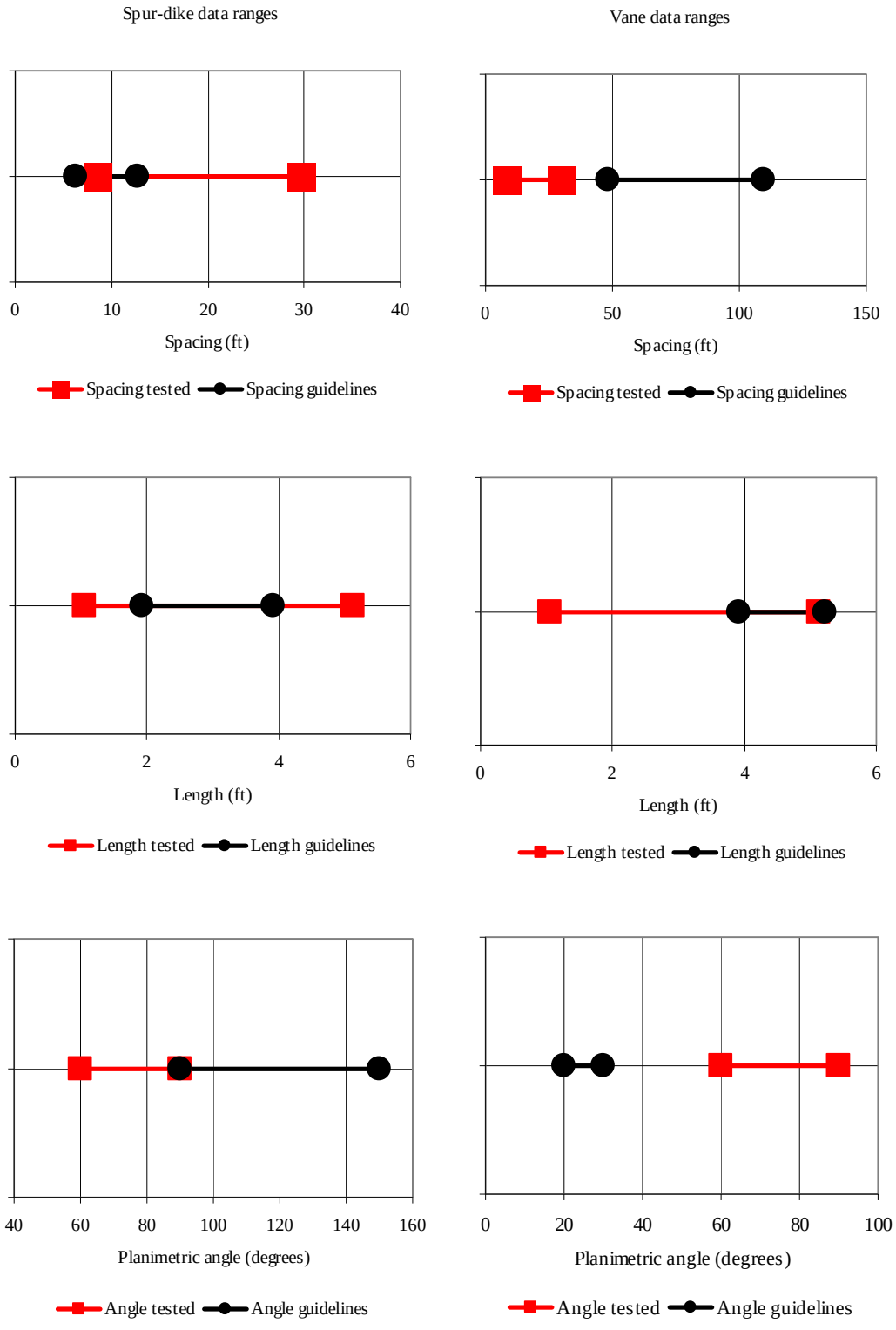


**Figure 48.** Ranges of laboratory data compared to design recommendations

# A2. Normalized hydraulic ratios

**Table 18.** Configuration maximum and average velocity ratios, regional analysis

| ID | Bend | $Q$ (ft³/s) | $MVR_O$ | $MVR_I$ | $MVR_C$ | $AVR_O$ | $AVR_I$ | $AVR_C$ |
|---|---|---|---|---|---|---|---|---|
| W01 | US | 8 | 0.438 | 1.509 | 1.337 | 0.159 | 1.259 | 1.195 |
| W01 | US | 12 | 0.210 | 1.537 | 1.302 | 0.110 | 1.370 | 1.179 |
| W01 | US | 16 | 0.263 | 1.493 | 1.298 | 0.142 | 1.344 | 1.158 |
| W01 | DS | 8 | 0.203 | 1.523 | 1.680 | 0.127 | 1.331 | 1.472 |
| W01 | DS | 12 | 0.194 | 1.630 | 1.803 | 0.178 | 1.513 | 1.539 |
| W01 | DS | 16 | 0.250 | 1.713 | 1.708 | 0.128 | 1.573 | 1.532 |
| W02 | US | 8 | 0.357 | 1.518 | 1.432 | 0.166 | 1.195 | 1.283 |
| W02 | US | 12 | 0.285 | 1.578 | 1.327 | 0.105 | 1.348 | 1.220 |
| W02 | US | 16 | 0.175 | 1.525 | 1.335 | 0.147 | 1.324 | 1.232 |
| W02 | DS | 8 | 0.267 | 1.490 | 1.653 | 0.191 | 1.208 | 1.343 |
| W02 | DS | 12 | 0.281 | 1.630 | 1.601 | 0.200 | 1.388 | 1.438 |
| W02 | DS | 16 | 0.401 | 1.674 | 1.750 | 0.254 | 1.490 | 1.478 |
| W03 | US | 8 | 0.398 | 1.492 | 1.399 | 0.183 | 1.208 | 1.261 |
| W03 | US | 12 | 0.354 | 1.549 | 1.514 | 0.129 | 1.258 | 1.196 |
| W03 | US | 16 | 0.400 | 1.530 | 1.305 | 0.146 | 1.298 | 1.170 |
| W03 | DS | 8 | 0.266 | 1.580 | 1.714 | 0.110 | 1.376 | 1.484 |
| W03 | DS | 12 | 0.229 | 1.619 | 1.682 | 0.104 | 1.453 | 1.486 |
| W03 | DS | 16 | 0.194 | 1.569 | 1.699 | 0.149 | 1.439 | 1.443 |
| W04 | US | 8 | 0.183 | 1.172 | 1.383 | 0.132 | 1.056 | 1.144 |
| W04 | US | 12 | 0.357 | 1.382 | 1.257 | 0.148 | 1.214 | 1.105 |
| W04 | US | 16 | 0.496 | 1.335 | 1.244 | 0.186 | 1.231 | 1.091 |
| W04 | DS | 8 | 0.765 | 1.147 | 1.288 | 0.272 | 1.043 | 1.136 |
| W04 | DS | 12 | 0.906 | 1.348 | 1.396 | 0.332 | 1.199 | 1.238 |
| W04 | DS | 16 | 0.978 | 1.387 | 1.380 | 0.233 | 1.265 | 1.210 |
| W05 | US | 8 | 0.382 | 1.340 | 1.151 | 0.154 | 1.140 | 1.106 |
| W05 | US | 12 | 0.438 | 1.345 | 1.182 | 0.165 | 1.199 | 1.091 |
| W05 | US | 16 | 0.530 | 1.427 | 1.279 | 0.176 | 1.269 | 1.173 |
| W05 | DS | 8 | 0.871 | 1.251 | 1.241 | 0.331 | 1.003 | 1.148 |
| W05 | DS | 12 | 0.857 | 1.290 | 1.322 | 0.360 | 1.101 | 1.111 |
| W05 | DS | 16 | 1.197 | 1.419 | 1.519 | 0.293 | 1.268 | 1.224 |
| W06 | US | 8 | 0.318 | 1.445 | 1.239 | 0.189 | 1.188 | 1.189 |
| W06 | US | 12 | 0.230 | 1.513 | 1.308 | 0.146 | 1.302 | 1.248 |
| W06 | US | 16 | 0.272 | 1.500 | 1.307 | 0.121 | 1.355 | 1.253 |
| W06 | DS | 8 | 0.390 | 1.324 | 1.477 | 0.173 | 1.101 | 1.246 |
| W06 | DS | 12 | 0.514 | 1.025 | 0.886 | 0.099 | 0.881 | 0.845 |
| W06 | DS | 16 | 0.546 | 1.507 | 1.456 | 0.126 | 1.256 | 1.370 |
| W07 | US | 8 | 0.317 | 1.477 | 1.342 | 0.169 | 1.264 | 1.245 |
| W07 | US | 12 | 0.262 | 1.514 | 1.269 | 0.136 | 1.287 | 1.230 |
| W07 | US | 16 | 0.295 | 1.301 | 1.518 | 0.145 | 1.233 | 1.332 |
| W07 | DS | 8 | 0.614 | 1.335 | 1.562 | 0.209 | 1.154 | 1.364 |
| W07 | DS | 12 | 0.699 | 1.392 | 1.478 | 0.188 | 1.264 | 1.369 |
| W07 | DS | 16 | 0.642 | 1.471 | 1.561 | 0.154 | 1.340 | 1.429 |
| W08 | US | 8 | 0.174 | 1.229 | 1.095 | 0.128 | 1.023 | 1.020 |
| W08 | US | 12 | 0.216 | 1.321 | 1.132 | 0.154 | 1.128 | 1.039 |
| W08 | US | 16 | 0.511 | 1.263 | 1.086 | 0.144 | 1.145 | 1.036 |
| W08 | DS | 8 | 0.612 | 0.794 | 1.336 | 0.158 | 1.040 | 1.200 |

| ID | Bend | $Q$ (ft³/s) | $MVR_O$ | $MVR_I$ | $MVR_C$ | $AVR_O$ | $AVR_I$ | $AVR_C$ |
|---|---|---|---|---|---|---|---|---|
| W08 | DS | 12 | 0.639 | 1.100 | 1.183 | 0.201 | 0.972 | 1.037 |
| W08 | DS | 16 | 0.774 | 1.265 | 1.289 | 0.175 | 1.139 | 1.185 |
| W09 | US | 8 | 0.138 | 1.266 | 1.067 | 0.107 | 1.037 | 1.025 |
| W09 | US | 12 | 0.275 | 1.256 | 1.083 | 0.131 | 1.099 | 1.025 |
| W09 | US | 16 | 0.442 | 1.234 | 1.079 | 0.120 | 1.126 | 1.021 |
| W09 | DS | 8 | 0.669 | 1.102 | 1.226 | 0.288 | 0.950 | 1.103 |
| W09 | DS | 12 | 0.753 | 1.178 | 1.306 | 0.189 | 1.062 | 1.167 |
| W09 | DS | 16 | 0.761 | 1.287 | 1.338 | 0.156 | 1.144 | 1.218 |
| W10 | US | 8 | 0.288 | 1.287 | 1.184 | 0.130 | 1.165 | 1.135 |
| W10 | US | 12 | 0.126 | 1.216 | 1.176 | 0.122 | 1.123 | 1.065 |
| W10 | US | 16 | 0.252 | 1.338 | 1.178 | 0.125 | 1.247 | 1.132 |
| W10 | DS | 8 | 0.269 | 1.398 | 1.443 | 0.133 | 1.160 | 1.296 |
| W10 | DS | 12 | 0.416 | 1.403 | 1.411 | 0.181 | 1.232 | 1.305 |
| W10 | DS | 16 | 0.518 | 1.467 | 1.430 | 0.130 | 1.356 | 1.360 |
| W11 | US | 8 | 0.199 | 1.304 | 1.142 | 0.140 | 1.127 | 1.107 |
| W11 | US | 12 | 0.255 | 1.300 | 1.203 | 0.118 | 1.185 | 1.131 |
| W11 | US | 16 | 0.307 | 1.308 | 1.196 | 0.163 | 1.213 | 1.122 |
| W11 | DS | 8 | 0.401 | 1.317 | 1.398 | 0.176 | 1.172 | 1.305 |
| W11 | DS | 12 | 0.503 | 1.429 | 1.452 | 0.215 | 1.250 | 1.333 |
| W11 | DS | 16 | 0.635 | 1.380 | 1.529 | 0.133 | 1.282 | 1.379 |
| W12 | US | 8 | 0.277 | 1.324 | 1.241 | 0.172 | 1.160 | 1.163 |
| W12 | US | 12 | 0.185 | 1.307 | 1.187 | 0.130 | 1.207 | 1.125 |
| W12 | US | 16 | 0.325 | 1.352 | 1.176 | 0.162 | 1.244 | 1.135 |
| W12 | DS | 8 | 0.164 | 1.461 | 1.700 | 0.143 | 1.303 | 1.436 |
| W12 | DS | 12 | 0.153 | 1.537 | 1.629 | 0.168 | 1.396 | 1.259 |
| W12 | DS | 16 | 0.374 | 1.605 | 1.580 | 0.132 | 1.431 | 1.418 |
| W13 | US | 8 | 0.280 | 1.333 | 1.205 | 0.177 | 1.106 | 1.135 |
| W13 | US | 12 | 0.313 | 1.289 | 1.146 | 0.123 | 1.176 | 1.104 |
| W13 | US | 16 | 0.365 | 1.308 | 1.290 | 0.182 | 1.183 | 1.148 |
| W13 | DS | 8 | 0.135 | 1.374 | 1.469 | 0.153 | 1.148 | 1.251 |
| W13 | DS | 12 | 0.273 | 1.447 | 1.452 | 0.146 | 1.277 | 1.311 |
| W13 | DS | 16 | 0.287 | 1.536 | 1.654 | 0.154 | 1.446 | 1.408 |
| W14 | US | 8 | 0.286 | 1.445 | 1.309 | 0.203 | 1.231 | 1.194 |
| W14 | US | 12 | 0.263 | 1.445 | 1.326 | 0.142 | 1.325 | 1.252 |
| W14 | US | 16 | 0.490 | 1.464 | 1.350 | 0.144 | 1.326 | 1.252 |
| W14 | DS | 8 | 0.180 | 1.606 | 1.691 | 0.172 | 1.345 | 1.438 |
| W14 | DS | 12 | 0.258 | 1.615 | 1.605 | 0.186 | 1.443 | 1.437 |
| W14 | DS | 16 | 0.262 | 1.560 | 1.631 | 0.142 | 1.486 | 1.460 |
| W15 | US | 8 | 0.368 | 1.588 | 1.403 | 0.203 | 1.306 | 1.321 |
| W15 | US | 12 | 0.390 | 1.421 | 1.309 | 0.117 | 1.286 | 1.235 |
| W15 | US | 16 | 0.379 | 1.391 | 1.378 | 0.150 | 1.309 | 1.242 |
| W15 | DS | 8 | 0.290 | 1.565 | 1.640 | 0.216 | 1.257 | 1.396 |
| W15 | DS | 12 | 0.271 | 1.547 | 1.478 | 0.151 | 1.400 | 1.400 |
| W15 | DS | 16 | 0.394 | 1.536 | 1.564 | 0.151 | 1.457 | 1.446 |
| W16 | US | 8 | 0.188 | 1.374 | 1.321 | 0.142 | 1.184 | 1.236 |
| W16 | US | 12 | 0.305 | 1.372 | 1.296 | 0.146 | 1.248 | 1.168 |
| W16 | US | 16 | 0.387 | 1.373 | 1.273 | 0.212 | 1.284 | 1.195 |
| W16 | DS | 8 | 0.302 | 1.375 | 1.566 | 0.150 | 1.161 | 1.389 |
| W16 | DS | 12 | 0.486 | 1.379 | 1.384 | 0.146 | 1.237 | 1.322 |

| ID | Bend | $Q$ (ft³/s) | $MVR_O$ | $MVR_I$ | $MVR_C$ | $AVR_O$ | $AVR_I$ | $AVR_C$ |
|---|---|---|---|---|---|---|---|---|
| W16 | DS | 16 | 0.579 | 1.474 | 1.493 | 0.203 | 1.336 | 1.406 |
| W17 | US | 8 | 0.190 | 1.407 | 1.236 | 0.154 | 1.170 | 1.199 |
| W17 | US | 12 | 0.269 | 1.369 | 1.285 | 0.150 | 1.242 | 1.185 |
| W17 | US | 16 | 0.423 | 1.345 | 1.305 | 0.223 | 1.298 | 1.212 |
| W17 | DS | 8 | 0.180 | 1.411 | 1.391 | 0.138 | 1.089 | 1.220 |
| W17 | DS | 12 | 0.416 | 1.423 | 1.474 | 0.117 | 1.330 | 1.385 |
| W17 | DS | 16 | 0.476 | 1.465 | 1.535 | 0.171 | 1.381 | 1.423 |
| W18 | US | 8 | 0.254 | 1.334 | 1.296 | 0.157 | 1.189 | 1.243 |
| W18 | US | 12 | 0.253 | 1.338 | 1.249 | 0.153 | 1.222 | 1.198 |
| W18 | US | 16 | 0.345 | 1.475 | 1.323 | 0.184 | 1.349 | 1.219 |
| W18 | DS | 8 | 0.243 | 1.339 | 1.452 | 0.146 | 1.089 | 1.313 |
| W18 | DS | 12 | 0.430 | 1.426 | 1.443 | 0.140 | 1.336 | 1.358 |
| W18 | DS | 16 | 0.565 | 1.500 | 1.549 | 0.192 | 1.421 | 1.462 |
| W19 | US | 8 | 0.160 | 1.413 | 1.281 | 0.144 | 1.198 | 1.203 |
| W19 | US | 12 | 0.286 | 1.357 | 1.214 | 0.156 | 1.241 | 1.135 |
| W19 | US | 16 | 0.486 | 1.424 | 1.233 | 0.277 | 1.296 | 1.163 |
| W19 | DS | 8 | 0.342 | 1.291 | 1.352 | 0.145 | 1.138 | 1.182 |
| W19 | DS | 12 | 0.549 | 1.395 | 1.429 | 0.130 | 1.251 | 1.310 |
| W19 | DS | 16 | 0.610 | 1.308 | 1.405 | 0.283 | 1.221 | 1.305 |
| W20 | US | 8 | 0.156 | 1.359 | 1.313 | 0.132 | 1.180 | 1.246 |
| W20 | US | 12 | 0.202 | 1.392 | 1.317 | 0.150 | 1.278 | 1.231 |
| W20 | US | 16 | 0.440 | 1.388 | 1.339 | 0.172 | 1.303 | 1.267 |
| W20 | DS | 8 | 0.388 | 1.337 | 1.577 | 0.138 | 1.229 | 1.361 |
| W20 | DS | 12 | 0.505 | 1.383 | 1.419 | 0.140 | 1.286 | 1.347 |
| W20 | DS | 16 | 0.595 | 1.413 | 1.437 | 0.120 | 1.336 | 1.361 |
| W21 | US | 8 | 0.199 | 1.323 | 1.247 | 0.141 | 1.185 | 1.208 |
| W21 | US | 12 | 0.481 | 1.237 | 1.190 | 0.194 | 1.150 | 1.095 |
| W21 | US | 16 | 0.699 | 1.282 | 1.253 | 0.225 | 1.214 | 1.165 |
| W21 | DS | 12 | 0.872 | 1.237 | 1.254 | 0.203 | 1.106 | 1.181 |
| W21 | DS | 16 | 1.030 | 1.345 | 1.373 | 0.185 | 1.194 | 1.291 |
| W22 | US | 8 | 0.193 | 1.331 | 1.210 | 0.137 | 1.145 | 1.164 |
| W22 | US | 12 | 0.442 | 1.263 | 1.181 | 0.164 | 1.132 | 1.101 |
| W22 | US | 16 | 0.740 | 1.317 | 1.238 | 0.242 | 1.218 | 1.130 |
| W22 | DS | 12 | 0.838 | 1.207 | 1.260 | 0.196 | 1.097 | 1.144 |
| W22 | DS | 16 | 0.988 | 1.245 | 1.368 | 0.120 | 1.163 | 1.240 |

**Table 19.** Configuration maximum and average boundary shear-stress ratios, point-based analysis

| ID | Bend | $Q$ (ft³/s) | $M\tau R_O$ | $M\tau R_I$ | $M\tau R_C$ | $A\tau R_O$ | $A\tau R_I$ | $A\tau R_C$ |
|---|---|---|---|---|---|---|---|---|
| W01 | US | 8 | 0.032 | 1.336 | 1.150 | 0.013 | 0.934 | 0.990 |
| W01 | US | 12 | 0.048 | 1.206 | 1.047 | 0.032 | 1.022 | 0.919 |
| W01 | US | 16 | 0.051 | 1.618 | 1.079 | 0.020 | 1.153 | 0.939 |
| W01 | DS | 8 | 0.150 | 4.785 | 7.317 | 0.054 | 4.552 | 5.270 |
| W01 | DS | 12 | 0.195 | 3.961 | 4.404 | 0.079 | 2.888 | 2.997 |
| W01 | DS | 16 | 3.141 | 7.902 | 4.677 | 0.948 | 4.703 | 3.342 |
| W02 | US | 8 | 0.015 | n/a | 1.418 | 0.004 | n/a | 1.069 |
| W02 | US | 12 | 0.086 | n/a | 1.203 | 0.020 | n/a | 0.936 |
| W02 | US | 16 | 0.003 | n/a | 1.073 | 0.000 | n/a | 0.861 |
| W02 | DS | 8 | 0.369 | 4.712 | 7.559 | 0.116 | 4.120 | 5.072 |

| ID | Bend | $Q$ (ft³/s) | $M\tau R_O$ | $M\tau R_I$ | $M\tau R_C$ | $A\tau R_O$ | $A\tau R_I$ | $A\tau R_C$ |
|---|---|---|---|---|---|---|---|---|
| W02 | DS | 12 | 0.219 | 2.607 | 3.277 | 0.065 | 2.194 | 2.227 |
| W02 | DS | 16 | 0.264 | 3.365 | 4.766 | 0.165 | 3.159 | 2.962 |
| W03 | US | 8 | 0.165 | 1.292 | 1.291 | 0.047 | 0.996 | 1.062 |
| W03 | US | 12 | 0.056 | 1.171 | 0.975 | 0.004 | 0.949 | 0.832 |
| W03 | US | 16 | 0.038 | 1.177 | 1.108 | 0.006 | 0.930 | 0.829 |
| W03 | DS | 8 | 0.215 | 4.621 | 7.524 | 0.047 | 3.769 | 4.780 |
| W03 | DS | 12 | 0.239 | 2.518 | 3.681 | 0.041 | 2.338 | 2.727 |
| W03 | DS | 16 | 0.418 | 3.828 | 3.732 | 0.121 | 2.980 | 3.016 |
| W04 | US | 8 | 2.757 | 1.778 | 1.662 | 1.402 | 1.267 | 1.100 |
| W04 | US | 12 | 1.375 | 1.895 | 1.574 | 0.787 | 1.544 | 1.463 |
| W04 | US | 16 | 0.884 | 1.915 | 1.541 | 0.741 | 1.630 | 1.432 |
| W04 | DS | 8 | 5.641 | 6.150 | 4.917 | 4.003 | 4.081 | 3.559 |
| W04 | DS | 12 | 2.416 | 3.149 | 3.586 | 1.755 | 2.595 | 2.715 |
| W04 | DS | 16 | 3.190 | 3.925 | 4.105 | 2.440 | 3.170 | 3.259 |
| W05 | US | 8 | 0.999 | 1.914 | 1.767 | 0.908 | 1.672 | 1.672 |
| W05 | US | 12 | 0.878 | 1.885 | 1.538 | 0.774 | 1.532 | 1.384 |
| W05 | US | 16 | 0.900 | 1.786 | 2.942 | 0.754 | 1.561 | 1.653 |
| W05 | DS | 8 | 5.138 | 4.503 | 5.087 | 3.448 | 3.944 | 4.262 |
| W05 | DS | 12 | 3.880 | 3.093 | 3.014 | 2.024 | 1.852 | 2.239 |
| W05 | DS | 16 | 3.561 | 3.804 | 4.911 | 2.761 | 3.166 | 3.827 |
| W06 | US | 8 | 0.929 | 2.065 | 2.021 | 0.903 | 1.770 | 1.854 |
| W06 | US | 12 | 0.757 | 2.240 | 1.897 | 0.721 | 1.751 | 1.614 |
| W06 | US | 16 | 1.818 | 1.845 | 1.858 | 0.961 | 1.084 | 1.491 |
| W06 | DS | 8 | 2.304 | 5.789 | 7.215 | 1.816 | 4.859 | 5.652 |
| W06 | DS | 12 | 1.272 | 3.872 | 3.414 | 0.918 | 2.677 | 2.655 |
| W06 | DS | 16 | 4.158 | 3.616 | 4.129 | 2.886 | 2.913 | 1.969 |
| W07 | US | 8 | 0.830 | 2.092 | 1.938 | 0.785 | 1.689 | 1.746 |
| W07 | US | 12 | 0.665 | 2.115 | 2.286 | 0.622 | 1.555 | 1.596 |
| W07 | US | 16 | 0.676 | 1.893 | 1.864 | 0.629 | 1.677 | 1.607 |
| W07 | DS | 8 | 2.237 | 5.453 | 6.828 | 1.752 | 4.786 | 5.674 |
| W07 | DS | 12 | 1.193 | 2.912 | 3.946 | 0.969 | 2.564 | 2.821 |
| W07 | DS | 16 | 1.723 | 4.004 | 4.492 | 1.394 | 4.002 | 3.822 |
| W08 | US | 8 | 0.802 | 1.815 | 1.664 | 0.517 | 1.189 | 1.532 |
| W08 | US | 12 | 0.799 | 2.095 | 1.485 | 0.676 | 1.330 | 1.399 |
| W08 | US | 16 | 0.904 | 2.055 | 1.571 | 0.665 | 1.608 | 1.435 |
| W08 | DS | 8 | 3.742 | 5.085 | 6.463 | 2.565 | 4.322 | 5.346 |
| W08 | DS | 12 | 1.886 | 2.971 | 3.763 | 1.378 | 2.445 | 2.822 |
| W08 | DS | 16 | 2.486 | 3.814 | 3.779 | 1.948 | 3.230 | 3.374 |
| W09 | US | 8 | 0.848 | 1.980 | 1.652 | 0.790 | 1.626 | 1.480 |
| W09 | US | 12 | 0.974 | 1.613 | 1.439 | 0.678 | 1.424 | 1.326 |
| W09 | US | 16 | 0.770 | 1.880 | 1.560 | 0.646 | 1.462 | 1.386 |
| W09 | DS | 8 | 3.365 | 4.994 | 6.343 | 2.323 | 4.157 | 5.044 |
| W09 | DS | 12 | 2.230 | 2.676 | 2.976 | 1.468 | 2.443 | 2.572 |
| W09 | DS | 16 | 3.685 | 3.520 | 4.100 | 2.017 | 3.321 | 3.471 |
| W10 | US | 8 | 0.758 | 1.830 | 1.954 | 0.731 | 1.429 | 1.542 |
| W10 | US | 12 | 0.616 | 1.513 | 1.551 | 0.591 | 1.266 | 1.304 |
| W10 | US | 16 | 0.657 | 1.870 | 1.737 | 0.573 | 1.466 | 1.463 |
| W10 | DS | 8 | 1.550 | 5.551 | 7.014 | 1.330 | 4.753 | 5.039 |
| W10 | DS | 12 | 1.005 | 2.811 | 3.339 | 0.780 | 2.634 | 2.800 |

| ID | Bend | $Q$ (ft³/s) | $M\tau R_O$ | $M\tau R_I$ | $M\tau R_C$ | $A\tau R_O$ | $A\tau R_I$ | $A\tau R_C$ |
|---|---|---|---|---|---|---|---|---|
| W10 | DS | 16 | 1.727 | 4.274 | 4.689 | 1.030 | 3.604 | 3.837 |
| W11 | US | 8 | 0.780 | 2.007 | 1.776 | 0.706 | 1.642 | 1.596 |
| W11 | US | 12 | 0.720 | 1.830 | 1.690 | 0.699 | 1.564 | 1.461 |
| W11 | US | 16 | 0.685 | 2.026 | 1.758 | 0.575 | 1.630 | 1.540 |
| W11 | DS | 8 | 1.720 | 5.733 | 8.138 | 1.503 | 5.075 | 5.432 |
| W11 | DS | 12 | 1.183 | 2.922 | 3.904 | 0.858 | 2.716 | 3.100 |
| W11 | DS | 16 | 1.882 | 4.180 | 4.391 | 1.070 | 3.446 | 3.702 |

# A3. Parameter response and sensitivity

## A.3.1 Velocity ratios

The all-structure maximum and average velocity ratio equations were presented in Table 9. Figure 49 provides the response of the all-structure equations to alteration of the six adjusted parameters. The plots of $L_{ARC}$, $R_C$, and θ do not have complex variable response; they only alter the dimensionless parameter on the abscissa axis and the response behaves according to the specified exponent in Table 9. Behavior of these variables was smooth throughout the laboratory ranges and showed appropriate responses from expectations of physical hydraulics depicted in the literature. Increased spacing increased outer-bank velocities, increased channel curvature decreased outer-bank velocity, and planimetric angle had a small, positive effect on all region hydraulics. Flat response of a dependent variable to parameter alteration indicated an exponent of zero and a dimensionless parameter determined not statistically significant during regression procedures.

Alteration of $L_{W\text{-}PROJ}$ indicated a direct impact on the shifted conveyance ratios and an indirect relationship with the outer-bank ratios. This corresponds well with physical expectations from the literature. With the exception of $MVR_O$, all hydraulic ratios responded to $L_{W\text{-}PROJ}$ gradually and smoothly through the laboratory data ranges and extrapolated well outside of laboratory bounds. The $MVR_O$ values for altered $L_{W\text{-}PROJ}$ approached a vertical asymptote near the lower range of the laboratory data and did not extrapolate well past the laboratory minimum; however, extrapolated smoothly past the maximum laboratory value. Values of $MVR_O$ calculated near the lower laboratory limit of the lateral contraction ratio should be evaluated cautiously.

Increased structure submergence produced increased velocity at the outer-bank and decreased velocity at the inner-bank and centerline. Results correspond to continuity principles and expected trends from the literature. The $MVR_O$ rapidly approached a vertical asymptote within the laboratory ranges, exceeding unity by relatively low $D_R$ of 1.5. Lack of applicability for $MVR_O$ throughout the full data range is attributed to the fact that there is a large, negative weight on $A^*$ for $MVR_O$ which is not regulated by a negative coefficient for $D_R$ (Table 9), and the combination of the vane and spur-dike datasets. $MVR_O$ was predicted accurately for the spur-dike ranges of $D_R$ and inaccurately for the vane ranges. Alteration of $T_W$ depicted an indirect relationship with the shifted conveyance zone and direct relationship with the outer-bank zone. Ratio response to $T_W$ alteration was smooth and extrapolates well to channel curvature values of naturally meandering rivers. Generally, functions behave gradually throughout the laboratory ranges with the exception of $D_R$ effects on $MVR_O$.

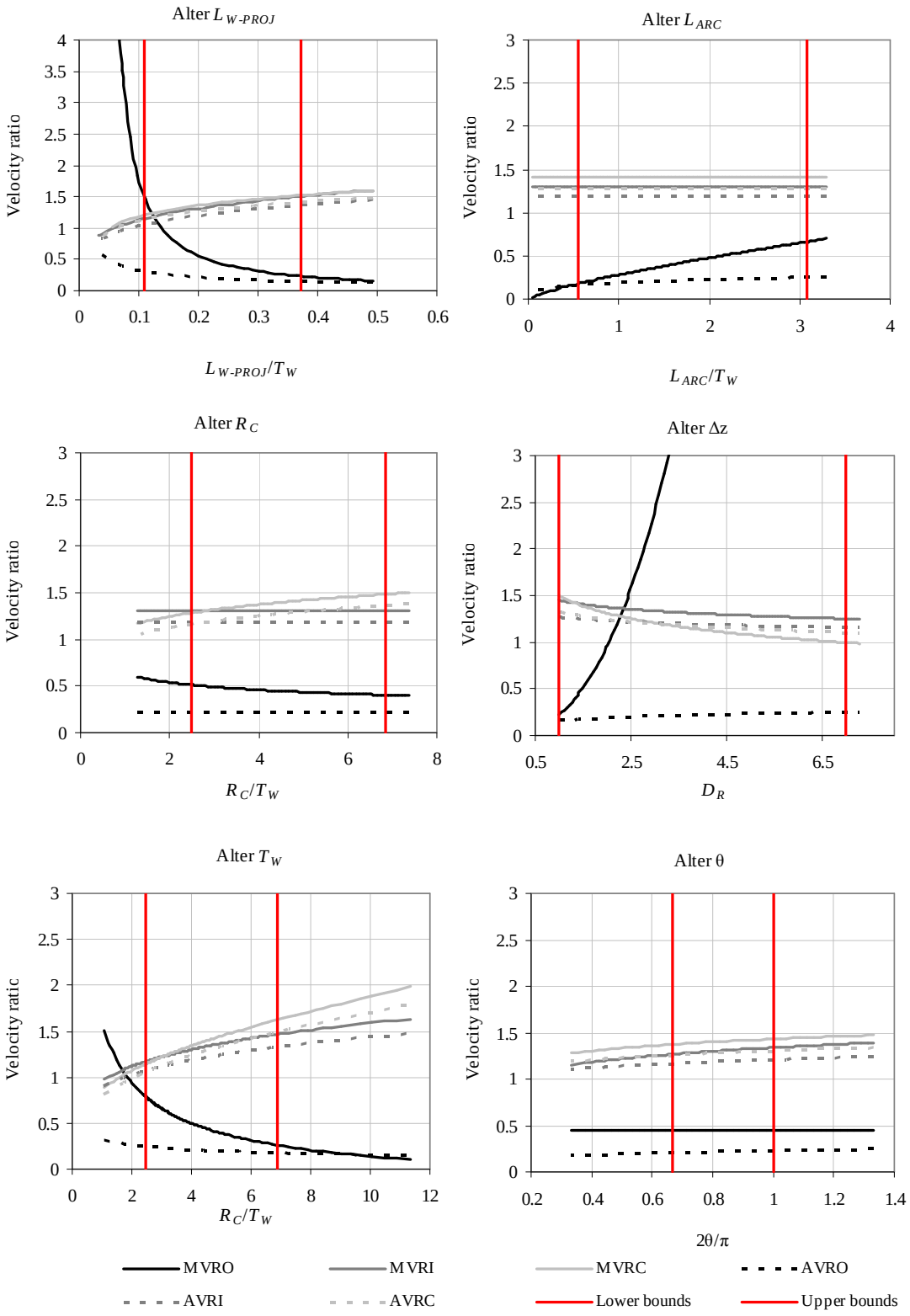


**Figure 49.** All-structure velocity equation parameter response

The spur-dike velocity ratio equations were detailed in Table 10. Spur-dike equation response and sensitivity to parameter alteration is graphically displayed in Figure 50. Plots of altered $L_{ARC}$, $R_C$, and $\theta$ behave according to the specific exponent of the containing dimensionless term from Table 10. When terms were found to be statistically significant, increased spacing ratio had a direct relationship with outer-bank velocity increase, increased channel curvature decreased outer-bank velocities and increased shifted conveyance, and planimetric angle increase showed a slight increase in shifted conveyance zone velocities. Increased projected weir length had the impact of reduced outer-bank velocities and associated increased inner-bank and centerline velocities.

Outer-bank velocities approached a vertical asymptote moving to the lower limit of the laboratory values of $L_{W\text{-}PROJ}/T_W$ such that extrapolations produce physically unrealistic values. Increase of the submergence had slight positive, or negligible, effects on all hydraulic ratios. Outer-bank increase is justified by overtopping and shifted conveyance to the bankline key-in. Joint increase of the outer-bank and shifted conveyance zones indicates that normalization conditions may have not fully accounted for hydraulics; the submergence ratio was directly related to volumetric flow rate such that increased submergence had higher stream velocities. Increasing $T_W$ was directly related to increased outer-bank velocities and inversely related to shifted conveyance velocities with functions behaving gradually and smoothly throughout the channel. Overall, all spur-dike velocity ratios were well behaved within the ranges of the laboratory data. Extrapolation past the laboratory ranges was typically smooth, with the exception of the outer-bank velocity ratios as function of the lateral contraction ratio.

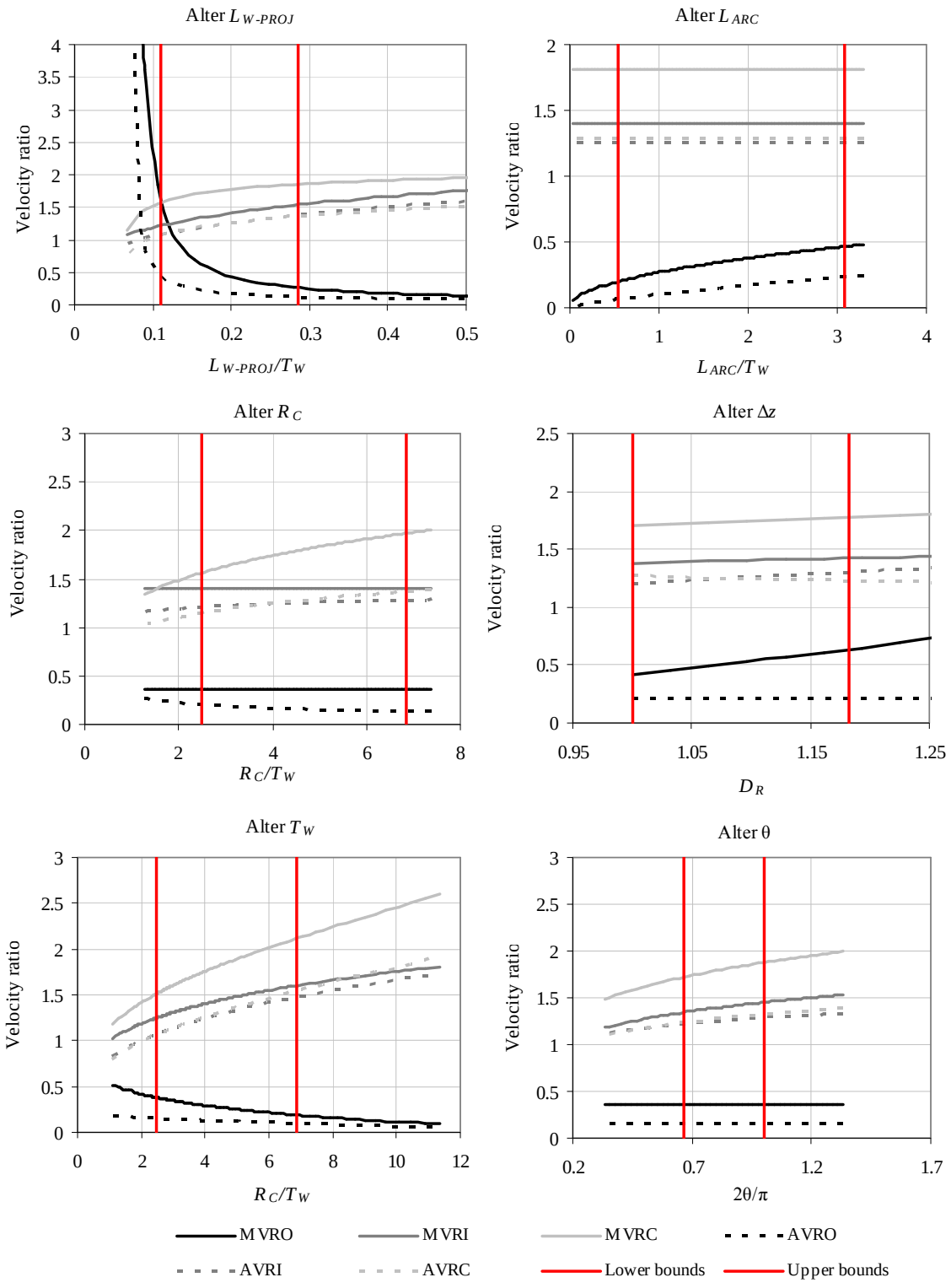


**Figure 50.** Spur-dike velocity equation parameter response

Vane velocity equations as summarized in Table 11 were subjected to parameter alteration for dependent variable response. Figure 51 illustrates plotted results of the analysis for all velocity ratios across the laboratory data ranges. Alteration of $L_{ARC}$, $R_C$, and θ behaved according to the specified regression weight in Table 11. Vane spacing ratio increase showed a decrease in the inner-bank velocity ratios and negligible effect on the outer-bank or centerline ratios. Increasing channel curvature resulted in increased velocities throughout the channel. Outer-bank velocity was reduced for increased curvature for the spur-dikes and the discrepancy may be explained by the differences between the design structure hydraulics. Flows overtopping the structure crest at all discharges may increase outer-bank velocity with channel curvature. No effect was determined for alteration of planimetric angle for vanes.

Increased $L_{W\text{-}PROJ}$ had an expected decrease in outer-bank velocity ratios and increase in the shifted conveyance ratios, corresponding to the all-structure and spur-dike responses. Shifted conveyance response was gradual throughout the laboratory ranges, while the outer-bank ratios approach a vertical asymptote passing the lower limit of the data. Submergence increase showed a negligible decrease in the shifted conveyance ratios, attributed to the conveyance diverted to the outer-bank; however, had a profound impact on the outer-bank ratios. By a submergence value of 2.75, both $MVR_O$ and $AVR_O$ had exceeded unity and showed behavior of rapidly approaching vertical asymptotes. Alteration of $T_W$ showed an increase in outer-bank velocities with increased $T_W$ and corresponding decrease in shifted conveyance velocities. Values behaved smoothly and gradually throughout the channel-curvature ranges of natural meandering systems. Ratios behaved did not exhibit abnormal response to parameter alteration with the exception of alteration of the submergence ratio at the outer-bank.

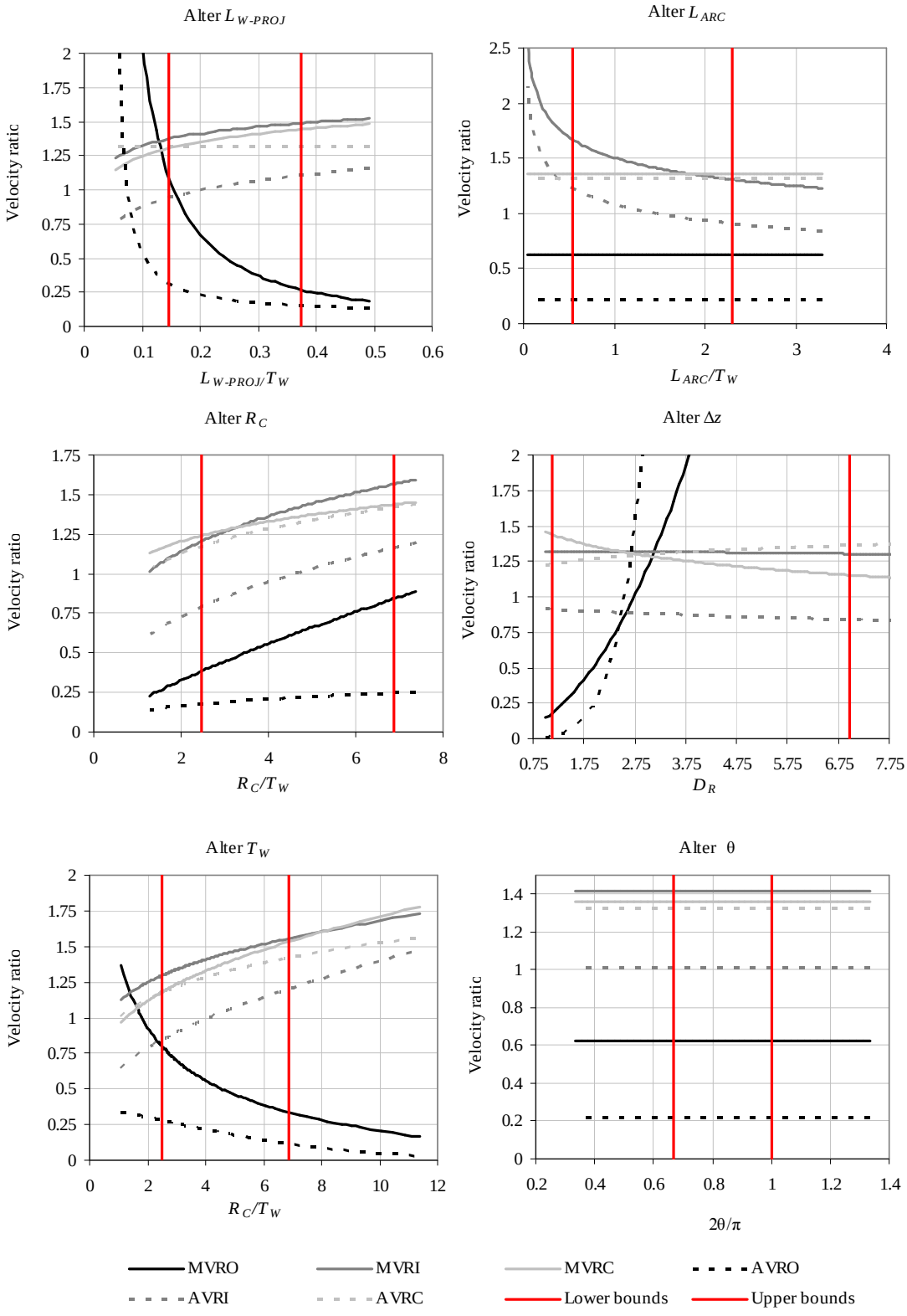


**Figure 51.** Vane velocity equation parameter response

### A.3.2. Boundary shear-stress ratios

Spur-dike boundary shear-stress regression equations were summarized in Table 12. Parameters were altered for the equations throughout the laboratory ranges and results are illustrated in Figure 52. Alteration of $L_{ARC}$, $R_C$, and θ behaved according to the specified regression weight in Table 12 with no response indicated for altered spacing or planimetric angle. Positive response was strongly observed with increased channel curvature for the shifted conveyance ratios and found mild or negligible for the outer-bank ratios. Lateral contraction ratio effects on the shear-stress ratios exhibited complex response for the shifted conveyance zone and a direct relationship for the outer-bank ratios. Inner-bank and centerline shear-stress exponentially decreased below the laboratory data limits, exhibited maximum ratio values near $L_{W\text{-}PROJ}/T_W$ approximately 0.15, and then gradually decayed through the upper ranges of the laboratory values. Outer-bank ratios exhibited behavior common to the velocity equation response and grew exponentially towards the lower limits of the laboratory data to reach a vertical asymptote beyond the laboratory range. Structure submergence affected all values to a negligibly or slightly positively with the exception of $M\tau R_I$ which exhibited a minimal decrease with increasing submergence. Similar behavior was noted for the alteration of $T_W$ where $M\tau R_I$ displayed a minimum value near curvature ratios of approximately 5. Other shifted conveyance ratios grew indirectly with increased $T_W$ and outer-bank ratio were directly related to increased $T_W$. Outer-bank shear-stress ratios as functions of $T_W$ were not found to extrapolate well past the lower laboratory limit. Vane outer-bank velocity ratios showed a more significant increase in the outer-bank velocity as a function of channel curvature. Inner-bank and centerline ratios showed a general trend of increase with increased channel curvature across all equation sets.

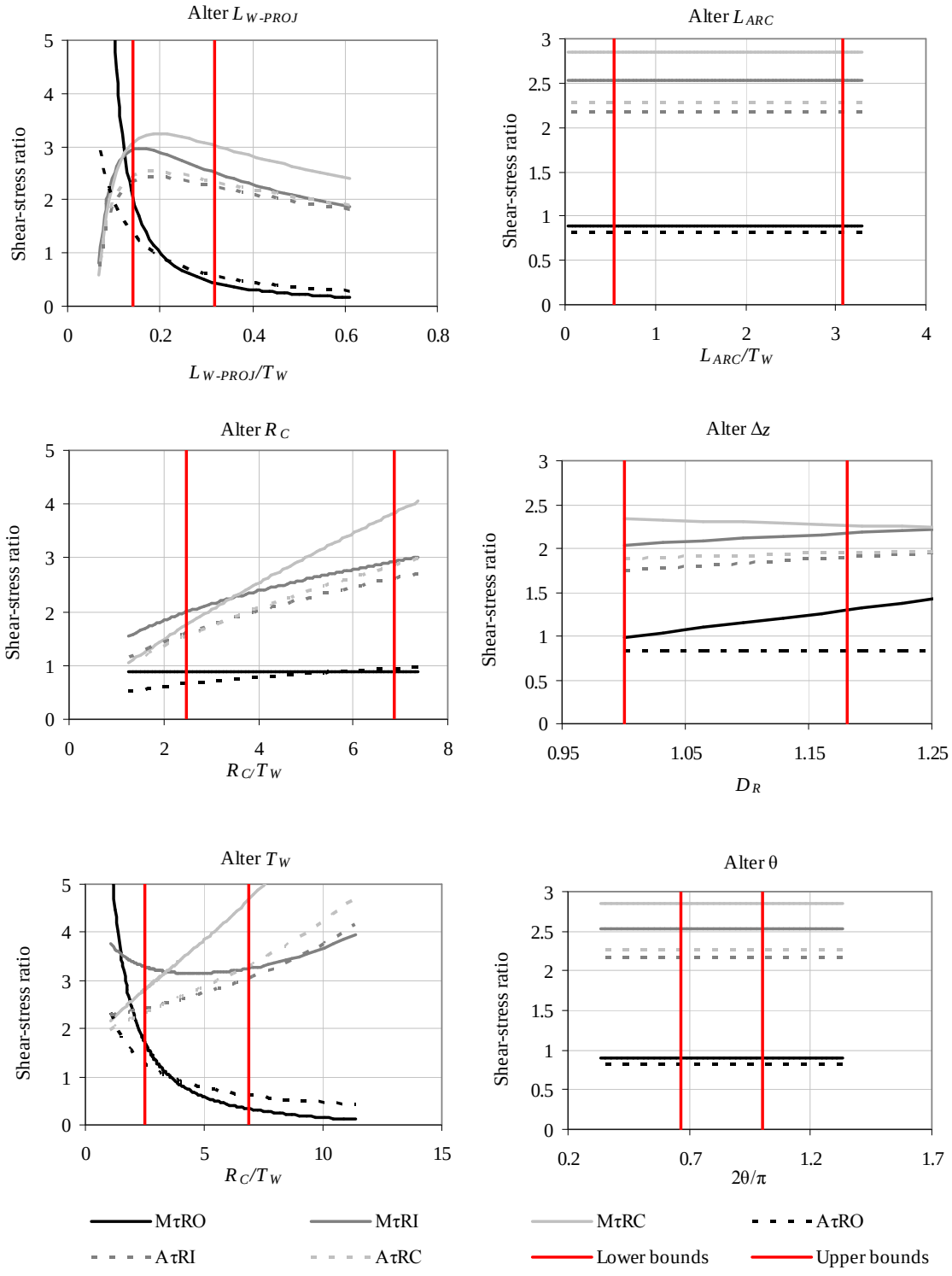


**Figure 52.** Spur-dike boundary shear-stress equation parameter response

# A4. Literature comparison

**Table 20.** Velocities from literature with normalization conditions

| Study | Configuration | $U_{AVG}$ ft/s | $MV_O$ ft/s | $MV_I$ ft/s | $MV_C$ ft/s | $AV_O$ ft/s | $AV_I$ ft/s | $AV_C$ ft/s |
|---|---|---|---|---|---|---|---|---|
| Lyn and Cunningham (2010) | H050-V22-T24A,B | 0.067 | 0.091 | 0.084 | 0.091 | 0.077 | 0.076 | 0.079 |
| | H050-V22-T48 | 0.067 | | 0.084 | 0.091 | | 0.072 | 0.091 |
| | H050-V25-T12A,B | 0.067 | | 0.091 | 0.099 | | 0.085 | 0.094 |
| | H075-V22-T48 | 0.067 | | 0.084 | 0.091 | | 0.074 | 0.084 |
| | H100-V22-T48 | 0.067 | | 0.084 | 0.091 | | 0.078 | 0.085 |
| Bui (2011) | 2,237 cfs | 3.320 | 0.760 | | 1.460 | 0.610 | | 1.430 |
| | 2,971 cfs | 3.770 | 0.810 | | | 0.680 | | |
| | 2,944 cfs | 3.760 | | | 1.160 | | | 1.090 |
| Thornton et al. (2011) | NW01 | 2.457 | 3.542 | 3.035 | 3.328 | 2.255 | 2.385 | 2.675 |
| | NW02 | 1.836 | 1.223 | 2.611 | 3.078 | 0.463 | 1.590 | 2.226 |
| | NW03 | 2.457 | 1.630 | 3.491 | 3.926 | 0.649 | 2.971 | 2.651 |
| | NW04 | 1.836 | 2.926 | 2.231 | 3.451 | 1.436 | 1.594 | 2.359 |
| Scurlock et al. (2013a) | BW01 | 1.702 | 1.470 | 3.113 | 3.113 | 0.943 | 2.056 | 2.056 |
| | BW02 | 1.409 | 2.529 | 2.745 | 2.745 | 0.646 | 2.451 | 2.451 |
| | BW03 | 2.457 | 1.701 | 4.153 | 4.153 | 1.009 | 2.605 | 2.605 |
| | BW04 | 1.836 | 1.684 | 3.654 | 3.654 | 0.556 | 2.748 | 2.748 |
| Scurlock et al. (2013b) | BW05 | 1.702 | 1.478 | 3.186 | 3.186 | 0.494 | 1.326 | 1.326 |
| | BW06 | 1.409 | 1.302 | 2.704 | 2.704 | 0.448 | 1.601 | 1.601 |
| | SD05 | 1.702 | 1.034 | 4.239 | 4.239 | 0.251 | 1.435 | 1.435 |
| | V05 | 1.702 | 0.999 | 3.127 | 3.127 | 0.324 | 1.379 | 1.379 |

**Table 21.** Predicted velocity ratios using Equation 11 and literature data

| Study | Configuration | $MVR_O$ - | $MVR_I$ - | $MVR_C$ - | $AVR_O$ - | $AVR_I$ - | $AVR_C$ - |
|---|---|---|---|---|---|---|---|
| Lyn and Cunningham (2010) | H050-V22-T24A,B | 0.640 | 1.375 | 1.245 | 0.156 | 1.231 | 1.180 |
| | H050-V22-T48 | | 1.375 | 1.245 | | 1.231 | 1.180 |
| | H050-V25-T12A,B | | 1.375 | 1.245 | | 1.231 | 1.180 |
| | H075-V22-T48 | | 1.418 | 1.220 | | 1.255 | 1.169 |
| | H100-V22-T48 | | 1.452 | 1.389 | | 1.245 | 1.106 |
| Bui (2011) | 2,237 cfs | 0.192 | 1.198 | 1.252 | 0.168 | 1.108 | 1.108 |
| | 2,971 cfs | 0.237 | 1.179 | 1.200 | 0.171 | 1.069 | 1.069 |
| | 2,944 cfs | | 1.180 | 1.203 | | 1.071 | 1.071 |
| Thornton et al. (2011) | NW01 | 1.009 | 1.424 | 1.834 | 0.342 | 1.268 | 1.337 |
| | NW02 | 0.348 | 1.404 | 1.512 | 0.181 | 1.225 | 1.188 |
| | NW03 | 1.711 | 1.465 | 1.585 | 0.583 | 1.344 | 1.248 |
| | NW04 | 0.218 | 1.380 | 1.738 | 0.113 | 1.170 | 1.272 |
| Scurlock et al. (2013a) | BW01 | 0.471 | 1.434 | 1.512 | 0.173 | 1.299 | 1.459 |
| | BW02 | 0.306 | 1.235 | 1.325 | 0.183 | 1.148 | 1.221 |
| | BW03 | 0.184 | 1.353 | 1.554 | 0.150 | 1.256 | 1.453 |
| | BW04 | 0.216 | 1.291 | 1.425 | 0.219 | 1.182 | 1.275 |
| Scurlock et al. (2013b) | BW05 | 0.475 | 1.491 | 1.430 | 0.111 | 1.339 | 1.405 |
| | BW06 | 0.282 | 1.440 | 1.395 | 0.157 | 1.270 | 1.270 |
| | SD05 | 0.365 | 1.419 | 1.795 | 0.138 | 1.296 | 1.359 |

| Study | Configuration | $MVR_O$ - | $MVR_I$ - | $MVR_C$ - | $AVR_O$ - | $AVR_I$ - | $AVR_C$ - |
|---|---|---|---|---|---|---|---|
| | V05 | 0.565 | 1.537 | 1.475 | 0.195 | 1.105 | 1.358 |

**Table 22.** Absolute error between observed and predicted values, literature studies to Equation 11

| Study | Configuration | $MVR_O$ - | $MVR_I$ - | $MVR_C$ - | $AVR_O$ - | $AVR_I$ - | $AVR_C$ - |
|---|---|---|---|---|---|---|---|
| Lyn and Cunningham (2010) | H050-V22-T24A,B | 0.723 | 0.125 | 0.119 | 0.996 | 0.095 | 0.043 |
| | H050-V22-T48 | | 0.125 | 0.119 | | 0.163 | 0.111 |
| | H050-V25-T12A,B | | 0.012 | 0.233 | | 0.041 | 0.093 |
| | H075-V22-T48 | | 0.168 | 0.143 | | 0.147 | 0.061 |
| | H100-V22-T48 | | 0.202 | 0.025 | | 0.080 | 0.059 |
| Bui (2011) | 2,237 cfs | 0.037 | | 0.812 | 0.015 | | 1.108 |
| | 2,971 cfs | 0.022 | | | 0.009 | | |
| | 2,944 cfs | | | 0.895 | | | 1.071 |
| Thornton et al. (2011) | NW01 | 0.433 | 0.189 | 0.479 | 0.575 | 0.350 | 0.367 |
| | NW02 | 0.318 | 0.018 | 0.165 | 0.072 | 0.973 | 0.321 |
| | NW03 | 1.048 | 0.044 | 0.013 | 0.319 | 1.080 | 0.039 |
| | NW04 | 1.376 | 0.165 | 0.142 | 0.669 | 0.388 | 0.404 |
| Scurlock et al. (2013a) | BW01 | 0.393 | 0.395 | 0.317 | 0.382 | 0.745 | 0.251 |
| | BW02 | 1.489 | 0.714 | 0.623 | 0.275 | 0.689 | 0.518 |
| | BW03 | 0.509 | 0.337 | 0.137 | 0.261 | 0.846 | 0.392 |
| | BW04 | 0.702 | 0.699 | 0.565 | 0.084 | 0.879 | 0.221 |
| Scurlock et al. (2013b) | BW05 | 0.393 | 0.381 | 0.442 | 0.180 | 1.049 | 0.626 |
| | BW06 | 0.642 | 0.480 | 0.524 | 0.161 | 0.952 | 0.133 |
| | SD05 | 0.243 | 1.072 | 0.696 | 0.010 | 1.148 | 0.516 |
| | V05 | 0.022 | 0.300 | 0.363 | 0.005 | 0.914 | 0.548 |

# List of Abbreviations

| | |
|---|---|
| CSU | Colorado State University |
| Reclamation | United States Bureau of Reclamation |
| USDA | United States Department of Agriculture |
| GRG2 | Generalized Reduced Gradient |
| RMSD | Root Mean Square Deviation |
| USACE | United States Army Core of Engineers |
| HEC-RAS | Hydrologic Engineering Center River Analysis System |